UNIVERSITEIT VAN PRETORIA
UNIVERSITY OF PRETORIA
YUNIBESITHI YA PRETORIA
Denkleiers • Leading Minds • Dikgopolo tša Dihlalefi

Investigation of non-prostatic *in vitro* prostate-specific membrane antigen expression in MCF-7 and MDA-MB-231 breast tumour cells

By

Malvin Thabani Tshabalala

A dissertation submitted in fulfilment of the requirements for the degree,

Magister Scientiae

in

Pharmacology

Department of Pharmacology, School of Medicine,
Faculty of Health Sciences
University of Pretoria

Supervisor

Professor Duncan Cromarty
Department of Pharmacology

Co-supervisors

Dr. Thomas Ebenhan

Department of Nuclear Medicine

Dr. June Serem

Department of Anatomy

Faculty of Health Sciences
University of Pretoria
Email: duncan.cromarty@up.ac.za

Faculty of Health Sciences

University of Pretoria

Email: thomas.ebenhan@gmail.com

Faculty of Health Sciences

University of Pretoria

Email: june.serem@up.ac.za

Abstract

Introduction

Breast and prostate cancer mutually represent the most commonly occurring malignancies worldwide in women and men, respectively. The mutative state, recurrence capacity, resistance to conventional chemotherapy, low success rate of surgery and risks associated with radiotherapy confound the management of both these malignancies. There are several similarities between breast and prostate cancer, like growth hormone dependence and similar chemotherapeutic interventions. Therapy based on radiopharmaceuticals targeting the prostate-specific membrane antigen (PSMA) is proving to be a cutting-edge theranostics intervention for prostate cancer. Clinical positron emission tomography (PET) scans have located anti-PMSA binding sites in breast cancer *in vivo*. This indicates possible non-prostatic expression of PSMA, therefore research focused on understanding the cellular kinetics, PSMA expression profiles using two breast cancer adenocarcinoma cell lines as breast cancer models. This approach was to assess PSMA as a biomarker molecule that can aid in development of more selective, effective and safe diagnostic and therapeutic alternatives for breast cancer. This study was aimed at evaluating PSMA expression of MCF-7 or MDA-MB-231 mammary adenocarcinoma cell lines in comparison to a known high PSMA expressing LNCaP prostate carcinoma and EA.hy926 hybrid vascular endothelial cell line.

Methods

In vitro cultures of LNCaP's , a prostatic adenocarcinoma cell line, MCF-7 and MDA-MB-231 breast adenocarcinoma cell lines and endothelial EA.hy926 cells were tested for expression of PSMA by flow cytometry. The LNCaP cells were used a positive control. Cellular localisation of PSMA was achieved utilising confocal microscopy and fluorescently-tagged antibodies in all the cell lines tested. PSMA was quantified in all the cell lines utilising ELISA. Prior to experimentation, a pilot study was undertaken to optimise cell detachment methods. Trypsinisation was compared to mechanical scraping to evaluate a cell detachment method that allowed optimal downline experimentation.

Results

Findings from three supporting and complementary techniques demonstrate positive PSMA identification, localisation and quantification in all the probed cell lines despite three cell types not having a prostrate origin. Quantitatively, LNCaP cells reported the highest

concentration of PSMA followed by the malignant MDA-MB-231 cells, then the MCF-7 cell line and least in EA.hy926 cells. The difference in fluorescence between LNCaP cells and all three investigational cell lines was statistically significant however the difference in fluorescence between the three investigational cell lines was not statistically significant. The PSMA antigen was localised on the cell membrane and diffused within the cytosol in LNCaP cells. The MDA-MB-231, MCF-7 and EA.hy926 cells all exhibited a differential expression pattern of PSMA. These cells showed diffuse cytosolic accumulation and intense circular region accumulation apparently bordering the cell membrane and the cell nucleus. The quantification of PSMA reported the highest concentration as being in LNCaP cells. The MDA-MB-231 cells were second, then the MCF-7 cells and the lowest concentration. Significant differences were seen between the positive control and the investigation cell lines. The difference in concentration between the investigational cell lines was not significant. Finally, cryotome sections of biopsies of tumours from two breast cancer patients were found to show detectable PSMA presence.

Discussion

Fluorescence is directly proportional to concentration. The high fluorescence of PSMA exhibited by LNCaP cells in the flow cytometry results can be equated to concentration. A fundamental point of departure from which PSMA expression in the breast carcinoma cell lines could be investigated was established. Expression of PSMA is associated with cancer aggression, metastatic progression and increased malignancy. These clinicopathological characteristics support the expression of PSMA seen in MDA-MB-231. Contrastingly, the same characteristics aren't seen in MCF-7 cells but expression of PSMA was observed. The expression is not entirely dismissible as other luminal A cell lines have also been shown to express PSMA. The EA.hy926 cells are somatic hybrids that are made up of lung A549 cells and HUVEC's. Lung cancer has been shown to also express PSMA when probed utilising histology. The expression of PSMA in EA.hy926 is the first of its kind but may be attributable to its lung carcinoma makeup. The pattern of expression in the LNCaP confocal microscopy images can be expected. The PSMA antigen is a transmembrane receptor and as such intense fluorescence was seen on the membrane. Expression of PSMA in the cytoplasm has been reported and was equally observed in the LNCaP cells. The investigation cell line showed accumulation of green fluorescence in vesicular bodies bordering the cell membrane and in juxtanuclear positions. The expression of PSMA has been reported in the mitochondria and the green fluorescence at the nucleus could be mitochondrial. The Golgi apparatus and endoplasmic reticulum have also been recognised as potential location of PSMA expression. The localisation of both these organelles at the nucleus along with the expression of PSMA seen close to the nucleus could be associated. Worth noting is the

internalisation properties of PSMA. The antigen has an internalisation signal that can be induced by ligand binding or in the absence of a ligand. Upon internalisation the receptors are vesicled and transported either for degradation of for recycling. The vesicular expression seen close to the membrane in the investigational cell lines could be PSMA that is being trafficked for recycling or degradation upon internalisation. The ELISA quantification revealed the levels of PSMA in the positive control are 100-fold greater than those in the investigation cell lines. The ability to translate PSMA targeting in clinical settings is questionable when considering the difference in concentration values. The probing of PSMA in histological slices was positive and showed patterns that are similar to those seen in the monolayer cultures. This shows continuity between two-dimensional cultures and heterogeneous tissue samples. The premise for investigation of PSMA as a potential theranostic target was established through positive identification, localisation and quantification across three independents methods.

Conclusion

This study is the first of its kind to report reproducible expression of PSMA in the two-dimensional cultures of breast adenocarcinoma MDA-MB-231 and MCF-7 cell lines as well as in the hybrid endothelial EA.hy926 cell line. The results were confirmed by three different techniques where different antibodies were used for the ELISA showing reproducibility in the findings. Moreover, the generated results support the apparent localisation of PSMA in breast cancer patients utilising PSMA targeting radionuclides in PET imaging in a clinical setting. The potential application of this study's result is stimulating. The success being realised in prostate cancer theranostics through PSMA targeting, may conceivably be realised in other carcinomas, particularly breast carcinoma theranostics.

Declaration

University of Pretoria
Faculty of Health Sciences
Department of Pharmacology

Full name (s) Malvin Thabani Tshabalala

Student number U14139899

Subject of study Investigation of non-prostatic *in vitro* prostate-specific membrane antigen expression in MCF-7 and MDA-MB-231 breast tumour cells

1. I understand what plagiarism is and am aware of the University's policy in this regard.
2. I declare that this dissertation is my own original work. Where other people's work has been used (either from a printed source, Internet or any other source), this has been properly acknowledged and referenced in accordance with departmental requirements.
3. I have not used work previously produced by another student or any other person to hand in as my own.
4. I have not allowed, and will not allow, anyone to copy my work with the intention of passing it off as his or her own work.

SIGNATURE: 

Acknowledgements

- I would like to thank Prof. Cromarty, Dr. Serem and Dr. Ebenhan. Your supervision and guidance allowed me develop and grow into a researcher who is confident in his work. You guided and natured as well directed my strengths, making me a better researcher.
- I would like to thank Shamiso and Hafiza. You allowed me to be myself albeit at a great cost to your peace and sanity. I honestly can never thank you enough but you should know that you have my utmost respect and appreciation and I wish you nothing but the best in everything.
- I would like to thank Ms Margo Nel, Voula, Andy, Chanel, Dr. Kleynhans, Solly, Amos, Petunia, Jacque, Dr. Taute and Dr. Van de Bout. Your help with different parts of this project made its completion possible.
- I would like to thank Tracey and Clement. You made all of this more bearable, provided support and comical relief. Consistently motivating and advising throughout the struggle. I'm eternally grateful.
- I would like to thank Noluthando, Sinethemba, Khanyisile, Faustino, Roberta, Bryant, Ncane Lucky, Maki, Patience, Uncle Evidence, KPFC, Ruth, Alan, Kerrin, Tumelo, Monde, Mthokozisi, Munashe, Khabo, Kerri, Lizette and Yolandi. You each played a part in this success.
- I would like to thank Mwila Saini, Thami Tsoka and Malumbo Kasanda. The past 15 years have been great, may the next 15 be even greater. I appreciate greatly your work gentlemen.
- To my sister Sandra and my brother Thembani, you have all my gratitude. I don't have the words to express how grateful I am but this would not have been possible at all without you. I love you with all that I am.
- To my parents, thank you for your love and patience. You allowed to me see this plan through and we are here now. This Masters is dedicated to you and your support of my dreams. I love you.
- To my God, I am undeserving yet you chose display your majesty through me. May I never forget from whence all blessings flow. Use me once more.

2 Corinthians 4:8-18

Table of Contents

Abstract iii

Acknowledgements vii

List of Figures: xi

List of Tables: xv

Abbreviations xvi

1 1

1 Introduction and literature review 1

1.1 Cancer 1

1.1.1 Breast cancer 2

1.1.2 Breast cancer classification 3

1.1.3 Molecular classification of breast cancer 6

1.1.4 Breast cancer diagnosis 7

1.1.5 Challenges in breast cancer diagnosis 9

1.1.6 Breast cancer treatment 10

1.2 Prostate cancer 12

1.3 Radiopharmaceuticals 13

1.3.1 Nuclear diagnostics - Positron emission tomography 14

1.3.2 Nuclear therapeutics - Theranostics 16

1.4 Prostate specific membrane antigen (PSMA) 17

1.4.1 PSMA and prostate cancer 19

1.4.2 PSMA function 19

1.4.3 Folate 19

1.4.4 Folate and one carbon metabolism 20

1.4.5 Folate, PSMA and prostate cancer 22

1.4.6 PSMA targeting radiopharmaceuticals 22

1.4.7 PSMA based theranostics 24

1.5 Non-prostatic PSMA expression 26

1.5.1 PSMA in breast cancer 26
1.5.2 Breast and prostate cancer overlap 28
1.6 Study rationale 28
1.7 Study Aim 29
1.8 Objectives 29
2 Materials and methods 31
2.1 Cell culturing 31
2.1.1 Description of cell Lines 31
2.1.2 Culture media and conditions 31
2.1.3 Preparation of cells for experiments 32
2.1.4 Cell counting 32
2.1.5 Cell culture reagents 32
2.1.6 Optimisation of cell culturing conditions for the detection of PSMA 33
2.1.7 Crystal Violet assay 34
2.2 Indirect flow cytometry detection of PSMA 36
2.2.1 Preparation of cells for flow cytometry 36
2.2.2 Antibody staining of cells for flow cytometry 36
2.2.3 Controls 37
2.2.4 Statistics for flow cytometry 37
2.2.5 Flow cytometry reagents 37
2.3 Indirect immunofluorescence analysis – PSMA localisation 38
2.3.1 Preparation of coverslips for immunofluorescence. 39
2.3.2 Preparation of cells for immunofluorescence 39
2.3.3 Seeding of cells for confocal microscopy 39
2.3.4 Staining of cells for confocal microscopy 39
2.4 ELISA - PSMA quantification 41
3 Results and Discussion 45
3.1 Phase contrast microscopy and Crystal Violet assay – Optimisation 45
3.1.1 Cell detachment methods 45

3.1.2 Phase contrast microscopy 45
3.2 Crystal Violet assay 47
3.3 Indirect flow cytometry - PSMA identification 50
3.3.1 LNCaP cells – Flow cytometry 50
3.3.2 MCF-7 cells – Flow cytometry 52
3.3.3 MDA-MB-231 cells – Flow cytometry 53
3.3.4 MCF-7 cells and MDA-MB-231 cells – Flow cytometry 55
3.3.5 EA.hy926 cells – Flow cytometry 57
3.3.6 Flow cytometry – All cells 59
3.4 Indirect immunofluorescence analysis – PSMA localisation 61
3.4.1 LNCaP cells – Confocal microscopy 61
3.4.2 MCF-7 cells – Confocal microscopy 62
3.4.3 MDA-MB-231 cells – Confocal Microscopy 65
3.4.4 MCF-7 and MDA-MB-231 cells – Confocal microscopy 69
3.4.5 EA.hy926 – Confocal microscopy 71
3.5 ELISA – PSMA quantification 73
3.6 Breast tissue – Confocal microscopy 75
4 Concluding discussion 83
4.1 Limitations and recommendations 86
4.2 Future work 88
5 References 89

List of Figures:

Figure 1-1 Global Cancer Observatory cancer statistics 2018 (Bray et al., 2018). (Used with permission) 2
Figure 1-2 Cancer development in breast ducts (A) and lobules (B) (Board, 2020a). (Used with permission) 4
Figure 1-3 Metastatic breast cancer (Board, 2020a). (Used with permission) 5
Figure 1-4 Diagrammatic depiction of the layout of the opposing detectors of a typical PET system (Kong et al., 2013). (Used with permission) 15
Figure 1-5 Breast PET scan showing a focus of intense radioligand uptake (orange arrow) in the upper inner quadrant of the right breast proven to be a breast carcinoma (Vercher-Conejero et al., 2015). (Used with permission) 15
Figure 1-6 Energy and penetration properties of alpha, beta and gamma rays. (Image formulated utilising Microsoft PowerPoint®) 17
Figure 1-7 PSMA receptor structure (Evans et al., 2016). (Used with permission) 18
Figure 1-8 Folic acid conversion into tetrahydrofolate (THF) through nicotinamide adenine dinucleotide phosphate (NADPH) oxidation and dihydrofolate reductase, R = para-aminobenzoate-glutamate (DHFR) (Zheng and Cantley, 2019). (Used with permission) 20
Figure 1-9 Folate 1C metabolism pathways in the cytosol and mitochondria (Zheng and Cantley, 2019). (Used with permission). Blue highlights indicate enzymes, pink highlights indicate chemical cofactors and green highlights indicated folate associated metabolites. .. 21
Figure 1-10 [68Ga] Ga-PSMA-11 labelling with metal chelator and peptide inhibitor. (Image formulated utilising Microsoft PowerPoint®) 23
Figure 1-11 A diagram of a combined 68-Gallium/177-Lutetium-PSMA-11 used in tandem for prostate cancer theranostics. (Image formulated utilising Microsoft PowerPoint®) 25
Figure 1-12 A combined PET/CT scan image of a 39-year-old woman with stage IV breast cancer following ^{68}Ga-PSMA-11 administration. PET demonstrated multiple osseous metastasis and a primary right breast cancer (Sathekge et al., 2017). Axial, coronal and sagittal PET/CT views of the patient confirm the presence of PSMA in breast tumour lesions. (Used with permission). 27
Figure 1-13 A flow diagram summarising the different methods applied and cell lines used in this study. 30
Figure 2-1 Optimisation of culturing conditions prior to PSMA expression evaluation. 34

Figure 3-1 Monolayer, trypsinised and scraped images phase contrast images of trypsinised and scraped LNCaP MCF-7, MDA-MB-231 and EA.hy926 cells at 10X magnification. Red arrows indicate cell clustering. (Image brightness adjusted)..... 46
Figure 3-2 Graphs representing growth of LNCaP (A), Ea.hy926 (B), MCF-7 (C) and MDA-MB-231 (D) monolayer cells at 48 and 72 hour time intervals after scraping (black) or trypsinisation (grey) assessed by the Crystal Violet assay. N= 3 repeats, (P <0.0001), error bars are representative of standard error of the mean (SEM). 48
Figure 3-3 Graph of the typical growth phases of mammalian cells in culture (Used with permission) 49
Figure 3-4 Flow cytometry histogram depicting PSMA binding in unstained (A) and stained (B) LNCaP cells (7500 events x 3 repeats). Note the gate position has remained constant. 51
Figure 3-5 Flow cytometry histogram depicting PSMA binding in unstained (A) and stained (B) MCF-7 cells (7500 events x 3 repeats). Note the gate position has remained constant. 52
Figure 3-6 Flow cytometry histogram depicting PSMA binding in unstained (A) and stained (B) MDA-MB-231 cells (7500 events x 3 repeats). Note the gate position has remained constant. 54
Figure 3-7 Half offset histogram overlay representing MCF-7 fluorescence intensity compared to MDA-MB-231 fluorescence intensity. 56
Figure 3-8 Flow cytometry histogram depicting PSMA binding in unstained (A) and stained (B) EA.hy926 cells (7500 events x 3 repeats). Note the gate position has remained constant. 57
Figure 3-9 Fluorescence intensity comparison across all cell lines. N= 3 independent repeats, (P <0.0001), error bars are representative of standard error of the mean (SEM). Significant differences across different cell lines are represented by (*). Multiple comparisons of a Repeated measures one-way Analysis of Variance (ANOVA). 60
Figure 3-10 Confocal fluorescent microscopy images of LNCaP cells stained with anti-PSMA primary antibody counterstained with a FITC labelled secondary antibody. Turquoise DAPI stains reveal the cell nucleus while, the green indicates PSMA antigen localisation. Control LNCaP cells stained with DAPI but not exposed to anti-PSMA antibodies are shown in the bottom row of images confirming that there was no non-specific binding. Images were taken at 100X magnification. Blue arrow indicates strong cytosolic green fluorescence and white arrows show membrane associated green fluorescence. (Image brightness adjusted)..... 61
Figure 3-11 Confocal fluorescent microscopy images of MCF-7 cells stained with anti-PSMA primary antibody counterstained with a FITC labelled secondary antibody.

Turquoise DAPI stains reveal the cell nucleus while, the green indicates PSMA antigen localisation. Control cells not treated with anti-PSMA antibody do not show green fluorescence, showing that there was no non-specific biding. Images were taken at 100X magnification. Blue arrows indicate diffuse cytosolic fluorescence and white arrows indicate circular intracellular fluorescence accumulation. (Image brightness adjusted)..... 63
Figure 3-12 MCF-7 cells visualised using confocal microscopy (B) contrasted with LNCaP immunoelectron microscopy image (A). Cell membrane (CM) (Troyer et al., 1997). White arrow indicates circular intracellular accumulation of fluorescence. (Used with permission). (Image brightness adjusted). Magnification (A) x97000 64
Figure 3-13 Graphical representation of the transportation, digestion and recycling of PSMA (Ghosh and Heston, 2004). Trans Golgi network (TGN), plasma membrane (PM), Adaptor complexes (AP). Brown circle indicates PSMA recycling, the pink circle shows the Trans Golgi network, the red circle indicates PSMA internalisation and the green circle indicate PSMA lysosome digestion. (Used with permission) 65
Figure 3-14 Confocal fluorescent microscopy images of MDA-MB-231 cells stained with anti-PSMA primary antibody counterstained with a FITC labelled secondary antibody. DAPI stain reveals the cell nucleus as turquoise while the green indicates PSMA antigen localisation. Control cells not treated with anti-PSMA antibodies indicating that there was no non-specific binding. Images were taken at 100X magnification. Blue arrow shows diffuse cytosolic fluorescence, red arrow shows fluorescence close to the nucleus. White arrow shows a smaller circle of green fluorescence and yellow arrow indicates bigger circle of green fluorescence (Image brightness adjusted)..... 66
Figure 3-15 MDA-MB-231 cells visualised using transmission electron microscopy (TEM) (A) (Wojtkowiak et al., 2012) and confocal fluorescent microscopy (B). Mitochondria (M), nucleus (N) and lysosome (LY) (Wojtkowiak et al., 2012). Red arrow indicates fluorescence bordering the nucleus, blue arrow shows vesicular intracellular fluorescence and white arrows depict diffuse cytosolic accumulation. (TEM image used with permission). (Image brightness adjusted) 67
Figure 3-16 Graphical representation of PSMA recycling (Ghosh and Heston, 2004). Recycling endosomal compartment (REC) and nuclear membrane (NM). Pink circle indicates REC compartment, dark blue circle indicates REC trafficking, PSMA interacts with filamin A indicated by light blue circle and vesicle receptors are indicated by red circles. (Used with permission)..... 68
Figure 3-17 Confocal microscopy comparison of MDA-MB-231 images and MCF-7 images. Blue arrow indicates diffuse cytosolic accumulation, red arrow show fluorescence next to the nucleus and the white arrow indicates vesicular expression close to the membrane. (Image brightness adjusted)..... 70

Figure 3-18 Confocal fluorescent microscopy images of EA.hy926 cells stained with anti-PSMA primary antibody counterstained with a FITC labelled secondary antibody. DAPI stain reveals the cell nucleus as turquoise while the green indicates PSMA antigen localisation. Controls not stained with anti-PSMA antibody showed no green fluorescence, indicating that there was no non-specific binding. Blue arrows indicate diffuse cytosolic fluorescence, white arrows show fluorescence close to the cell membrane, yellow arrows show fluorescence close to the nucleus and red arrows show fluorescence close to the plasma membrane. Images were taken at 100X magnification. (Image brightness adjusted) 71
Figure 3-19 EA.hy926 cells visualised using TEM EA.hy926 cells (A) (Eremeeva and Silverman, 1998) and confocal fluorescent microscopy (B). Red arrow indicates intracellular nuclear associated fluorescence, blue arrow indicates intracellular circular fluorescence close to the membrane and yellow arrow shows fluorescence at the plasma membrane. (TEM image used with permission). (Image brightness adjusted) 72
Figure 3-20 PSMA quantification utilising ELISA in LNCaP, MDA-MB-231, MCF-7 and EA.hy926 cell lysates. N= 3 repeats, (P <0.0001), error bars are representative of standard error of the mean (SEM). Significant differences across different cell lines are represented by (*). Multiple comparisons of a Repeated measures one-way ANOVA. 74
Figure 3-21 Confocal fluorescent microscopy images of luminal A tumour samples stained with anti-PSMA primary antibody counterstained with a FITC labelled secondary antibody. DAPI stain reveals the cell nuclei as turquoise while, the green indicates PSMA antigen localisation. Images were taken at 20X, 40X and 63X magnification. Blue arrows indicate intense green fluorescence, pink arrow indicate membrane associated fluorescence. The white circles indicate multiple cells showing intense green fluorescence (PSMA). (Image brightness adjusted) 77
Figure 3-22 Luminal A tissue samples visualised using confocal fluorescent microscopy (63X magnification) (A) compared with MCF-7 cells (B). MCF-7 (100X magnification). Red arrow shows membrane associated fluorescence in tissue samples, blue arrows show diffuse cytosolic fluorescence and white arrow shows circular accumulation in MCF-7 cells. (Image brightness adjusted) 78
Figure 3-23 Confocal fluorescent microscopy images of HER-2 positive tumour samples stained with anti-PSMA primary antibody and counterstained with a FITC labelled secondary antibody. DAPI stain reveals the cell nucleus as turquoise while, the green indicates PSMA localisation. Images were taken at 20X, 40X and 63X magnification. White arrows indicate intracellular fluorescence and blue arrows indicate membrane associated fluorescence. (Image brightness adjusted) 79

Figure 3-24 Consensus PSMA RNA sequence data form of HPA internally generated RNA sequence data, RNA sequence data from the Genotype-Tissue Expression (GTEx) project and Cap Analysis of Gene Expression (CAGE) data from FANTOM5 project (Thul et al., 2017). The black rectangles indicate PSMA expression in prostate, liver, breast, cervix and lung tissue from highest to lowest. (Used with permission) 81
Figure 3-25 Consensus PSMA RNA expression in pathological tissue data form of HPA internally generated mRNA sequence data (Thul et al., 2017). The brown rectangle indicates PSMA expression in lung cancer, the blue rectangles indicate PSMA expression in prostate cancer and the pink rectangle indicates PSMA expression in breast cancer. (Used with permission) 82

List of Tables:

Table 1.1 Main molecular classifications of breast cancer (Feng et al., 2018). 7
Table 3.1 Table showing numeric values of PSMA quantified in LNCaP, MDA-MB-231, MCF-7 and EA.hy926 utilising ELISA. Multiple comparisons of a Repeated measures one-way ANOVA. 75

Abbreviations

1C	One carbon
5-FU	5-Flourouracil
ANOVA	Analysis of variance
AP	Adaptor complexes
AR	Androgen receptor
ATCC	American type culture collection
BRCA	Breast cancer gene
BSE	Breast self-examination
Ca^{2+}	Calcium ion
CAGE	Cap analysis of gene expression
CDK	Cyclin dependent kinase
CNB	Core needle biopsy
CNS	Central nervous system
CO_2	Carbon dioxide
CT	Computed tomography
CV	Crystal violet
DAPI	4′, 6-diamidino-2-phenylindole
DCIS	Ductal carcinoma *in-situ*
DHF	Dihydrofolate
DHFR	Dihydrofolate reductase
DHT	Dihydrotestosterone
DMEM	Dulbecco's Modified Eagles Medium
DNA	Deoxyribonucleic acid

DOTA	Dodecane tetraacetic acid
DRE	Digital rectal exam
dUMP	Deoxyuridine monophosphate
dTMP	Deoxythymidine monophosphate
ELISA	Enzyme linked immunosorbent assay
ER	Endoplasmic reticulum
ER	Oestrogen receptor
ERα	Oestrogen receptor alpha
FCS	Foetal calf serum
FITC	Fluorescein isothiocyanate
FNAC	Fine needle aspiration cytology
g	Gravity
GTEx	Genotype-Tissue expression
H&L	Heavy and light chain
HBED-CC	N,N′-bis[2-hydroxy-5-(carboxyethyl)benzyl]-6 ethylenediamine-N,N′-diacetic acid
HER-2	Human epidermal receptor 2
HPA	Human protein atlas
HRP	Horseradish peroxidase
HUVEC	Human umbilical vein endothelial cells
IDC	Invasive ductal carcinoma
ILC	Invasive lobular carcinoma
LCIS	Lobular carcinoma *in situ*
LET	Linear energy transfer
Mg^{2+}	Magnesium ion

MRI	Magnetic resonance imaging
MTHFD1/L	Methylene tetrahydrofolate dehydrogenase 1/Like
MTHFD2/L	Methylene tetrahydrofolate dehydrogenase 2/Like
MTHFR	Methylene tetrahydrofolate reductase
mTOR	Mammalian target of rapamycin
MTT	3-[4, 5-dimethylthiazole-2-yl]-2, 5-diphenyltetrazolium bromide
MTX	Methotrexate
NAAG	N-acetyl aspartylglutamate
$NADP^+$	Nicotinamide adenine dinucleotide phosphate
NE	Normalised expression
NM	Nuclear membrane
PALB2	Partner and localizer 2
PARP	poly-ADP ribose polymerase
PBS	Phosphate buffer saline
PBST	Phosphate buffered saline and tween®
PEM	Positron emission mammography
PET	Positron emission tomography
PET/CT	Positron emission tomography – computed tomography
PM	Plasma membrane
PMT	Photomultiplier tube
PR	Progesterone receptor
PSA	Prostate specific antigen
PSMA	Prostate specific membrane antigen
RNA	Ribonucleic acid
SAM	S-adenosylmethionine synthase

SEM	Standard error of mean
SHMT	Serine hydroxyl methyl transferase
SPECT	Single photon emission computed tomography
TEM	Transmission electron microscopy
TGN	*Trans* Golgi network
THF	Tetrahydrofolate
TMB	Tetramethyl benzidine
TNBC	Triple negative breast cancer
TRUS	Trans rectal ultrasound
TYMS	Thymidylate synthase
Zn^{2+}	Zinc (II) ion

1 Introduction and literature review

1.1 Cancer

Cancer is a state when a healthy cell within the body begins to undergo uncontrolled proliferation that can then generally form a solid tumour (Arneth, 2020). Tumorigenesis is a multistep process that is caused by genetic alterations in cell cycle promoters and inducers in select cells (Arneth, 2020, Sarkar *et al.,* 2013). This results in the limitless replication potential and the loss of growth control demonstrated by these cells (Arneth, 2020, Sarkar *et al.,* 2013). The accumulation of multiple abnormalities in cell regulatory systems can be summarised in the six original hallmarks of cancer as described by Hanahan and Weinberg (2000). These include but are not limited to; self-sufficiency in growth signals, insensitivity to antigrowth signals, evasion of apoptosis, promotion of angiogenesis, limitless replicative potential and tissue invasion and metastasis (Hanahan and Weinberg, 2000). Emerging hallmarks have also been identified. These are; reprogramming of energy metabolism and evasion of immune destruction. All the above-mentioned hallmarks are facilitated by two characteristics namely, genomic instability and mutation as well as chronic tumour promoting inflammation.

Cancer today, persists as one of the most fatal non-communicable diseases in the world (Wild *et al.,* 2020). It is the first or second leading cause of premature death in 134 out of 183 countries (Wild *et al.,* 2020). With an increasing average number of new cases reported every year, the global cancer disease burden continues to grow (Bray *et al.,* 2018). An overwhelming portion of this increase in incidence is observed largely in low and middle-income countries, adding considerably to their existing socioeconomic challenges (Arneth, 2020, Bray *et al.,* 2018). In 2018, there were an estimated 18.1 million newly diagnosed cancer cases and 9.6 million cancer related deaths worldwide. Female breast cancer accounts for 11.6% of the global cancer incidence, with prostate cancer statistically representing 7.1% of global cancer incidence (Figure 1.1) (Bray *et al.,* 2018). In Africa, the most common malignancies are also breast cancer in women and prostate cancer in men (Wild *et al.,* 2020).

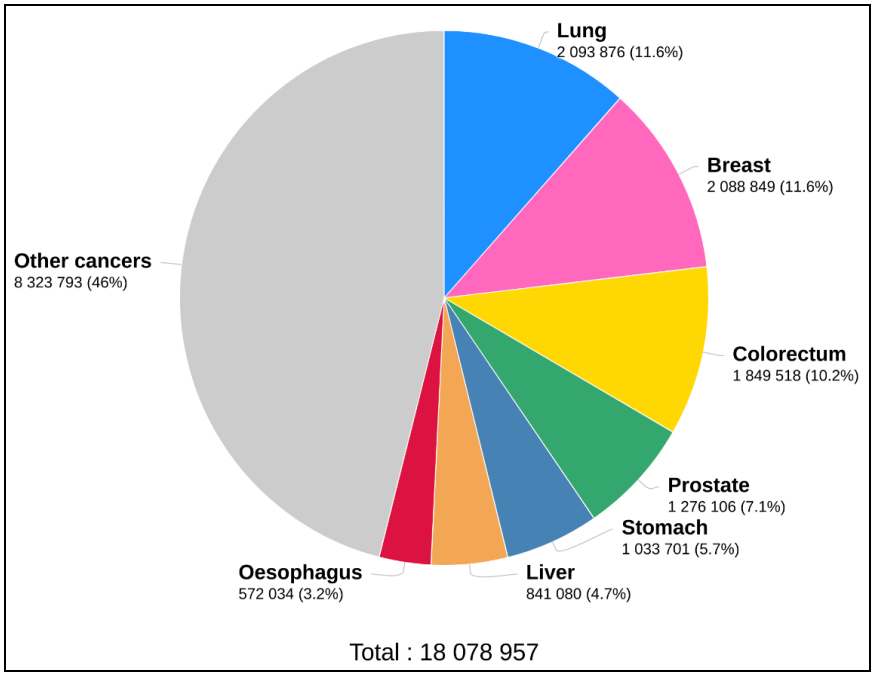

Figure 1-1 Global Cancer Observatory cancer statistics 2018 (Bray et al., 2018). (Used with permission)

1.1.1 Breast cancer

Breast cancer is a heterogeneous disease that occurs as distinct malignancies mainly in the mammary glands and milk ducts (Alkabban and Ferguson, 2019). Equally worth noting is that, breast cancer can occur in men but prevalence is not comparable to the levels seen in women (Bray *et al.,* 2018, Wild *et al.,* 2020). It is the most diagnosed cancer in 154 out of 185 countries and presents as the foremost cause of cancer related death in a 100 countries (Bray *et al.,* 2018). In 2018 an estimated 2.1 million cases of breast cancer were diagnosed, second only to lung cancer (Bray *et al.,* 2018). More than half of the diagnosed breast cancer cases manifest in low- and middle-income countries, of which South Africa is one.

A family history of breast cancer contributes to susceptibility, particularly in first-degree relatives (Kamińska *et al.,* 2015, Momenimovahed and Salehiniya, 2019). Patients can inherit breast cancer susceptibility gene mutations, especially mutations in the breast cancer genes (BRCA) 1, 2 and the partner and localiser gene 2 (PALB2) (Momenimovahed and Salehiniya, 2019). These genes are involved in the repair of double-stranded deoxyribonucleic acid (DNA) and genome maintenance. Expression of these mutated genes confers genomic instability that contributes substantially to the breast cancer development (Macedo *et al.,* 2019). Individuals presenting with these mutations have a two-fold higher risk

of developing breast cancer (Godet and Gilkes, 2017). Additionally, non-cancerous breast pathology conditions such as ductal hyperplasia, intraductal papilloma's and fibroadenomas further increase the risk of breast cancer development (Bray *et al.,* 2018).Taken together, the above-mentioned hereditary and genetic predisposing factors are associated with approximately 10% of total breast cancer incidence (Bray *et al.,* 2018, Godet and Gilkes, 2017).

Non-hereditary factors are the principal drivers of the observed breast cancer incidence rates (Bray *et al.,* 2018). Extrinsic risk factors such as early menarche, delayed menopause, high breast tissue density, late age first pregnancy, increased exogenous hormone intake, high alcohol consumption, fat rich diet, tobacco use, low physical activity, and radiation exposure remain the supreme contributors to the breast cancer incidence (Bray *et al.,* 2018, Brewster *et al.,* 2014, Stratton, 1997). The relationship between breast cancer risk and increase in age is proportional. The median age for breast cancer progression is 60 years (Bray *et al.,* 2018). Moreover, certain ethnic populations such as Caucasians are more predisposed than African, Asian and Hispanic population groups (Bray *et al.,* 2018, Brewster *et al.,* 2014). The rise in breast cancer incidence correlates to the increase of these extrinsic factors (Wild *et al.,* 2020).

1.1.2 Breast cancer classification

Classification of breast cancer is primarily determined by which cells are involved. Staging then extends to the degree of invasiveness relative to the primary tumour site (Feng *et al.,* 2018, Harris and McCormick, 2010). Discerning the class of breast cancer is crucial as there is a direct implication on the treatment and prognosis outcome (Feng *et al.,* 2018). Breast cancer is classified into three categories specifically, in-situ (non-invasive), invasive and metastatic breast cancer (Barnard *et al.,* 2015, Feng *et al.,* 2018, Harris and McCormick, 2010).

Ductal carcinoma *in situ* (DCIS) involves the epithelial cells that line the ducts responsible for delivery of milk to the nipples (Figure 1.2A). It is essential to note that although DCIS is initially non-invasive, there is potential to develop further into invasive carcinoma (Feng *et al.,* 2018, Barnard *et al.,* 2015). Early therapeutic intervention is pertinent and usually sufficient in averting progression to an invasive state (Feng *et al.,* 2018). Invasive ductal carcinoma (IDC) describes cancer cells that have invaded beyond the basal membrane of the ducts into the adjacent stromal tissue of the breast (Barnard *et al.,* 2015). IDC cells have

the potential to spread and metastasise by entering the surrounding lymph nodes and beyond to other parts of the body (Barnard *et al.,* 2015). Approximately 80% of observed breast cancer cases are of the IDC subtype, manifesting frequently in women over the age of 55 (Barnard *et al.,* 2015).

Lobular carcinoma *in situ* (LCIS) presents within the lobules of the milk producing glands (Figure 1.2B). The LCIS subtype, also known as ALH, is classified as benign, but women with LCIS face a greater risk of developing invasive cancers (Feng *et al.,* 2018). Similarly without early antineoplastic intervention, an invasive form of lobular carcinoma can develop (Feng *et al.,* 2018). Invasive lobular carcinoma (ILC) is the subsequent spreading form of LCIS breast cancer. More commonly manifesting later in life, ILC occurs mostly in women in their early 60's (Barnard *et al.,* 2015). It accounts for 10-15% of reported breast cancer cases (Barnard *et al.,* 2015, Brewster *et al.,* 2014). Together, IDC and ILC account for 95% of all reported breast cancer cases. They each demonstrate distinct molecular abnormalities, treatment and prognosis outcomes (Feng *et al.,* 2018).

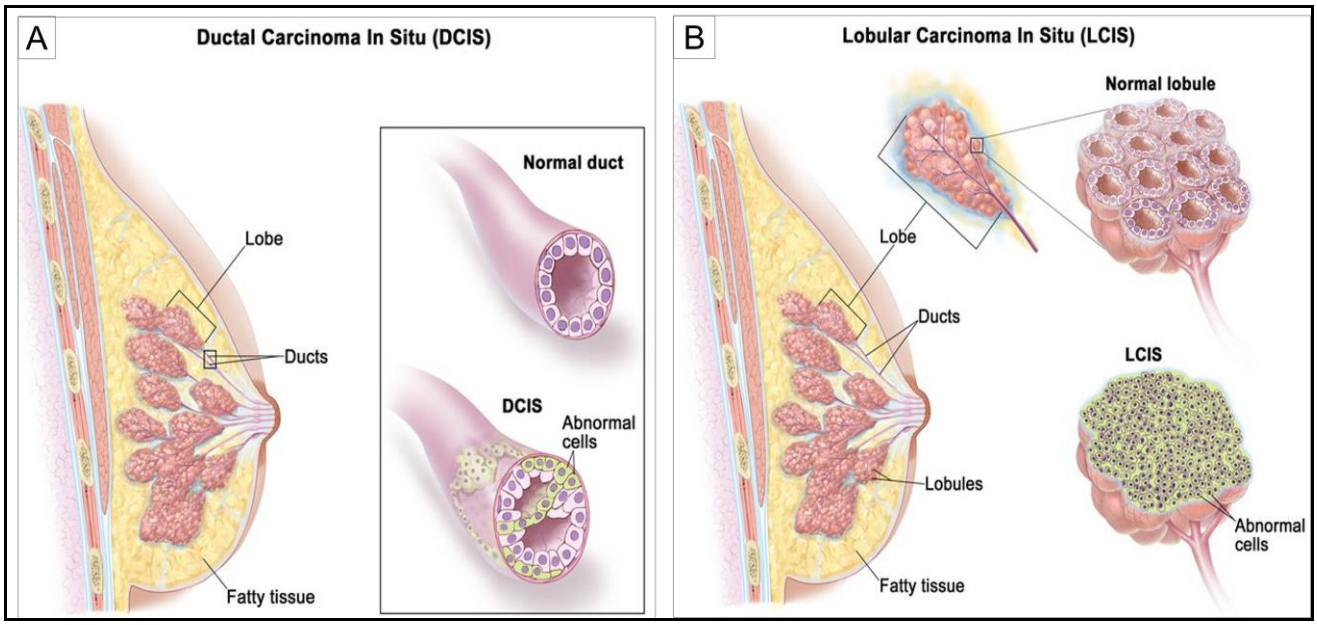

Figure 1-2 Cancer development in breast ducts (A) and lobules (B) (Board, 2020a). (Used with permission)

Breast cancer can haematologically or lymphatically spread to neighbouring or distant tissues and organs. Breast cancer metastases are the main cause of breast cancer-associated deaths (Jin and Mu, 2015). Breast carcinoma metastases are typically found in the axillary lymph nodes located in the armpit area (Figure 1.3). Other regions of typical metastasis include the lungs, bones, liver and brain (Feng *et al.,* 2018, Jin and Mu, 2015).

Microscopic tumour cells that are able to evade therapeutic intervention and possess a self-renewal capability have been observed to remain after therapeutic intervention in metastatic breast cancer (Wang, 2015). These surviving microscopic deposits are generally secondary pioneer-cells causing breast cancer recurrence (Feng *et al.,* 2018, Jin and Mu, 2015). This further complicates the management of metastatic breast cancer. Regrettably, up to 30% of patients diagnosed with early-stage breast cancer will develop metastatic breast cancer (Feng *et al.,* 2018).

Mucinous, papillary, tubular and inflammatory breast carcinomas are less prevalent and less invasive forms of breast cancer. Together they represent the remaining classes of breast cancer along with male and adolescent breast cancer (Feng *et al.,* 2018).

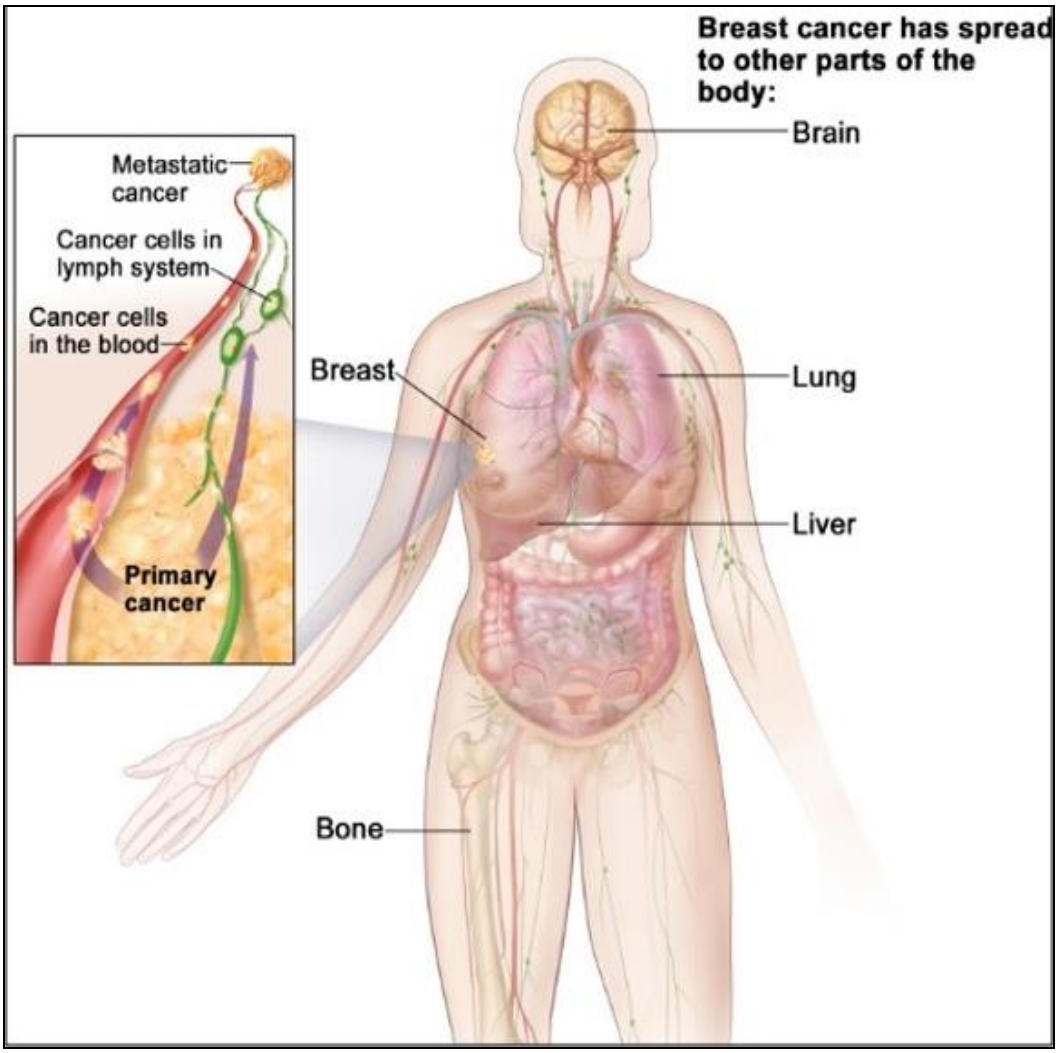

Figure 1-3 Metastatic breast cancer (Board, 2020a). (Used with permission)

1.1.3 Molecular classification of breast cancer

Breast cancer is a highly heterogeneous disease and it is classified into distinct molecular subtypes according to its hormone receptor expression profiles. It is divided into five molecular subtypes based on the expression pattern of certain genes that relate to the expression of oestrogen receptors (ER), human epidermal growth factor 2 (HER-2) and progesterone receptors (PR) (Table 1.1) (Barnard *et al.,* 2015, Feng *et al.,* 2018). All the hormone receptor subtypes independently infer differing prognostic, pathologic and therapeutic outcomes (Barnard *et al.,* 2015, Feng *et al.,* 2018).

Oestrogen is the primary facilitatory hormone in hormone-dependent breast cancer oncogenesis (Lumachi *et al.,* 2013). The biological effect of oestrogen is mediated by the nucleus associated oestrogen receptor alpha (ER-α). This receptor functions as a ligand-inducible transcription factor that promotes cell growth (Lumachi *et al.,* 2013, Tian *et al.,* 2018). The amplification of the cell surface expressed HER-2 receptor has been demonstrated to play an essential role in the growth and differentiation of epithelial breast cancer cells (Albagoush and Limaiem, 2018, Lumachi *et al.,* 2013). Progesterone is a steroidal hormone which is crucial in female adolescent breast development and preparation for lactation in pregnant women. In breast cancer, it facilitates cancer cell proliferation and differentiation (Lange and Yee, 2008, Tian *et al.,* 2018).

Of the five subtypes of breast cancer, the luminal A subtype accounts for approximately 40% of all presenting breast cancer cases. Luminal A carcinomas are slow-growing, low-grade carcinomas. They have reduced aggression and demonstrate the best prognosis compared to the other four subtypes. This is due to their expression of both ER and PR, which are susceptible to endocrine targeted therapy (Barnard *et al.,* 2015, Feng *et al.,* 2018). Luminal B carcinomas represent less than 20% of all breast carcinomas. They express all three receptors along with high levels of Ki-67. This subtype shows poorer prognosis, higher-grade tumours, increased aggression compared to the luminal A subtype (Feng *et al.,* 2018, Parise and Caggiano, 2014).

Quantitatively, HER-2 subtypes make up 10-15% of breast cancer cases. They lack both the ER and PR. As a result, the subtype shows higher aggressiveness, faster tumour growth rates and poor prognosis (Feng *et al.,* 2018). Treatment is achieved through targeting of HER-2 receptors using monoclonal antibodies such as Trastuzumab (Feng *et al.,* 2018).

Basal cell and claudin-low subtypes are classified as triple-negative breast cancers (TNBC's). They do not express high levels of HER-2, progesterone or oestrogen receptors (Feng *et al.,* 2018). Statistically, 20% of all breast cancers are triple-negative. Additionally, 75% of triple-negative breast cancers fall into the basal-like subtype (Feng *et al.,* 2018). When compared to the luminal subtypes, TNBC is generally of a higher grade with high aggressiveness, showing only partial response to chemotherapy, higher recurrence rate and reduced patient survival (Parise and Caggiano, 2014).

The prognostic differences associated with each cancer subtype emphasises the need for accurate subtype diagnosis that allows for the development of an appropriate treatment regimen that is more specific toward the prognostic demands of each subtype (Shah *et al.,* 2014).

Table 1.1 Main molecular classifications of breast cancer (Feng et al., 2018).

Classification	Characteristics
Luminal A	Lack HER-2 expression but are positive for both ER and PR.
Luminal B	Positive for HER-2, ER and PR.
Basal	Lack HER-2, ER and PR (triple-negative).
Claudin-low	Triple negative, but differ in their low claudin – a protein important for formation of tight junctions between cells
HER-2	Positive for HER-2, but lack ER and PR.

1.1.4 Breast cancer diagnosis

The cornerstone of breast cancer treatment is early detection. A reliable diagnosis is pivotal as well as decisive in the determination and outcome of a therapeutic intervention strategy. The benefit of early and accurate diagnosis is shown by the encouragingly higher survival rate of women who undergo early diagnostic screening (Gøtzsche and Jørgensen, 2013, Shah *et al.,* 2014). One fact remains consistent when considering the complex prognostic inferences of the different breast cancer subtypes; early-stage cancer cell detection has the best prognosis (Wang, 2017). For this reason, deliberate efforts have been undertaken particularly in low- and middle- income countries to promote early diagnosis and screening

(Ginsburg *et al.,* 2020). There are several diagnostic approaches that can be applied that range from physical examinations, radiographic imaging tests and biopsies (Wang, 2017).

Breast cancer self-diagnosis can be undertaken by the individual through regular physical breast self-examination (BSE) (Shah *et al.,* 2014). Regular and consistent BSE encourages women to take the initiative with regard to their personal healthcare. If done regularly enough, the individual becomes accustomed to their normal breast anatomy. This allows them to be able to detect and report any anatomical inconsistencies such as change in size, lumps, sensitive foci or changes in skin colour (Ahmed *et al.,* 2018, Henderson and Ferguson, 2019). The reported inconsistencies can then be clinically investigated by professionals utilising more predictable and accurate diagnostic methods (Board, 2014).

.

Breast mammography is the standard method applied in breast cancer screening. It is a radiographic diagnostic method used for early diagnosis (Gøtzsche and Jørgensen, 2013, Keen and Keen, 2009, Løberg *et al.,* 2015). A mammogram is an X-ray image of the breast by which clinicians can identify breast tissue masses or microcalcifications at an early, curable stage (Løberg *et al.,* 2015, Naseem *et al.,* 2015). Microcalcifications are calcium mineral deposits, which indicate the presence of benign cysts and can indicate early presence of breast cancer (Bailey *et al.,* 2005, Karssemeijer *et al.,* 2012).

Another method used in breast cancer diagnosis is magnetic resonance imaging (MRI). This method displays higher diagnostic sensitivity for cancer detection, especially in high-risk women (Knisely *et al.,* 2020). High risk women include women with prior breast augmentation, prior therapeutic chest radiation, women with dense breast tissue and those with a 20-25% risk of breast cancer development (Knisely *et al.,* 2020, Shah *et al.,* 2014). It is nonetheless inferior in specificity when compared to mammography (Menezes *et al.,* 2014). As a result, women showing average risk do not benefit from MRI screening (Radhakrishna *et al.,* 2018). Alternatively, it is used mostly as a supplementary method for mammography and ultrasound to measure tumour size and localise other tumours within the breast (Radhakrishna *et al.,* 2018).

Whole breast ultrasound is used when mammography fails to confidently identify breast tumours from benign lesions (Madjar, 2010, Thigpen *et al.,* 2018). Dense breast tissue and

tumour lesions both appear lighter when imaged using mammography hence the adjunctive option of whole breast ultrasound diagnosis (Madjar, 2010, Thigpen *et al.,* 2018). Ultrasound leverages the echoic differences in tissue density to improve cancer detection in women with dense breasts. Dense tissue is echogenic whilst cancerous tissue is hypoechoic, allowing a contrast to be observed in ultrasound diagnostic imaging (Madjar, 2010, Thigpen *et al.,* 2018).

The remaining common method applied in breast cancer diagnosis is a breast tissue biopsy (Nounou *et al.,* 2015). Cells or tissue samples are removed from a lump or suspicious area of the breast and histologically assessed for any signs of cancer (Board, 2019, Nounou *et al.,* 2015).There are different types of biopsies that are used in breast cancer diagnosis namely, fine needle aspiration cytology (FNAC) and core needle biopsy (CNB). Of the two, FNAC is quicker and less invasive (Nounou *et al.,* 2015). Despite concerns regarding their invasive nature, breast tissue biopsies remain the most definitive and accurate method in breast cancer diagnosis (Nounou *et al.,* 2015).

1.1.5 Challenges in breast cancer diagnosis

Over diagnosis, false-positives and false-negatives are of particular concern when considering breast cancer diagnosis. Over diagnosis is defined as “the detection of tumours at screening that might never have progressed to become symptomatic or life-threatening in the absence of screening” (Løberg *et al.,* 2015). The harm associated with radiation exposure from mammographic screening is not negligible. For women aged between 40 and 59 who undergo annual screening, the estimated radiation-induced mortality rate ranges from 2/100 000 to 11/100 000 (Houssami, 2017). Mammography still plays a non-substitutable role is reducing breast cancer death through early diagnosis, however, over diagnosis is a silent risk that deserves attention (Houssami, 2017). Breast tissue biopsies cannot be done in patients on anticoagulant medication or those with bleeding disorders. Moreover there are concerns of infection, bruising and pain (Nounou *et al.,* 2015).

False-positive diagnosis occur when individuals are clinically diagnosed with breast cancer, but thereafter, mandatory follow-up screening discloses no signs of breast cancer (Seely and Alhassan, 2018). Both mammography and MRI screening have been shown to have a noteworthy rate of false-positives. Most of the false positives are resolved in follow up screenings but they cause needless anxiety and depressive feelings in patients (Seely and

Alhassan, 2018). False-negatives occur when mammography is unsuccessful in tumour localisation and detection. They occur mostly in pre-menopausal women as they have denser breast tissue, which challenges the ability of mammography to diagnose breast cancer (Seely and Alhassan, 2018). If diagnosis is delayed by mammographic false negatives, the outcome of treatment may be negatively affected. This effect is counterproductive as the goal of breast cancer screening is early diagnosis to achieve better treatment outcomes (Brewer *et al.,* 2007, Wang, 2017).

In an attempt to mitigate the different disadvantages of each diagnostic method while simultaneously exploiting their individual advantages, combination screening techniques are used. A triple test consisting of clinical breast examinations, breast imaging and tissue biopsies is used (Nounou *et al.,* 2015). The result is 100% sensitivity and selectivity (Kharkwal and Sameer, 2014). Unfortunately, this benefit is experienced by only those who can afford the financial costs. Patients in developing countries often cannot afford triple tests (Kharkwal and Sameer, 2014). As a result, research addressing the mandate to develop accurate, efficient, and cost-effective diagnostic methods remains pertinent.

1.1.6 Breast cancer treatment

The next step following positive diagnosis is the development of a management and treatment regimen that is aimed at complete cancer remission (Board, 2019, Hyatt, 2009). Before treatment is initiated, certain factors such as the age of the patient, patient health status and presence of co-morbidities have to be considered (Board, 2014, Siegel *et al.,* 2016). Additionally, the tumour should be tested to determine the type of breast cancer, the recurrence capacity, the cancer stage, metastasis potential and the molecular subtype as well as any prior treatment (Board, 2019, Morimoto *et al.,* 2010). These factors have an influence on treatment options and prognosis and should be addressed before any treatment strategy is undertaken (Board, 2019, Morimoto *et al.,* 2010).

Breast cancer treatment could incorporate neoadjuvant chemotherapy, surgery, radiation, chemotherapy and endocrine therapy. Depending on the diagnosis, any one of these or a combination may be appropriate to address the therapeutic demands (Board, 2014). Surgery alone is mostly used to achieve local control and prevent metastasis. Partial or total mastectomy may be performed depending on the stage of the cancer (Alkabban and Ferguson, 2019). Radiation therapy is usually applied postoperatively (Board, 2020a).

Adjuvant radiation therapy addresses recurrence, eliminating the residual tumour deposits that can pioneer late-stage recurrence (Alkabban and Ferguson, 2019). However, radiation cannot be used in patients over 70 years of age or in hormone positive cancers. In these cases radiation has not been shown to significantly improve survival (Alkabban and Ferguson, 2019, Board, 2020a). Radiation can also be used palliatively, to reduce pain associated with bone metastasis in breast cancer (Board, 2020a).

Chemotherapy involves the use of cytotoxic or cytostatic chemical drugs either to kill or stop cancer cell growth respectively (Board, 2020a). Antimetabolites such methotrexate and 5-flourouracil deprive cancer cells of crucial DNA precursors, inhibiting cancer cell propagation. Anthracycline antibiotics such as doxorubicin and taxanes such as paclitaxel are also commonly used (Alkabban and Ferguson, 2019). The latter drugs achieve the same cytotoxic and cytostatic effects but the treatment regimen uses combinations based on cancer stage and disease progression (Anampa *et al.,* 2015).

Endocrine therapy utilises agents which block hormone receptors to stop cancer growth in hormone receptor positive cancer (Board, 2020a). Agents such as tamoxifen realise their antiproliferative effects through competitively inhibiting oestrogens. Tamoxifen is used both in localised and metastatic breast cancer (Board, 2020a). Post-surgery adjuvant therapy with tamoxifen has been shown to reduce the recurrence rate by close to half in the first 10 years and reduce treated breast cancer mortality by about 30% (Alkabban and Ferguson, 2019, Anampa *et al.,* 2015, Board, 2020a).

Targeted therapy is indicated for breast cancers which overexpress HER-2 (Dieci *et al.,* 2019). Trastuzumab is a monoclonal antibody that directly targets HER-2 receptors (Alkabban and Ferguson, 2019). Other targeted therapies include cyclin dependent kinase (CDK) inhibitors, poly-ADP ribose polymerase (PARP) inhibitors and mammalian target of rapamycin (mTOR) inhibitors (Board, 2020a). Targeted therapy is usually combined with chemotherapy. Combination of trastuzumab and chemotherapy has been reported to result in a 52% and 33% reduction in recurrence and death respectively in HER-2 positive breast cancer if early treatment is initiated (Alkabban and Ferguson, 2019).

Whilst the different treatment strategies may be effective in eliminating cancerous cells, the pernicious effects to the surrounding healthy cells cannot be ignored (Pearce *et al.,* 2017). Physical side effects include but aren't limited to; infection, radiation pneumonitis, nausea, vomiting, alopecia, myelosuppression, pain, heart failure, infection and premature menopause. More concerning is the development of secondary cancers such as leukaemia's, sarcomas and lung cancer in non-smokers (Board, 2020a, Pearce *et al.,* 2017). Over and above the side effect profile, depressive states are commonly seen in patients during chemotherapy (Pearce *et al.,* 2017). Occurrence of depression in cancer patients is three times higher compared to healthy individuals (Smith, 2015). The result of this anxiety is a decreased quality of life, suicide, poorer treatment outcomes and higher rates of mortality. Depressed patients also stay in hospital longer, increasing their health expenditure and the overall cost of treatment (Smith, 2015). This is the same cost which already presents an access barrier for a majority of patients in southern Africa (Wild *et al.,* 2020).

1.2 Prostate cancer

Prostate cancer is akin to breast cancer in that it is a hormone-driven cancer. It is an adenocarcinoma which is driven principally by androgen receptor (AR) stimulation for proliferation (Tan *et al.,* 2015). The glandular function of the prostate is mediated by androgens, mainly testosterone and dihydrotestosterone (DHT). Under oncogenic conditions, the AR develops autonomous activation, which in turn promotes the survival and growth of the prostate cells through binding of these androgens (Robinson *et al.,* 2015). During 2018, an estimated 1.2 million individuals were diagnosed with prostate cancer globally, resulting in a mortality burden of 359 000 (Figure 1.1) (Bray *et al.,* 2018, Cooperberg and Chan, 2017). It is the leading cause of cancer death in men in over 46 countries particularly countries in sub-Saharan Africa and the Caribbean (Bray *et al.,* 2018). The highest incidence rates are observed in Australia and Europe however the highest mortality rates are seen in Benin, South Africa, Zambia, Zimbabwe, Barbados, Jamaica and Haiti. This disparity is partly due to limited access to early screening and therapy for the latter (Bray *et al.,* 2018).

There are four conventional methods in prostate cancer diagnosis: the physical digital rectal exam (DRE), the prostate specific antigen (PSA) blood level test, trans-rectal ultrasound (TRUS), and prostatic tissue biopsy (Descotes, 2019). Each method varies in specificity and sensitivity (Board, 2020b). Prostate cancer can only be confidently confirmed by a combination of a TRUS and prostate needle biopsy (Eastham, 2017). Typically, DRE and

PSA results are used as precursors for further testing using the more reliable TRUS imaging and prostate biopsy (Board, 2020b, Eastham, 2017). Gleason scores ranging from 2 to 10 are assigned to measure the extent of metastasis. The higher the Gleason score the greater the metastasis risk (Board, 2020b). Unfortunately, the diagnostic challenges experienced in breast cancer stretch to prostate cancer diagnosis. Positive DRE and PSA level blood test results can be indicative of benign prostate hyperplasia and not necessarily prostate carcinoma (Prcic *et al.,* 2016). Correspondingly, some reported side effects of TRUS include haematuria, haematospermia, rectal bleeding and infection (Efesoy *et al.,* 2013, Huang *et al.,* 2019). As a consequence, the research mandate aimed at development of superior diagnostic methods persists.

Equally, factors such as age, health status, recurrence capacity and extent of metastasis should be deliberated before any therapeutic strategy is undertaken in prostate cancer (Board, 2020b). Different therapeutic strategies can be applied in prostate cancer. A unique approach in prostate cancer therapy is the active surveillance strategy (Board, 2020b). It is reserved solely for localised prostate cancer (Board, 2020b). In active surveillance, the patient is not given treatment but disease progression is monitored. If the cancer starts progressing, treatment is given to cure the cancer (Board, 2020b, Stephen *et al.,* 2020). Surgery, radiation, endocrine therapy and chemotherapy remain the conventional options in prostate cancer therapy (Stephen *et al.,* 2020, Board, 2020b). The side effects of these therapeutic strategies include, impotence, shortening of penis, pain, infection and depression amongst others (Board, 2020b). Once again, the pernicious effects of these conventional treatment approaches cannot be evaded, even in prostate cancer treatment. As a result, the research mandate extends further for development of better diagnostic and therapeutic alternatives. Alternative approaches must fewer false positive or negative results, have improved side effect profiles and must be considered.

1.3 Radiopharmaceuticals

Radiopharmaceuticals are pharmacological ligands that have accompanying radioactivity (Sgouros, 2019). They are introduced in sub-pharmacological or pharmacological doses for quantitative assessment of physiologic parameters and therapeutic intervention (Munjal and Gupta, 2020). Radiopharmaceutical targeting exploits the nature of carcinomas to up-regulate the expression of certain proteins and metabolism of growth molecules (Kapoor and Kasi, 2020). After administration these radiotracer can interact with these up-regulated cellular targets; thus may accumulate at the tumour site (Figure 1.4) (Capitanio *et al.,* 2016).

Through this metabolic trapping principle, the diagnostic and therapeutic applications of radiopharmaceuticals are realised (Du and Dizdarevic, 2017, Kapoor and Kasi, 2020). Radiopharmaceutical targeting has been acknowledged as a highly promising, safe, effective and economically viable therapeutic modality in oncology (Sgouros *et al.,* 2020). Radiopharmaceutical diagnosis can be achieved through nuclear imaging procedures, particularly positron emission technology (PET) (Kapoor and Kasi, 2020).

1.3.1 Nuclear diagnostics - Positron emission tomography

PET is a nuclear medicine technique for *in vivo* quantitative measurement of physiologic parameters (Saha, 2015). A radiotracer is administered and images are acquired using a sensitive camera that is capable of detecting the radioactivity emanating from the patient (Kapoor and Kasi, 2020). This technique has found great success in medical diagnostics for assessing disease progression non-invasively. The method provides high molecular specificity and allows for use of biologics in a manner that doesn't modify their functionality (Saha, 2015).

A positron is the antiparticle of an electron. It has the same mass but differs in charge (Singh, 2016). The functioning of PET is through the emission of a positron from a positron emitting radionuclide that has kinetic energy. The energy is lost due to collisions with other electrons in the surrounding tissue. The loss of energy through radioactive decay, results in the combination of the positron and electron (Saha, 2015). When an electron and positron collide, they annihilate and their mass is converted into energy. The energy is emitted as two 511-keV photons travelling in opposite directions, producing gamma-radiation (Figure 1.4) (Saha, 2015, Singh, 2016). A pair of scintillation detectors coupled to photomultiplier tubes (PMT) detect positron emission by measuring the two photons in coincidence (Saha, 2015). Using the PMT, the photons are converted into an electrical pulse. The electrical pulses can be amplified and processed to provide information regarding the intensity and the nature of the radiation (Saha, 2015). The coincidental emission of the photons is the basis for detection and localisation in PET. The detectors move at 180° to each other opposite the source of the positron emission source in a circular arrangement (Dahlbom, 2017, Saha, 2015). This allows for radiation to be measured from different angles and distances. The information gathered is used to generate tomographic images that localise the regions of radioactivity at high spatial resolution (Figure1.5) (Dahlbom, 2017, Saha, 2015). The advantage of PET scans over conventional diagnostic methods is that they appear to be more accurate (Liu *et al.,* 2017, Stephen *et al.,* 2020) allowing for anatomical diagnostics (when combined with CT or MRI) while eliciting cellular, molecular and biochemical properties of targeted neoplasms (Liu *et al.,* 2017, Vercher-Conejero *et al.,* 2015).

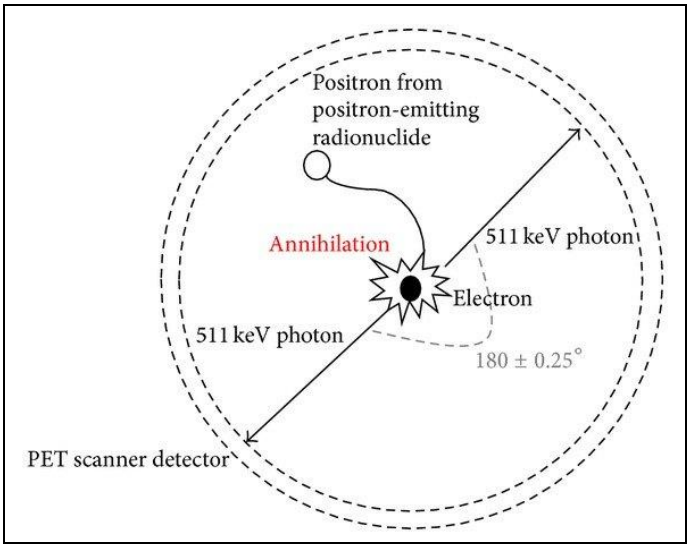

Figure 1-4 Diagrammatic depiction of the layout of the opposing detectors of a typical PET system (Kong et al., 2013). (Used with permission)

Nowadays, due to the selectivity and specificity of certain radiotracers, a large contrast between untargeted tissue and targeted pathologic tissue may be achieved. The resultant high signal-to-noise ratios addressing concerns with respect to false-negative findings (Figure 1.5) (Vercher-Conejero *et al.,* 2015). Given these advantages there is a growing development and interest for radiopharmaceutical therapeutics.

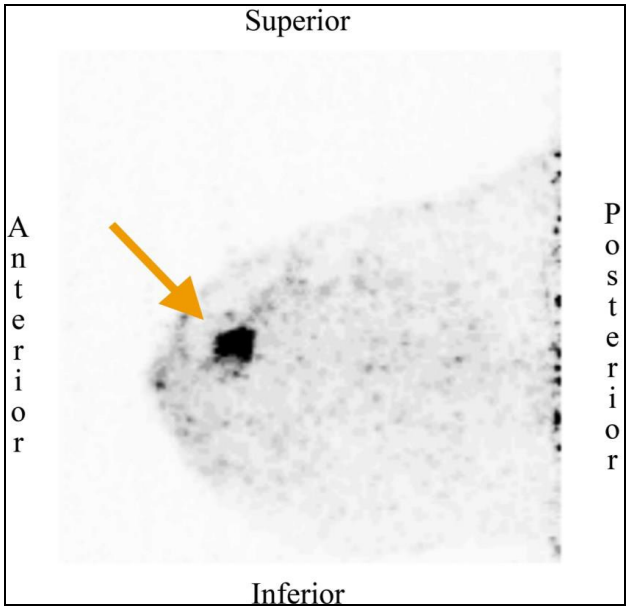

Figure 1-5 Breast PET scan showing a focus of intense radioligand uptake (orange arrow) in the upper inner quadrant of the right breast proven to be a breast carcinoma (Vercher-Conejero et al., 2015). (Used with permission)

1.3.2 Nuclear therapeutics - Theranostics

Theranostics is defined as “the integration of two modalities, being, clinical therapy and medical imaging into a single package material for overcoming the undesirable variations in therapeutic efficacy and biodistribution” (Ding and Wu, 2012, Turner, 2018). The goal of theranostics exceeds simple disease identification and treatment. The concept is based on the long term ability to identify and monitor disease progression, assess drug delivery kinetics and drug efficacy as well as the possibility to influence therapy down to small cell masses at an individual patient level (Kelkar and Reineke, 2011). Taking the varying pharmacogenetic profiles of the population into consideration, integration of nuclear medicine and pharmacology in the form of theranostics is a step in the direction toward personalised medicine. Various approaches such as the metabolic trapping principle can be applied to radioligand products carrying suitable radionuclides to induce localised cytotoxic therapeutic effects (Du and Dizdarevic, 2017). Simultaneous nuclear imaging is achieved by using compounds carrying radionuclides that have low energy gamma or positron emission and that have short decay half-lives (Nairne *et al.,* 2015). Radiation deriving from positrons or gamma rays can therefore penetrate tissue easily allowing accurate tumour localisation deep within the body (Donya *et al.,* 2015). The radionuclides used for targeted antitumoural therapy need to emit radiation with higher energy ranges over a short path length. This is so that the energy is locally deposited to minimise whole-body irradiation (Hyatt, 2009, Kramer-Marek and Capala, 2012); hence, beta emitters are commonly used as radiotherapeutics. They have a penetration path length of 0.8–5.0 mm and low linear energy transfer (LET) of roughly 0.2 keV/μm (Kramer-Marek and Capala, 2012). This path length may also result in targeting non-cancerous cells surrounding the tumour, sometimes causing unwanted nonspecific cell toxicity (Kramer-Marek and Capala, 2012, Hyatt, 2009). Notwithstanding the aforementioned concern, beta emitting radioligands can be effectively used in treating poorly perfused and bulky tumours; however be less appropriate for targeting small metastases (Kramer-Marek and Capala, 2012). Alternately, alpha particles have a higher energy of 4–9 MeV (Figure 1.6) but travel over short distances in tissue, typically between 40–100 μm (Kramer-Marek and Capala, 2012, Hyatt, 2009). This characteristic circumvents the cross-firing effect exhibited by beta-emitting radionuclides. Moreover, they could possibly address the target specificity shortfalls exhibited by conventional chemotherapeutics. Due to alpha particles higher energy, they may be able to realise higher biological efficacy compared to beta emitters (Kramer-Marek and Capala, 2012). Studies still in progress have shown highly effective and specific tumour cell killing in cell culture and clinical models (Shinohara *et al.,* 2018, Ku *et al.,* 2019). .

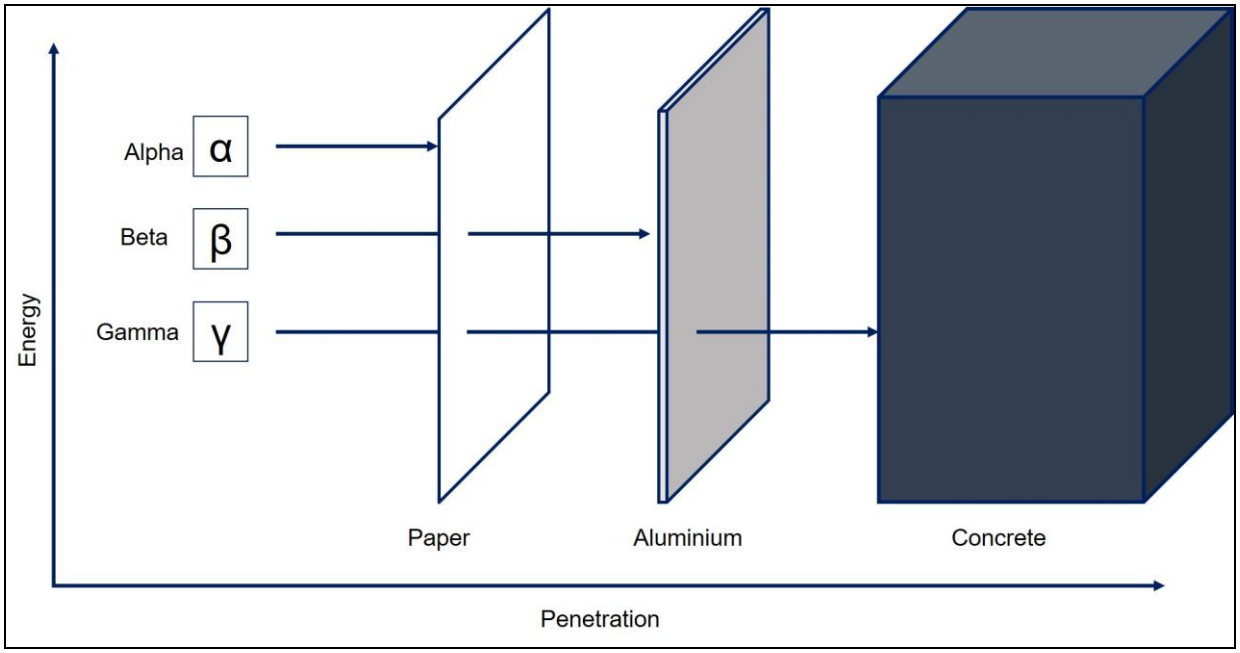

Figure 1-6 Energy and penetration properties of alpha, beta and gamma rays. (Image formulated utilising Microsoft PowerPoint®)

The potential of radiotherapeutics in oncology presents too valuable an opportunity not to investigate. Due diligence demands rigorous and critical scientific investigations to reveal the full clinical possibilities of radiotherapeutics. Even more promising is the development of radiopharmaceuticals that combine diagnosis and therapy (Du and Dizdarevic, 2017). This indication that synchronous diagnosis and therapy is a feasible clinical outcome in our lifetime has become a prevailing idea in radiopharmaceutical research, particularly in the oncology (Kalash *et al.,* 2016). For example, prostate cancer has realised some success in theranostics by targeting the overexpressed prostate specific membrane antigen (PSMA) which has shown to be an excellent target for theranostic radiopharmaceuticals (Bouchelouche and Choyke, 2016).

1.4 Prostate specific membrane antigen (PSMA)

As the search for predictive diagnostic and therapeutic biomarkers continues, one of the promising targets evaluated is PSMA. It has realised extensive application in prostate carcinoma theranostics (Flores *et al.,* 2017). This antigen is an extensively studied 80-100 kDa type II membrane protein consisting of an extracellular C-terminal region, a cytoplasmic N-terminal domain and a helical transmembrane region (Figure 1-7) (Ristau *et al.,* 2014, Sathekge *et al.,* 2017). The extracellular portion makes up the bulk of the protein structure

and is subdivided into three domains, namely; the protease/catalytic domain, the apical domain and the C-terminal or dimerization domain. These three domains together accomplish PSMA's substrate binding function (Evans *et al.,* 2016). The extracellular binding domain forms an active dimer binding two zinc ions (Zn^{2+}). There are two separate binding pockets, the glutamate-sensing pocket and a non-pharmacophore pocket (Foss *et al.,* 2012)

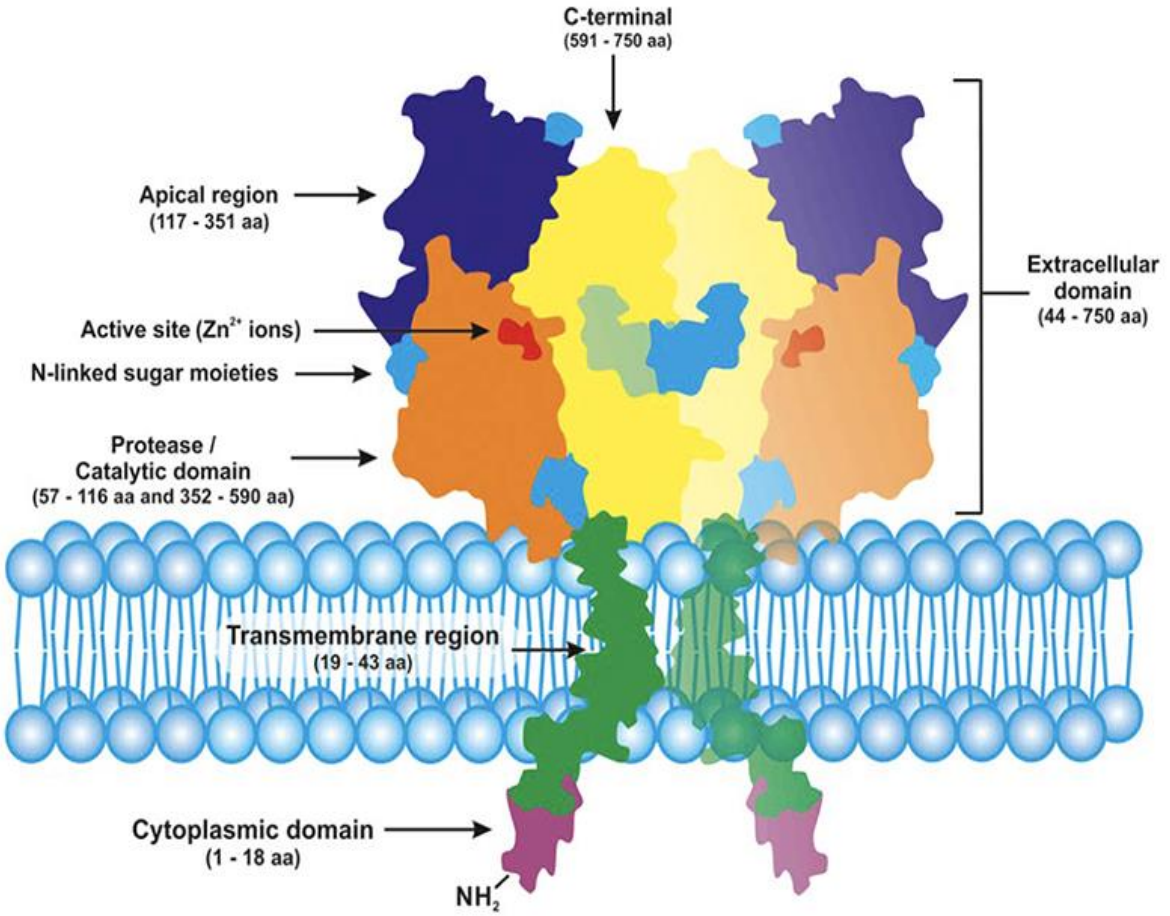

Figure 1-7 PSMA receptor structure (Evans et al., 2016). (Used with permission)

Presently, four sites have been confirmed as exhibiting PSMA expression under healthy physiologic conditions. It is predominantly expressed by prostate cells, but other tissue sites include the proximal tubules of the kidney, glial cells in the central nervous system (CNS) and the jejunal brush border of the small gastrointestinal tract (Ristau *et al.,* 2014).

1.4.1 PSMA and prostate cancer

When compared to healthy prostatic tissue, PSMA expression is 100-1000 fold greater within carcinoma cells derived from the prostrate (Udovicich *et al.,* 2017). An increase in prostatic tumour cell aggression correlates to an increased PSMA expression (Chen *et al.,* 2017). Likewise, expression increases from non-cancerous prostatic tissue to benign epithelial tissue to high-grade intraepithelial neoplasia and finally malignant cells (Hupe *et al.,* 2018). The association between PSMA expression and prostate cancer progression provides a foundation to clinically make use of PSMA in prostatic cancer imaging diagnosis and therapy (Chen *et al.,* 2017).

1.4.2 PSMA function

PSMA function appears to be dependent on the site of expression (Murray *et al.,* 2014). In the CNS the function is defined and less argued. It is reported to function in the hydrolysis of N-acetyl aspartylglutamate (NAAG) into glutamate and N-acetylaspartate (Evans *et al.,* 2016, O'Keefe *et al.,* 2018). This increases neuronal glutamate levels and inhibits growth factor β secretion by astrocytes (Evans *et al.,* 2016). In the jejunal brush border, PSMA acts as a folate hydrolase, assisting in folate absorption and transportation into the systemic circulation. Through cleavage of the C-terminal glutamates of dietary folate, PSMA permits enteral folate absorption (Evans *et al.,* 2016, Ristau *et al.,* 2014). In the kidney the PSMA function is not clear, although it has been proposed to function in reuptake of excreted folate (O'Keefe *et al.,* 2018, Ristau *et al.,* 2014). Elevated PSMA expression in prostatic carcinoma results in an increased ability to process folate (Evans *et al.,* 2016) within the cancer cells. Folic acid is an endogenous PSMA-targeting ligand through which significant theranostic progression has been realised (Emmett *et al.,* 2017). Its enzymatic activity has been shown to hydrolyse polyglutamated folates into folate and glutamates (Evans *et al.,* 2016). This highlights the association of PSMA and folate. Moreover, when considering the generally reported role of folate in cancer, the increase in PSMA expression from non-cancerous to cancerous tissue is validated (O'Keefe *et al.,* 2018).

1.4.3 Folate

Folates are large molecules classified as one of the B vitamins that are obtained through dietary sources (Ducker and Rabinowitz, 2017, Zheng and Cantley, 2019). Folic acid is a synthetic folate whose biologically active derivative, tetrahydrofolate (THF) functions as a cofactor in amino acid and nucleotide metabolic reactions (Ducker and Rabinowitz, 2017). The main cellular role of folates is found in one carbon metabolism (Ducker and Rabinowitz,

2017, Zheng and Cantley, 2019). One carbon metabolism, supported by folate, mediates DNA synthesis through biosynthesis of purines, pyrimidines and especially thymidine. Folate one carbon metabolism is furthermore involved in amino acid homeostasis of serine, glycine and methionine (Ducker and Rabinowitz, 2017, Zheng and Cantley, 2019).

1.4.4 Folate and one carbon metabolism

Under healthy physiological conditions, folate is obtained through dietary sources. Once in the body, it can be transported into cells or enters the cells by diffusion. In the cell it is transported to its mitochondrial and cytosolic metabolic targets through vesicular endocytosis or in a reduced monoglutamyl conformation (Zheng *et al.,* 2018, Zheng and Cantley, 2019). Polyglutamated folate cannot be utilised by cells. For this reason, polyglutamated folate hydrolysis to monoglutamyl folate by PSMA is essential for cellular use (Flores *et al.,* 2017). In the cell, folate is converted into dihydrofolate (DHF) by dihydrofolate reductase (DHFR) using nicotinamide adenine dinucleotide phosphate (NADPH) oxidation to NADP+. Through a second NADPH oxidation reaction, DHFR converts DHF to THF, the biologically active folate derivative (Figure 1.8) (Zheng and Cantley, 2019).

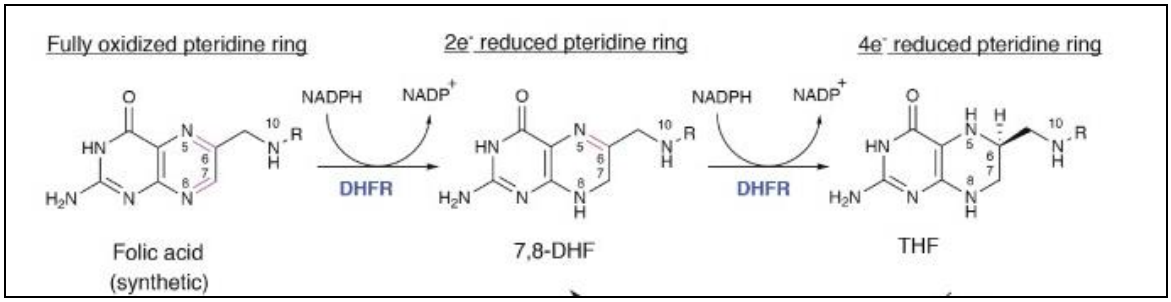

Figure 1-8 Folic acid conversion into tetrahydrofolate (THF) through nicotinamide adenine dinucleotide phosphate (NADPH) oxidation and dihydrofolate reductase, R = para-aminobenzoate-glutamate (DHFR) (Zheng and Cantley, 2019). (Used with permission)

Depending on the requirement of the cell, THF can go through different chemical transformations mediated by its ability to accept one carbon (1C) units (Ducker and Rabinowitz, 2017). The 1C units are covalently bound to the 5-position nitrogen atom on the pteridine ring of THF. Parallel cytosolic and mitochondrial pathways use folate mediated 1C metabolism (Figure 1.9). In the mitochondria and the cytosol, serine hydroxyl methyl transferase (SHMT) simultaneously converts THF into 5,10-methylene-THF through donation of methyl and hydroxyl groups. At the same time, glycine is synthesised from serine in a reversible reaction (Ducker and Rabinowitz, 2017, Zheng and Cantley, 2019). The mitochondrial 1C pathways produce more glycine compared to the cytosolic pathway (Zheng

and Cantley, 2019). Additionally, in a 5,10-methylene-THF dependent reaction, thymidylate synthase (TYMS) converts deoxyuridine monophosphate (dUMP) to deoxythymidine monophosphate (dTMP). The dTMP produced is essential for DNA biosynthesis.(Ducker and Rabinowitz, 2017)

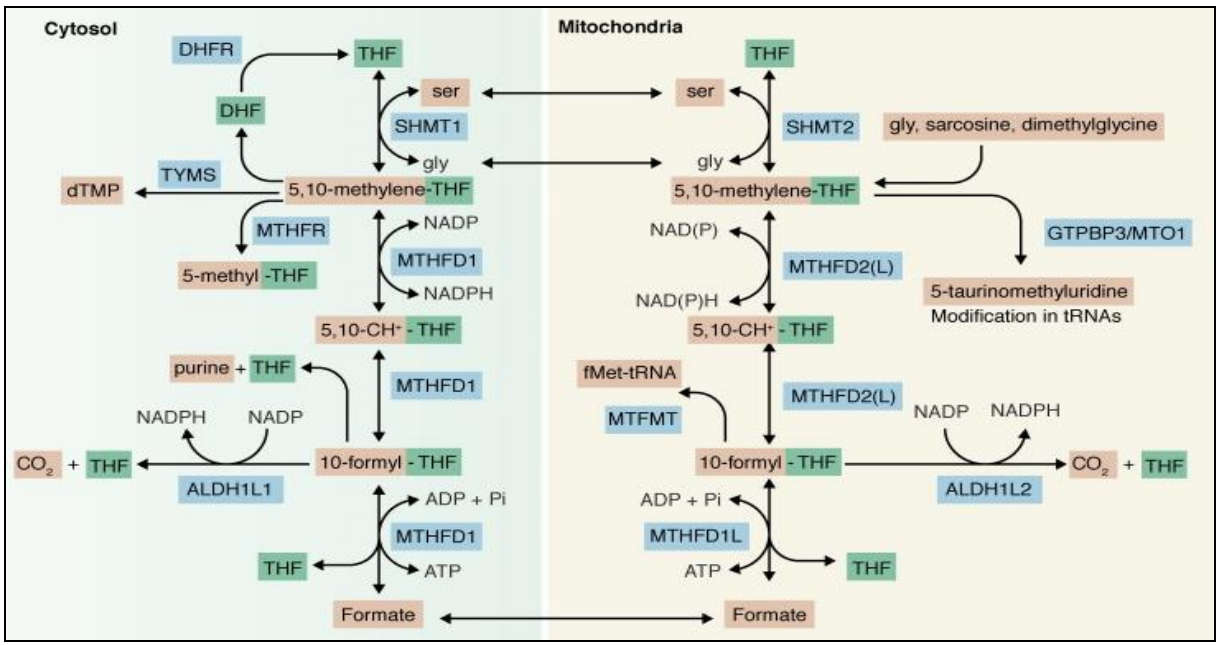

Figure 1-9 Folate 1C metabolism pathways in the cytosol and mitochondria (Zheng and Cantley, 2019). (Used with permission). Blue highlights indicate enzymes, pink highlights indicate chemical cofactors and green highlights indicated folate associated metabolites.

In the cytosol, methylene tetrahydrofolate reductase (MTHFR) through NADPH, produces 5-methyl-THF from 5,10-methylene-THF (Ducker and Rabinowitz, 2017). The produced 5-methyl-THF is used for methylation of homocysteine to form methionine (Ducker and Rabinowitz, 2017). Methionine is a substrate for S-adenosylmethionine synthase (SAM), an important co-factor in sulphur metabolism and creatine synthesis. Finally, methylene tetrahydrofolate dehydrogenase 2/Like (MTHFD2/L) oxidises 5,10-methylene-THF in the mitochondria to form 10-formyl-THF. The formed 10-formyl-THF is hydrolysed into formate by methylene tetrahydrofolate dehydrogenase 1/L (MTHFD1/L) (Ducker and Rabinowitz, 2017, Meiser *et al.,* 2016). Formate connects the mitochondrial and cytosolic folate 1C metabolism pathways. Mitochondrial 1C pathways produce formate, which is in turn used by the cytosolic pathway for purine synthesis (Ducker and Rabinowitz, 2017, Zheng and Cantley, 2019).

1.4.5 Folate, PSMA and prostate cancer

For most cancers, once a cell has transformed from healthy to neoplastic, folate depletion rapidly slows tumour growth (Rycyna *et al.,* 2013). This is the motivation why folate antimetabolites have been used successfully in cancer therapy. Methotrexate (MTX) is a folic acid antagonist that inhibits DHFR. It is used as a chemotherapeutic agent in several cancers (Hannoodee and Mittal, 2020). 5-flouro-uracil (5-FU) is a potent inhibitor of TYMS, targeting synthesis of nucleotides required by the folate 1C pathway, consequently inhibiting cancer progression (Casale and Crane, 2019).

Interestingly, folate has been shown to control the expression of PSMA *in vitro*. Cells that express PSMA exhibited a two-fold increase in folate uptake in contrast to PSMA-negative cells (O'Keefe *et al.,* 2018, Yao and Bacich, 2006). For this reason, PSMA has been implicated in folate uptake and transport in prostatic tissue. The official name of the *PSMA* gene product is folate hydrolase 1 (FOLH1) (O'Keefe *et al.,* 2018). As a folate hydrolase, it is understood to play a role in cell survival and proliferation through folate ligand binding (Emmett *et al.,* 2017). The overexpression of PSMA in prostrate carcinoma cells and its association with folate binding provides premise for its application in prostate cancer nuclear theranostics.

1.4.6 PSMA targeting radiopharmaceuticals

Before a radiopharmaceutical can be successfully used, its biological target should meet specific requirements (Lee *et al.,* 2019). The target should be abundantly expressed and accessible to radiopharmaceuticals for adequate target binding. Its expression characteristics should be stable to allow for a reliable use. Targets should ideally be located within the cells to avoid rapid clearance of the radiopharmaceutical from the blood. The target should also be tissue and cell type specific. Advantageously, PSMA meets the ideal requirements for radiopharmaceutical targeting. (Jadvar and Ballas, 2018)

As PSMA is a receptor, it can be targeted by use of a ligand or inhibitor. The inhibitor structure mimics NAAG and following binding to PSMA, metabolism stops (Kiess *et al.,* 2015). Urea-based inhibitors, such as Glu-urea-Lys (Glu-NH-CONH-Lys (Ahx)) are low-molecular-weight peptidomimetics used to target PSMA (Eder *et al.,* 2012). Phosphate-based inhibitors and thiol-based inhibitors can also be used as PSMA inhibitors but urea-based inhibitors show the highest affinity for PSMA (Barinka *et al.,* 2012). Traditionally, radiolabelled antibodies against PSMA were used to target the protein. However, due to their large size, extended circulation times adding to background signal and poor tissue

penetration of antibodies, small peptides have become the preferred alternative (Banerjee *et al.,* 2010). In comparison to antibodies, peptide inhibitors are smaller, more agile in tissues and they accumulate rapidly in tumours resulting in higher tumour-absorbed doses (Violet and Hofman, 2017). They clear quickly from the circulation limiting toxicity and significantly reduce background radioactivity (Violet and Hofman, 2017).

Metal ion chelators are required for radiopharmaceutical stability under physiological conditions (Nairne *et al.,* 2015). If the radionuclide (like lutetium-177 or gallium-68) is not incorporated fully into the chelator, the biodistribution of released isotope can lead to the imaging artefacts that complicate interpretation. Chelators such as N,N′-bis[2-hydroxy-5-(carboxyethyl)benzyl] ethylenediamine-N,N′-diacetic acid (HBED-CC) and dodecane tetraacetic acid (DOTA), are used for gallium-68 chelation and provide high stability *in vivo* (Eder *et al.,* 2014, Nairne *et al.,* 2015). The conjugation of the metal chelator HBED-CC to the PSMA peptide inhibitor, Glu-NH-CO-NH-Lys (Ahx) is radiolabelled with gallium-68 (Figure 1.10) (Banerjee *et al.,* 2010, Eder *et al.,* 2014).

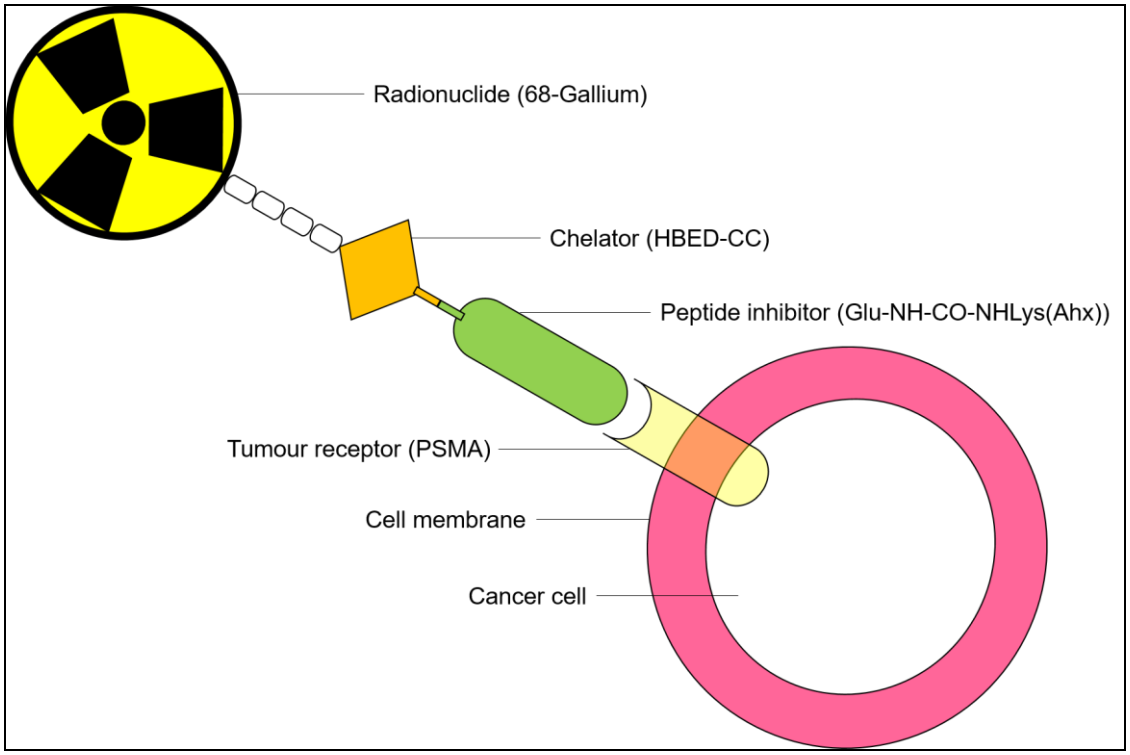

Figure 1-10 [68Ga] Ga-PSMA-11 labelling with metal chelator and peptide inhibitor. (Image formulated utilising Microsoft PowerPoint®)

1.4.7 PSMA based theranostics

New radiotracers that are efficient at targeting PSMA are being developed using isotopes such as gallium-68. Gallium-68 has shown high diagnostic efficacy (Raval *et al.,* 2016). Due to selective and stable targeting of PSMA, it is possible to detect metastasis within lymph nodes, an important marker of cancer progression in both prostate and breast cancers (Raval *et al.,* 2016). Rapid and efficient methods for labelling PSMA ligands with gallium-68 have been developed, particularly for use in PET and single photon emission computed tomography (SPECT) imaging (Sathekge *et al.,* 2017). The PSMA inhibitor, PSMA-11, labelled with gallium-68 and used in PET imaging was shown to be more accurate for the detection of recurrent prostate carcinoma compared to conventional imaging modalities (Sathekge *et al.,* 2017). Furthermore, [^{68}Ga]Ga-PSMA-11 shows superior early detection rates of recurrence and metastases (Roach *et al.,* 2018).

The use of [^{68}Ga]Ga-PSMA-11 in prostate cancer diagnosis has culminated in [^{68}Ga]Ga-PSMA-11 positron emission tomography/computed tomography (PET/CT) imaging being universally viewed as the new gold standard for imaging and for staging of recurrent prostate cancer (Lenzo *et al.,* 2018). Its effectiveness in PET imaging has led to the development of rapid bench-top preparation kits for easy preparation of the labelled ligand. These kits are capable of providing high-yield, high-purity and rapid labelling of the PSMA-11 at room temperature. This method does not require expensive automated synthetic systems, with kits presently being used in imaging centres in France and Australia (Lenzo *et al.,* 2018). This cost-shedding ingenuity aligns to the idea of developing cost-considerate alternatives in cancer diagnosis and therapy.

In recent years, [^{68}Ga]Ga-PSMA-11 PET/CT has been used theranostically to guide therapy using the labelled therapeutic radiopharmaceutical [^{177}Lu]Lu-PSMA-617 (Lenzo *et al.,* 2018, Turner, 2018). Phase 2 theranostic clinical trial studies using 68-Gallium/177-Lutetium-PSMA have shown promising results especially in castration-resistant metastatic prostate cancer (Figure 1.11) (Turner, 2018). The favourable physical properties of Lutetium-177 have made it desirable for therapy as it has a short range of emission and is completely excreted within 48 hours following administration via the renal route (Emmett *et al.,* 2017). At the same time, gallium-68 exhibits positron emission, making it ideal for nuclear imaging (Lenzo *et al.,* 2018).

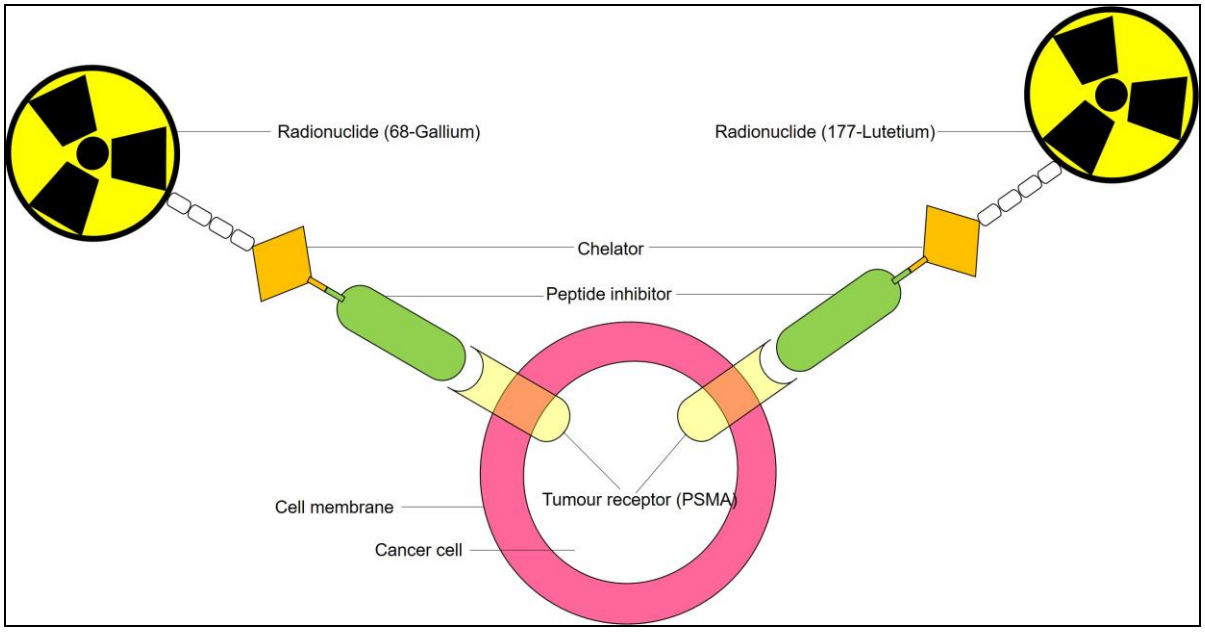

Figure 1-11 A diagram of a combined 68-Gallium/177-Lutetium-PSMA-11 used in tandem for prostate cancer theranostics. (Image formulated utilising Microsoft PowerPoint®)

Theranostics is an emerging field that is progressing at a rapid pace worldwide (Kalash *et al.,* 2016). Inherent genetic variability between patient groups manifests in conventional therapeutic drugs all too often failing in clinical trials, despite having shown significant efficacy in preclinical trials (Kalash *et al.,* 2016). Redirection of effort and resources toward theranostics is the next logical step in scientific research. This is a potential application in personalised healthcare, that is regarded as the future of health care (Kalash *et al.,* 2016). Where conventional diagnostic techniques experience challenges, PET together with PSMA-targeting tracers are finding oncological diagnosis and monitoring of treatment success. The technique is presently providing predictive and reliable diagnosis as well as impending therapeutic prospects (Eder *et al.,* 2012).

The above-mentioned radiotracers provide a method for investigation of theranostic intervention in prostate cancer by offering diagnosis and therapy which is reliable, minimally-invasive, quantifiable, traceable and most importantly effective (Emmett *et al.,* 2017, Flores *et al.,* 2017, Jadvar and Ballas, 2018, Lenzo *et al.,* 2018, Pearce *et al.,* 2017, Roach *et al.,* 2018, Sathekge *et al.,* 2017). Citing this success in PSMA targeting, the possibilities and potentially accompanying benefits demand of researchers to explore possible applications beyond prostate cancer (Jadvar and Ballas, 2018, Lenzo *et al.,* 2018, Sathekge *et al.,* 2017).

1.5 Non-prostatic PSMA expression

Though termed “prostate specific”, PSMA, is not entirely specific for prostate cancer (Jadvar and Ballas, 2018). Initial PSMA investigation was constrained to prostate cell expression but there are reports and well-studied non-prostatic expression of PSMA in the vasculature of other cancers (Wernicke *et al.,* 2014). The transmembrane PSMA is, however, not found in normal non-cancerous vascular endothelium (Nomura *et al.,* 2014).

Non-prostatic expression of PSMA has been reported in oesophagus, stomach, small intestine, colon, adrenal gland, testes, lung, and pertinent to this study, breast cancers (Kinoshita *et al.,* 2006, Nomura *et al.,* 2014, Silver *et al.,* 1997, Wernicke *et al.,* 2014). The name suggests prostate specificity but, current new research directed at PSMA is proving that the term “specific” is incorrect (Tolkach *et al.,* 2018). The non-prostate expression of PSMA in solid tumours makes it a suitable biomarker for investigation of its diagnostic and therapeutic applications beyond prostate carcinomas (Wernicke *et al.,* 2014). In breast cancer, PSMA expression has been reported in the neovasculature of both primary and metastatic carcinomas (Nomura *et al.,* 2014, Wernicke *et al.,* 2014).

1.5.1 PSMA in breast cancer

In breast cancer, PSMA appears to be expressed in the newly formed blood vessels of primary breast cancer tumours and for the most part in breast cancer metastases (Wernicke *et al.,* 2014). In breast carcinoma, patients with higher PSMA expression (>50% in tumour-associated vasculature) have larger median tumour size compared to those with lower PSMA expression (<50%). Furthermore, patients with high PSMA expression present with higher expression of the proliferative marker Ki-67 (Wernicke *et al.,* 2014). Patients that exhibit basal breast carcinomas are likely to have a higher PSMA expression compared to patients presenting with luminal A and luminal B subtypes (Wernicke *et al.,* 2014).

Breast cancer that is ER/PR-negative, and has a high expression of Ki-67 is characteristically more invasive (Aysola *et al.,* 2013). These same characteristics are reported to exhibit higher expression of PSMA. The exact physiological result of this higher PSMA expression is unclear. However, as PSMA is found in the neovasculature of many tumours, it is thought to aid in the regulation of angiogenesis (Alzahrani *et al.,* 2012, Conway *et al.,* 2006). Its postulated role in angiogenesis is believed to involve vascular endothelial growth factor (VEGF) to some extent. This is not a universal consensus as other researchers think otherwise (Alzahrani *et al.,* 2012, Conway *et al.,* 2006).

There have been reports of non-prostatic tissues showing PSMA-PET positive accumulation. Sathekge *et al.,* (2017) were the first researchers to image a patient with breast cancer using PSMA targeting radiopharmaceuticals. Up to this point, PSMA has been reported in breast tumour neovasculature, but not in solid tumoroal tissue. Using PET/CT, a female patient demonstrated positive binding of [^{68}Ga]Ga-PSMA-11 ligand in the right breast (Figure 1.12) as well as to detect bone and liver metastases in the patient (Sathekge *et al.,* 2017). This non-prostate PSMA expression potentially meant that the success realised in prostate cancer through PSMA radiopharmaceuticals could be potentially followed for therapy of breast cancer patients. This unexpected observation called for research aimed at understanding cellular kinetics, hormone expression profiles and genomic make-up of breast cancer to explain the reason for the radiopharmaceutical accumulation. This may lead to the possible discovery of underlying biomarkers in breast cancer such as PSMA that could aid in the development of more effective, safe, accessible and predictable diagnostic and therapeutic alternatives (Shah *et al.,* 2014).

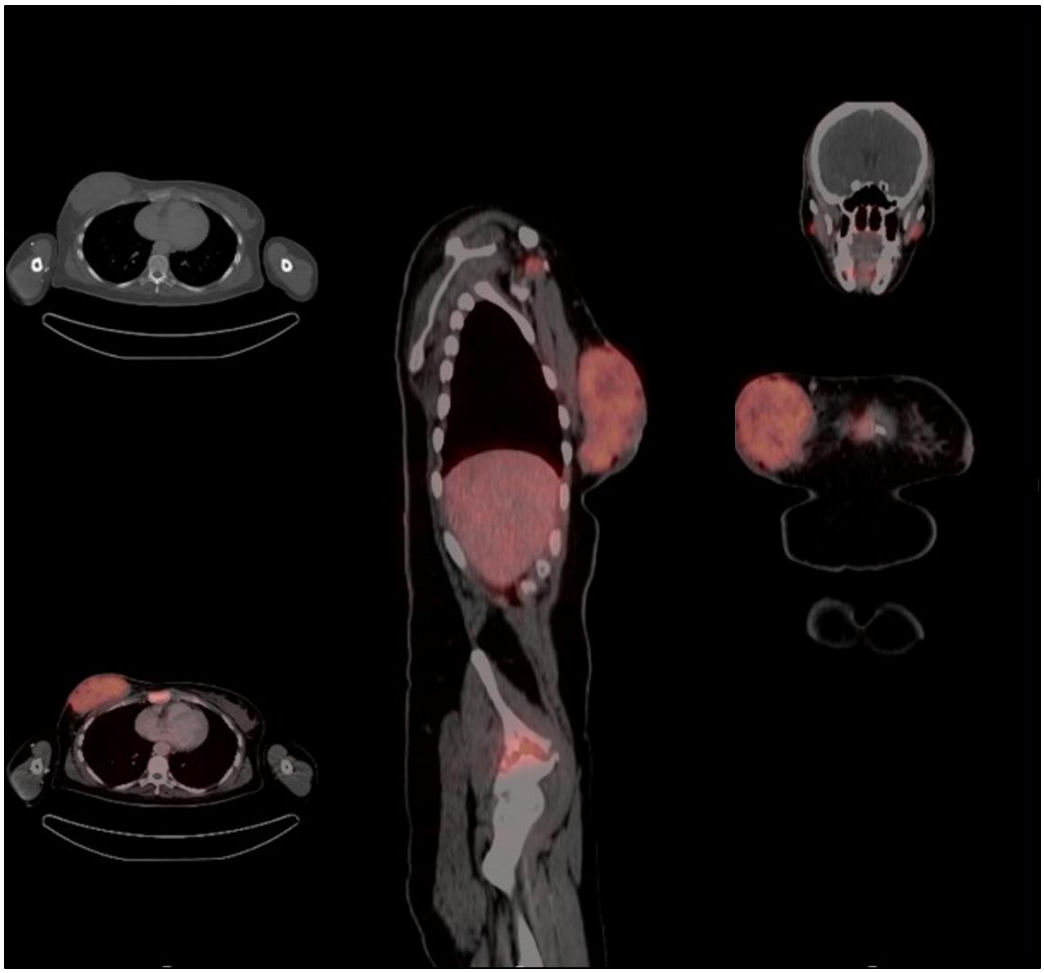

Figure 1-12 A combined PET/CT scan image of a 39-year-old woman with stage IV breast cancer following ^{68}Ga-PSMA-11 administration. PET demonstrated multiple osseous metastasis and a primary right breast cancer (Sathekge et al., 2017). Axial, coronal and sagittal PET/CT views of the patient confirm the presence of PSMA in breast tumour lesions. (Used with permission).

1.5.2 Breast and prostate cancer overlap

Although the breast and prostate glands are different with regard to their anatomy and physiological function, tumours that arise from both these glands have noteworthy underlying biological resemblances (Risbridger *et al.,* 2010). Men and women are both equally capable of oestrogen and androgen synthesis (Risbridger *et al.,* 2010). Intriguingly, in 90% of ER-positive and 55% of ER-negative breast tumours, AR is the most prevalent sex steroid hormone receptor expressed (Hu *et al.,* 2011, Lakis *et al.,* 2014). The role of AR stimulation in breast carcinoma is similar to that of HER-2 and has been investigated as a potential prognostic marker and a therapeutic target in breast cancer (Hu *et al.,* 2011, Lakis *et al.,* 2014). In prostate cancer, ER-β mediates the malignant effects of oestrogen, resulting in prostate cell inflammation and proliferation (Di Zazzo *et al.,* 2018).

Both extrinsic and intrinsic predisposing factors for prostate cancer have also been described in breast cancer. Mutations in the breast cancer linked *BRCA1* and *BRCA2* genes are associated with development of cancers in male, specifically prostate cancer (Castro and Eeles, 2012). Additionally, the mortality rates between prostate and breast cancer are shown to be strikingly similar (López-Abente *et al.,* 2014). Not only does a family history of prostate cancer infer genetic susceptibility but familial breast cancer presence significantly increases prostate cancer risk. This further supports the growing evidence that the molecular similarity between prostate and breast cancer is closer than previously believed (Barber *et al.,* 2018, López-Abente *et al.,* 2014). These two cancers are more similar than they are different (Risbridger *et al.,* 2010). This crosstalk between oestrogen and androgen receptor presence between these two cancers, the similarity in the mortality rates and the corresponding extrinsic and intrinsic predisposing factors collectively provide reasons to support this study. PSMA may well be an underlying biomarker in breast cancer where its role is still undetermined.

1.6 Study rationale

Cancer is a progressive disease and as such, needs management strategies that can cope with its mutative demands. The limitations of the existing diagnostic and therapeutic modalities confound the management of cancer even further. Breast cancer in particular exhibits these limitations in diagnosis and therapy. As such alternative, contemporary and effective methods of intervention need to be developed. Through radiopharmaceutical targeting of prostate cancer, PSMA is proving to be a cutting-edge, contemporary and progressive means of addressing the shortcomings of conventional cancer management. Based on the similarity between prostate and breast cancer cells, the success and progress

in treatment being realised in prostate cancer may be transferred and realised in breast cancer. Theranostic targeting of PSMA can potentially shorten hospital stays and the associated operational expenses with the promise of better treatment outcomes and partially addresses the depressive incidences seen in conventional cancer management. The goal of PSMA theranostics speaks to the goal of developing novel, personalised, affordable and reliable alternatives for cancer diagnosis and therapy. In breast cancer, targeting the PSMA may provide an alternative paradigm in achieving these diagnostic and therapeutic goals. *In vitro* proof of PSMA expression in breast carcinoma tissue is fundamental to the success of prospective clinical applications for both diagnosis and potential radiotherapeutic treatment of breast cancers. In this study, two dimensional breast carcinoma monolayer *in vitro* cultures were used to elucidate non-prostatic PSMA expression. Histological slices were also probed for PSMA expression however due to a lack of sample availability; only two slices could be probed.

1.7 Study Aim

This study was aimed at evaluating PSMA expression by MCF-7 or MDA-MB-231 mammary adenocarcinoma cell lines in comparison to a known high PSMA expressing LNCaP prostate carcinoma and EA.hy926 hybrid vascular endothelial cell line.

1.8 Objectives

The aim was achieved through the following objectives (summarised in Figure 1.13 below)

- Optimisation of monolayer cell culture conditions for the detection of PSMA for each of EA.hy926, MCF-7 MDA-MB-231 and LNCaP cell lines.
- Identification of PSMA expression in EA.hy926, MCF-7 MDA-MB-231 and LNCaP cell lines using:
    - Flow-cytometry
- Determining the spatial location of PSMA in EA.hy926, MCF-7, MDA-MB-231 and LNCaP cell lines using:
    - Immunofluorescence
    - Confocal microscopy
- Quantification of PSMA expression in the tested cell lines using
    - Enzyme linked immunosorbent assay

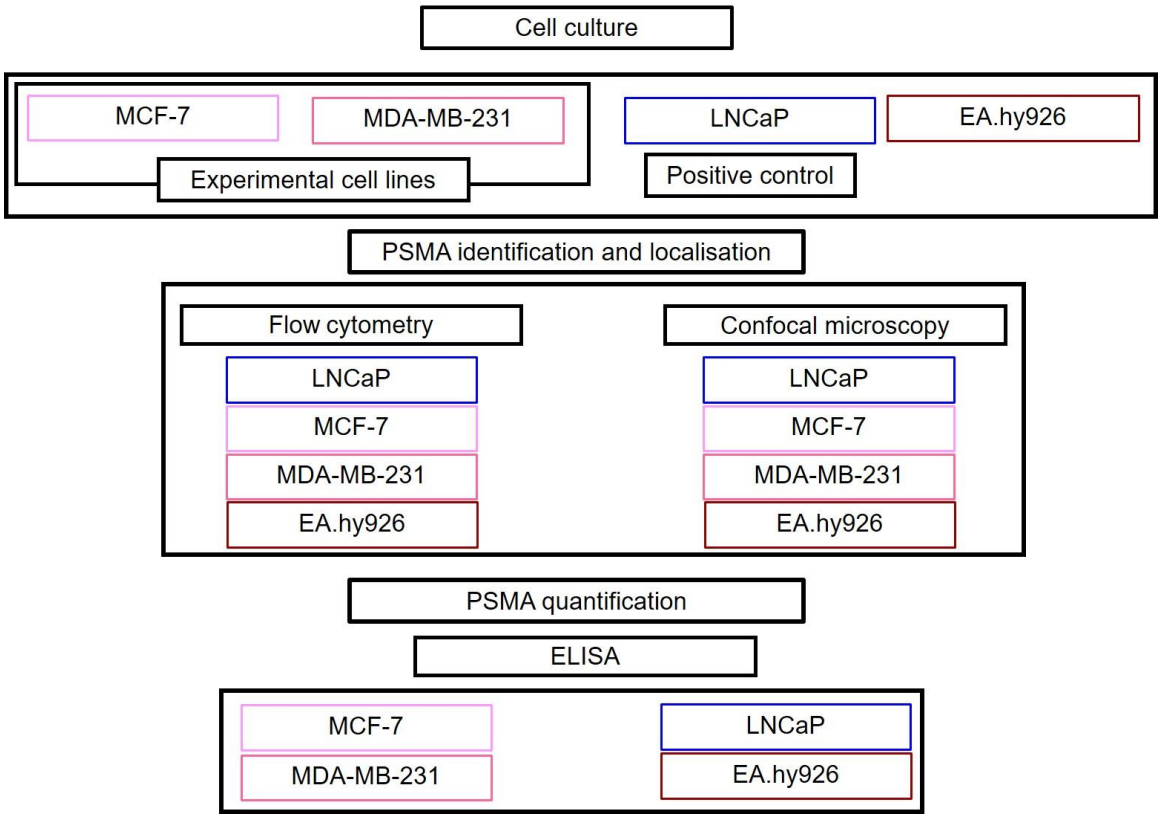

Figure 1-13 A flow diagram summarising the different methods applied and cell lines used in this study.

2 Materials and methods

All reagents and solvents were of highest purity available and generally of analytical grade or better. These were purchased from reputable chemical vendors. Where specific vendors are used these are mentioned after the reagent is mentioned in each section.

2.1 Cell culturing

Hybrid vascular endothelial EA.hy926 cells (ATCC®CRL-2922™), MCF-7 (ATCC® HTB-22™), and MDA-MB-231 breast adenocarcinoma cells (ATCC® HTB-26™) and LNCaP (ATCC® CRL-1740™) prostate adenocarcinoma cells were originally obtained from the American type tissue collection (ATCC, Manassas, VA. USA) then maintained and cultured in the Department of Pharmacology and Anatomy of the University of Pretoria. All experiments were conducted under the guidelines listed within the South African Human Tissue Act (No. 65 of 1983). Ethics approval was obtained from the Faculty of Health Sciences Research and Ethics Committee of the University of Pretoria (Ethics approval number: 379/2018)

2.1.1 Description of cell Lines

Endothelial EA.hy926 cells are somatic cell hybrids of primary human umbilical vein endothelial cells (HUVEC's) and A549 human alveolar basal epithelial adenocarcinoma cells that show typical endothelial cell characteristics (Edgell *et al.,* 1983, Liu *et al.,* 2011). The MCF-7 cell line is a hormone-responsive breast adenocarcinoma cell line originally isolated from the pleural effusion of a patient with breast adenocarcinoma (Chavez *et al.,* 2010). MCF-7 cells constitutively express ER and PR but without HER-2 amplification (Bajou *et al.,* 2002, COMŞA *et al.,* 2015). The triple-negative MDA-MB-231 cell line exhibits a stellate morphology in culture, further characterised by absence of either ER, PR or abundant HER-2 receptors (Liu *et al.,* 2003). The LNCaP human prostate adenocarcinoma cell line, originally characterised in 1977, was used as a positive control as they show abundant PSMA expression. Monolayer cultures exhibit spindle-like morphology *in vitro* and are reported to express both ER and PR receptors in addition to abundant PSMA expression (Laidler *et al.,* 2005, McKeithen *et al.,* 2010).

2.1.2 Culture media and conditions

The Ea.hy926, MCF-7, and MDA-MB-231 cells were grown in Dulbecco's Modified Eagle's Medium (DMEM), pH 7.2 while LNCaP cells were grown in Dulbecco's Modified Eagle's Medium/Ham's F12 Nutrient Mixture (DMEM/F12) (1:1), pH 7.2. Culture medium was supplemented with 1% penicillin/streptomycin (10 mL/L) and L-glutamine (10 mL/L). Additionally, medium was supplemented with 10% foetal calf serum (FCS) (Gibco, Fisher Scientific Rockford, IL, USA) for Ea.hy926, MCF-7 and MDA-MB-231 cell lines and 15%

FCS (Gibco, Fisher Scientific Rockford, IL, USA) for the LNCaP cell line. The cells were cultured at 37˚C in a humidified atmosphere with 5% CO_2 in 75 cm^2 CELLSTAR® culture flasks purchased from Greiner Bio-One International (Frickenhausen, Germany).

2.1.3 Preparation of cells for experiments

All cell culture apparatus was sterilised by autoclaving for 30 minutes at 121°C or using ultraviolet (UV) light for 30 minutes before use. Cell sub-culturing and experimentation was conducted in a laminar flow cabinet using aseptic techniques to maintain the sterility of the cultured cells. After cells reached approximately 80% confluence, they were harvested for experiments after briefly washing with phosphate-buffered saline (PBS), and either physically detached using scraping or detached by proteolytic trypsinisation, depending on the experiment being undertaken. Cells were collected using centrifugation (200 x *g* for 5 min) and counted using the trypan blue exclusion assay.

2.1.4 Cell counting

The trypan blue exclusion assay, which assesses membrane integrity and determines the percentage cell viability, was used to count cells preceding experimental use of cells. An aliquot of 20 µL of a 1 mL (medium) cell suspension was added to 180 µL of counting fluid [0.2 % (m/v) trypan blue solution]. The cell suspension was then loaded onto a haemocytometer and the cells were counted using an Olympus® IX71 inverted microscope. The cell suspensions were diluted to the required cell concentrations for each experiment.

2.1.5 Cell culture reagents

Dulbecco's Modified Eagles Medium (DMEM)

Gibco® DMEM was purchased from Thermo Fisher Scientific (Rockford, IL, USA) and supplemented with 1% penicillin/streptomycin (10 mL/L), L-glutamine (to 1.0 mM) and 10% heat inactivated foetal calf serum (FCS) (Gibco, Fisher Scientific Rockford, IL, USA). The prepared medium was stored at 4ºC.

Dulbecco's Modified Eagle's Medium/Ham's F12 Nutrient Mixture (DMEM/F12)

Gibco® Dulbecco's Modified Eagle's Medium/Ham's F12 Nutrient Mixture DMEM/F12 (1:1) was purchased from Thermo Fisher Scientific (Rockford, IL, USA) and supplemented with 1% penicillin/streptomycin (10 mL/L), L-glutamax® (to 1.0 mM) and 15% FCS (Gibco, Fisher Scientific Rockford, IL, USA). The prepared medium was stored at 4ºC

Bovine Foetal Calf Serum (FCS)

Gibco® heat inactivated FCS was purchased from Thermo Fisher Scientific (Rockford, IL, USA) and added to the cell culture medium to a final concentration of 10% for the Ea.hy926, MCF-7 and MDA-MB-231 cells and 15% for LNCaP cells.

Penicillin/Streptomycin

A penicillin/streptomycin solution containing 10 000 units of penicillin and 10 000 µg of streptomycin was added to the culture medium to a final concentration of 1% (v/v). (BioWhittaker; Walkersville, USA)

Phosphate Buffered Saline (PBS)

Phosphate buffered saline was made up by weighing out 9.23 g of FTA Hemagglutination buffer powder (PBS) (BD Bioscience; San Jose, USA) and dissolving in 1.0 litre of deionised water. The pH was adjusted to 7.4 and the PBS was autoclaved for 30 minutes at 121°C.

Trypsin/Versene solution

Trypsin/Versene solution (Highveld Biological; Johannesburg, RSA) was used to detach adherent cells. The solution consisted of 0.25% trypsin with 0.1% EDTA in Ca^{2+} and Mg^{2+} free phosphate buffered saline.

Cell counting fluid

Cell counting fluid was made up using trypan blue powder (Sigma-Aldrich: St. Louis, USA). The counting fluid was made up to 0.2% by weighing out 100 mg of trypan blue powder to in 50 mL PBS, pH 7.4.

2.1.6 Optimisation of cell culturing conditions for the detection of PSMA

Experimental methodology

Prior to final experimentation, a pilot study was undertaken to optimise methodology and experimental conditions (Figure 2.1). Culture plates of 24, 48 and 72-hour were tested alongside each other to determine the effect of scraping and trypsinisation comparatively on protein and DNA content as well as cell morphology. Phase contrast microscopy was used to assess cell morphology and the Crystal Violet assay to determine cell viability by assessing DNA and protein content of EA.hy926, MCF-7, MDA-MB-231 and LNCaP cells.

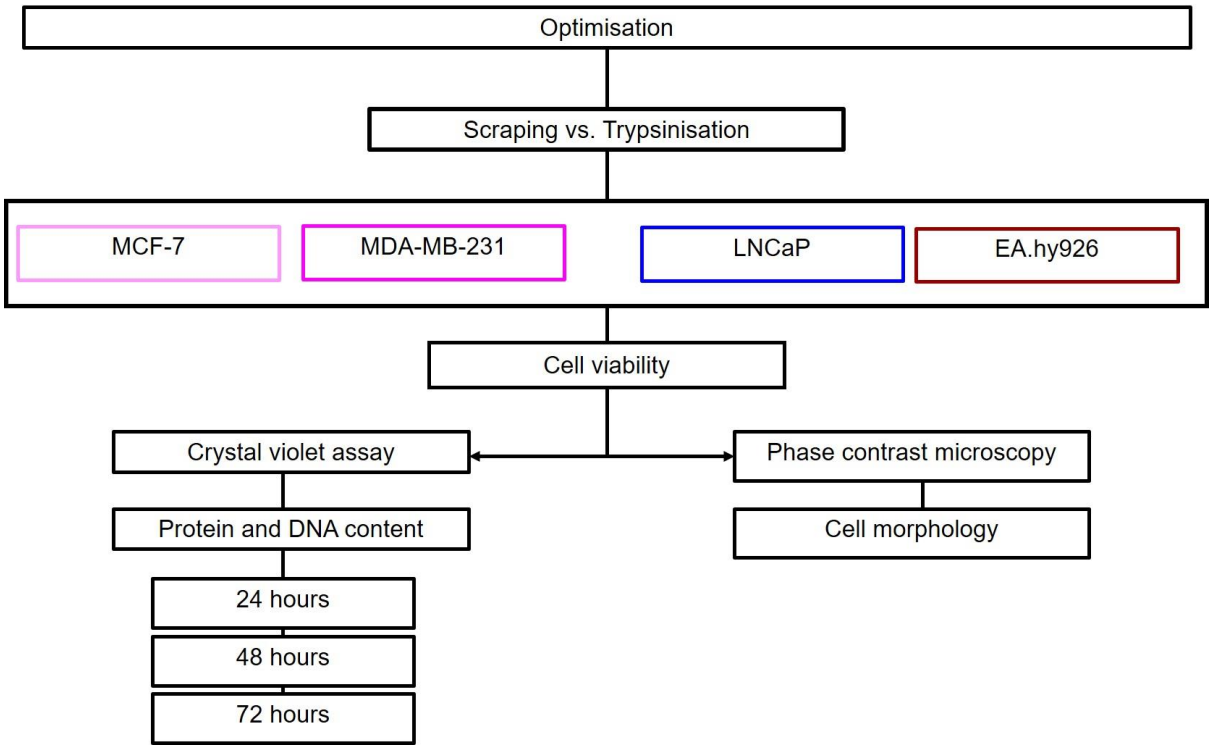

Figure 2-1 Optimisation of culturing conditions prior to PSMA expression evaluation.

2.1.7 Crystal Violet assay

The assay was performed according to the method reported by Kueng *et al,* (1989). Crystal Violet (CV) is a positively charged dye that binds to negatively charged cellular structures such as DNA and protein-containing negatively charged amino acids such as aspartic and glutamic acids. Staining results in accumulation of a purple colour that is proportional to the number of cells (Pugsley and Vega, 2011). From this data, after 24, 48 and 72 hours the relative change in cell count was obtained for scraped and trypsinised cell cultures.

2.1.7.1 Preparation of cells for Crystal Violet assay

Cell reached 80% confluence during their logarithmic phase of growth. The cells were washed twice with PBS to remove all growth media. All cells were grown concurrently in separate culture flasks, at the same passage number. In one flask, cells were chemically detached using 2 mL of trypsin and in an equivalent flask; cells were physically detached using a CELLSTAR® cell scraper purchased from Greiner Bio-One International (Frickenhausen, Germany). Following detachment, cells were harvested using centrifugation at 200 *x g* for five minutes and aliquots counted using the trypan blue exclusion assay then the cells were diluted to a concentration 40 000 cells/mL using the appropriate growth medium to provide 2 000 cells/well on a CELLSTAR® 96 well tissue culture plate.

2.1.7.2 Seeding cells for the Crystal Violet assay

Cells were seeded in a CELLSTAR® 96 well plate (Greiner Bio-One International, Frickenhausen, Germany). Cells were seeded at 2 000 cells/well in a total volume of 100 µL for each well and incubated for 24, 48 and 72 hours to determine the effect of the different cell detachment methods on cell viability over time.

2.1.7.3 Crystal Violet assay

After the 24, 48 and 72-hour incubation times, cells were fixed by adding 10 µL of 20% formaldehyde (v/v) to each well to achieve a final concentration of 2% in each well. Cells were fixed for 20 minutes at 37ºC. The fixative solution was removed by gently washing the plate under running water and the plates then allowed to air-dry. Following drying, 100 µL of Crystal Violet dye at a 0.1% (w/v) concentration was added to each well and allowed to incubate for 30 minutes at room temperature. The excess dye was removed by gently washing the plate under running water. The plate was then again allowed to air dry. Following the second drying step 200 µL of 10% acetic acid (v/v) solution was added to each well to dissolve the bound CV dye and the plate read in a Emax® Plus microplate reader (Molecular Devices, California, USA) measuring the absorbance at 570 nm with a reference at 630 nm.

2.1.7.4 Statistics for the relative change in cell count

A minimum of three independent inter-day repeats were conducted for each cell line. The passage number for each culture at every repeat was recorded. Data were measured and presented as Microsoft Excel 2016 spreadsheets that were further processed. Statistical analysis was conducted using GraphPad® Prism 6 (GraphPad Software, Inc. La Jolla, California, USA). Protein concentrations between scraped and trypsinised cell cultures were compared after a further 24-, 48- and 72-hours incubation as a determinant of the effect of the detachment method on the cell viability over time. The viability is expressed as the mean (± standard error of the mean) of the repeat measurements. The Kruskal-Wallis test was conducted to compare the mean cell viability against each cell detachment method and $p < 0.05$ was deemed as a significant difference in viability over the incubation periods.

2.1.7.5 Crystal Violet reagents

<u>20% Formaldehyde</u>

Formaldehyde for fixation was prepared from a 37% (v/v) formaldehyde (Sigma-Aldrich: St. Louis, USA) solution to a final working concentration of 20%. A volume of 540.5 mL of 37% formaldehyde (v/v) was added to 459.5 mL of deionised water (dH_2O) to provide a final concentration of 20% (v/v) formaldehyde in a final volume of 1 litre. The solution was stored at 4ºC in the dark.

0.1% Crystal Violet solution

The 0.1% (m/v) Crystal Violet solution was made from Crystal Violet powder (Sigma-Aldrich, St. Louis, USA). Exactly 100 mg of the powder was added to 0.75% (v/v) formic acid (Sigma-Aldrich, St. Louis, USA) made by adding 0.75 mL formic acid to 99.25 mL double deionised water (ddH_2O). The pH was confirmed to be 3.5.

10% Acetic acid solution

A 10% (v/v) acetic acid (Sigma-Aldrich: St. Louis, USA) was prepared by diluting 10 mL of acetic to a final volume of 100 mL with ddH_2O.

2.2 Indirect flow cytometry detection of PSMA

Flow cytometry analysis was used to measure PSMA presence in EA.hy926, MCF-7, MDA-MB-231 and LNCaP cell lines using an anti-PSMA antibody according to Tykvart et al. (2014)

2.2.1 Preparation of cells for flow cytometry

Upon reaching approximately 80% confluence in logarithmic growth phase in a T75 culture flask, growth media was poured off and the cells quickly washed twice with PBS then enzymatically detached using a 2 mL trypsin solution. Cells were harvested using centrifugation at 200 x *g* for five minutes and an aliquot of the pelleted cells counted using the trypan blue exclusion assay then diluted to a cell concentration of 1 000 000 cells/mL. After transferring 500 000 cells (500 µL) to new 15 mL centrifuge tubes, the cell suspensions were centrifuged at 200 x *g* for five minutes and washed with ice-cold PBS. Cells were then fixed by adding 1 mL of ice-cold 80% methanol (v/v) dropwise over five minutes while gently vortex mixing. Following fixation, cells were washed once with 1 mL PBS and collected at 200 x *g* for five minutes. Cells were permeabilised by incubating in 1 mL of 0.1% (v/v) Tween® 20 for 10 minutes at room temperature on a slowly rotating plate shaker then washed twice with PBS and collecting by centrifuging at 200 x *g* for five minutes for cell collection.

2.2.2 Antibody staining of cells for flow cytometry

Following fixation and permeabilisation, non-specific binding was blocked with a 3% BSA (m/v) and 10% FCS (v/v) in PBS for 1 hour. The cells were harvested by centrifugation and the blocking solution discarded. The cells were washed twice in PBS then treated with 0.2 µg YPSMA-1 mouse derived anti-human PSMA monoclonal antibody per million cells in 1 mL of 3% BSA (m/v) in PBS solution. The tubes were then incubated in the dark for 30 min at 22°C on a slowly rotating plate shaker. Unbound antibody was removed by washing cells three times with 1 mL of PBS with cells collected by centrifugation at 200 x *g* for 5 minutes

between washes. A secondary goat anti-mouse IgG antibody, conjugated to fluorescein isothiocyanate (FITC) (Heavy and Light chain) H&L was diluted 1/2000 in 3% BSA (m/v) and the cells resuspended in 500 µL of the secondary antibody solution and incubated for 30 min at 22°C in the dark on a slowly rotating plate shaker. The cells were then washed three times with PBS and centrifuged at 200 x *g* for 5 minutes after each wash. The cells were resuspended in 500 µL PBS containing 3% BSA and 1% sodium azide (m/v). Flow cytometric analysis was undertaken on a Beckman Coulter Cytoflex® flow cytometry analyser. A minimum of 7500 events were recorded where FITC excitation was achieved using a blue 488 nm argon laser and emission was measured at 525 nm with a 500 nm cut-off filter. The resulting data was analysed using Kaluza C® software (Beckman Coulter, Brea, CA, USA). A minimum of three independently prepared inter-day repeats were conducted for each cell line. The passage number for each culture at every repeat was recorded. The repeats from different days were combined for each cell line and presented as a composite univariate histogram.

2.2.3 Controls

Control samples of cells from the same cultures as the experimental groups were subjected to the same experimental conditions and processes including staining with the secondary antibody but without exposure to the primary anti-PSMA antibody staining. Control samples were analysed together with the stained samples. A minimum of three independent inter-day repeats were conducted for each cell line.

2.2.4 Statistics for flow cytometry

A minimum of three independent inter-day repeats were conducted for each cell line. The passage number for each culture at every repeat was recorded. Fluorescence was measured and processed utilising Kaluza C® software. Statistical analysis was conducted using GraphPad® Prism 6 (GraphPad Software, Inc. La Jolla, California, USA). The fluorescence is expressed as the mean (± standard error of the mean) of the repeat measurements. Significant differences across different cell lines are represented by (*). Multiple comparisons of a Repeated measures one-way Analysis of Variance (ANOVA).

2.2.5 Flow cytometry reagents

80% Methanol (v/v)

Methanol for fixation was prepared from a 100% methanol (Sigma-Aldrich: St. Louis, USA) solution to a final working concentration of 80%. Cells were resuspended in 200 µL PBS and 800 µL of methanol was slowly added while the cells were being gently vortex mixed to a final concentration of 80%.

0.1% Tween® 20 (v/v)

The permeabilising solution was made by adding 50 µL of Tween® 20 (Sigma-Aldrich: St. Louis, USA), to 49.95 mL of PBS to a final concentration of 0.1% in 50 mL. The solution was stored in the dark at room temperature.

Antibodies

The primary YPSMA-1 antibody (Abcam: ab19071, Cambridge, UK) upon delivery was aliquoted at assay dependent concentrations and stored at -20ºC according to manufacturer's instructions to avoid freeze thaw cycles. The secondary goat anti-mouse IgG H&L conjugated to FITC (Abcam: ab6785, Cambridge, UK) was stored at 4ºC as per manufacturer's instructions.

3% Bovine serum albumin (m/v)

Antibodies were made up in 3% BSA (m/v) solution made up by weighing 3 g of BSA (Sigma-Aldrich: St. Louis, USA) and adding it to 100 mL of PBS. The solution was stored at 4ºC and kept away from light. The solution was used for diluting the antibody.

PBS with 3% BSA (m/v) and 10% FCS (v/v)

The solution was made up by first adding 10 mL of FCS to 90 mL of PBS then adding 3.0 g of BSA to the final solution and gently mixing till dissolved. The solution was used for blocking non-specific binding. The solution was kept at 4ºC in the dark.

PBS, 3% BSA (m/v), 1% sodium azide (m/v)

The solution was used to resuspend cells after staining with secondary antibody and for analysis on the Cytoflex® flow cytometry analyser. The solution was made up by weighing 3.0 g of BSA and adding it to 100 mL of PBS. When completely solubilised 1.0 g of sodium azide (Sigma-Aldrich: St. Louis, USA) was then added and gently mixed to avoid foaming until completely dissolved. The solution was kept at 4ºC in the dark.

2.3 Indirect immunofluorescence analysis – PSMA localisation

Immunofluorescence is a technique that uses fluorescence microscopy and the specificity of antibody-antigen binding to target select molecules within a sample and allow visualisation and identification (Mandrell *et al.,* 1988). Confocal fluorescent microscopy has the added advantage of performing multiple high resolution third dimension layer stacking and several different fluorescent signals that can be overlaid. Confocal microscopy was performed according to the method established by Dowling *et al,* (2019).

2.3.1 Preparation of coverslips for immunofluorescence.

Glass coverslips (22 X 22 mm) were purchased from Thermo Fisher Scientific (Rockford, IL, USA). The coverslips were washed in an alkaline wash solution made up of a working concentration of 5% sodium hydroxide (NaOH) (w/v) and 30% ethanol (v/v). Both solutions were prepared separately in ddH_2O thus; 25 mL of 10% NaOH (m/v) and 25 mL 60% ethanol (v/v) stock solutions were added together to make 50 mL of working solution. After the washing step all work henceforth was done under strict sterile conditions. The coverslips were incubated in the alkaline wash solution for two hours on an orbital shaker. Following incubation, coverslips were rinsed five times in ddH_2O. Coverslips were covered with 100% ethanol (Sigma-Aldrich: St. Louis, USA) for 30 minutes then allowed to air-dry under laminar flow. After drying, coverslips were coated with poly-L-lysine (0.01%) (Sigma-Aldrich: St. Louis, USA) using 1 mL of solution per coverslip in a covered and autoclaved Petri dish. The coverslips were incubated for two hours on the orbital shaker. Following incubation, the poly-L-lysine solution was discarded and the coverslips were washed ten times by dipping into sterile deionised water. The coverslips were placed in a laminar flow cabinet for three days then stored in covered sterile Petri dishes at room temperature.

2.3.2 Preparation of cells for immunofluorescence

Cells at approximately 80% confluence during logarithmic growth phase in a T75 culture flask were quickly washed twice with PBS and enzymatically detached using 2 mL of trypsin solution. Cells were harvested using centrifugation at 200 x *g* for five minutes then counted using the trypan blue exclusion assay and cell concentration adjusted to 100 000 cells in 3 mL of FCS supplemented cell growth medium.

2.3.3 Seeding of cells for confocal microscopy

Poly-l-lysine coated coverslips were placed individually into wells of sterile CELLSTAR® 6 well culture plates purchased Greiner Bio-One International (Frickenhausen, Germany). Cell suspensions (100 000 cells in 3 mL) were seeded. The cells were incubated for 24 hours to allow for cell attachment onto the coverslips.

2.3.4 Staining of cells for confocal microscopy

Following incubation, cells were washed with phenol red-free DMEM/F12 purchased from Thermo Fisher Scientific (Rockford, IL, USA). The phenol red-free medium was removed and the cells were then fixed with 10% formalin for 20 minutes at room temperature. Cells were washed twice with sterile PBS on a plate shaker and permeabilised using 0.1% Tween® 20 for 10 minutes at room temperature. Following permeabilisation, cells were washed twice with PBS on a shaker for 5 minutes at each wash step. Non-specific binding was blocked with 3% BSA in PBS for 45 minutes at room temperature then rinsed twice with

PBS. A volume of 1 mL of YPSMA-1 mouse anti-human PSMA monoclonal antibody at a 1:500 dilution in 3% BSA was added to the coverslips to entirely submerge the surface of the coverslip in the antibody solution. The cells were incubated with the primary antibody for 24 hours at 4ºC. Following primary antibody incubation, cells were washed twice with PBS and stained in the dark at room temperature with 4′, 6-diamidino-2-phenylindole (DAPI) at a final concentration of 1 µg/mL in PBS for 10 minutes. After DAPI staining, cells were washed twice in PBS and stained at room temperature with a 1 mL of secondary goat anti-mouse IgG H&L antibody conjugated to FITC in 3% BSA solution prepared at a 1:100 dilution. The cells were stained whilst the plate was covered in foil, to protect from light. After secondary antibody incubation, cells were rinsed twice with PBS on a plate shaker. The slides were removed and allowed to dry before being mounted with 5 drops of the antifade mounting medium onto 25 x 75 x 1.0 mm microscope slides purchased from Thermo Fisher Scientific (Rockford, IL, USA). The cells were left to dry at room temperature whilst protected from light for 24 hours. A minimum of three independent inter-day repeats were conducted for each cell line.

2.3.4.1 Control confocal samples

Control samples from the same cell cultures were subjected to the same experimental conditions and processes as those used for the experimental samples except, that the primary antibody was not added to the incubation buffer during initial staining. Control samples were analysed together with the stained samples. A minimum of three independent inter-day repeats were conducted for each cell line.

2.3.4.2 Visualisation of cells using confocal microscopy

Visualisation of cells was undertaken using a LSM 880 Elyra, AxioObserver® confocal laser scanning microscope. Cells were viewed under an Alpha Plan-Apochromat 100x/1.46 Oil DIC M27 Elyra objective at 100x magnification. Fluorescence was examined using an argon laser at an excitation wavelength of 488 nm and emission wavelength of 548 nm for FITC fluorescing cells. DAPI fluorescence showing cell nuclei were analysed at an excitation wavelength of 405 nm and emission wavelength of 450 nm respectively. The detector gain was set at 946 V for FITC and 568 V for DAPI detection. All image analysis was accomplished using Carl Zeiss Microscopy GmbH: Zen 2.6 (Blue edition, 2018) software. Imaged cells were selected based on the presence of cellular green fluorescence under the objective when the pinhole is set between 0.25 and 1 Airy unit (AU). A minimum of three different randomly selected fields were captured per slide. The intensity of fluorescence of stained cells was not quantitatively measured and the unstained samples were used as an expression threshold.

2.3.4.3 Immunofluorescence reagents

Alkaline wash solution

Sodium hydroxide (NaOH) pellets (10 g) purchased from Merck (Darmstadt, Germany) were weighed out and added to 100 mL of dH_2O to prepare a 10% NaOH (m/v) stock solution. A volume of 60 mL of 100% ethanol purchased from Sigma-Aldrich (St. Louis, USA) was poured out into a 100 mL measuring cylinder. The measuring cylinder was filled with dH_2O until it reached the 100 mL mark to prepare a 60% (v/v) ethanol stock solution. The alkaline wash solution of was prepared by adding 25 mL of each stock solution to make up a 50 mL of 5% sodium hydroxide (NaOH) (w/v) and 30% ethanol (v/v) solution.

Phenol red-free DMEM/F12

Gibco phenol red-free DMEM/F12 supplemented with L-Glutamax® (1.0 mM) was purchased was from Thermo Fisher Scientific (Rockford, IL, USA).

10% Formalin (v/v)

Formalin for fixation was prepared from a 37% formaldehyde (Sigma-Aldrich: St. Louis, USA) solution to a final working concentration of 10%. A volume of 270 mL of 37% formaldehyde was added to 730 mL of PBS to a final concentration of 10% formaldehyde in a final volume of 1 litre. The solution was stored at 4ºC in the dark.

4′, 6-diamidino-2-phenylindole (DAPI)

DAPI was purchased from Sigma-Aldrich (St. Louis, USA). A stock of 10 mg/mL (m/v) was prepared by weighing out 10 mg and adding it to 1 mL of PBS. The working concentration of 1 µg/mL was made from this DAPI stock by diluting 5 µL to 50 mL.

Antifade mounting medium

ProLong® antifade slide mountant (10 mL) was purchased from Thermo Fisher Scientific (Rockford, IL, USA) and was used to mount the coverslips onto microscope slides to prevent photobleaching and signal preservation of the fluorescently labelled cells.

0.01% Poly-L-lysine

Poly-L-lysine (P8920, 0.1%) was purchased from Sigma-Aldrich (St. Louis, USA) and was used to coat glass coverslips to facilitate cell attachment during cell culture.

2.4 ELISA - PSMA quantification

A Elabscience® human PSMA enzyme-linked immunosorbent assay (ELISA) (E-EL-H5413) kit was used for quantifying the PSMA protein in the cells. In this study, sandwich ELISA was

used for quantifying PSMA present in all cell cultures. The micro ELISA plate is pre-coated with a capture antibody specific for PSMA. A series of standards or cell sample lysates from different cell cultures were added to individual wells of the ELISA plate and PSMA allowed to be captured during 1.5 hours incubation at 37°C. After extensive washing a detection antibody specific for PSMA conjugated to biotin was added to each well. After an incubation time of 1 hour at 37°C and extensive washing to remove unbound secondary antibody, a horseradish peroxidase (HRP) conjugated to streptavidin was added. A substrate solution (included in the ELISA kit) was added and the optical density of the reaction was measured spectrophotometrically to give an absolute concentration of the PMSA present in the sample (Saita *et al.,* 2017).

2.4.1.1 Cell preparation for ELISA

Cells at approximately 80% confluence during logarithmic growth phase in a T75 culture flask were quickly washed twice with PBS and enzymatically detached using 2 mL of trypsin solution. Cells were harvested using centrifugation at 200 x *g* for five minutes then counted using the trypan blue exclusion assay and cell concentration adjusted to 2 000 000 cells in 600 µL of PBS. The cells were washed three times with 600 µL of pre-cooled PBS. The cells were resuspended in 600 µL of a 1:6 dilution of PBS in cOmplete® protease inhibitor (25X). The cells were subjected to five freeze-thaw cycles with a 10 minute sonication step at each freeze-thaw interval to achieve complete cell lysis. The cell lysates were then centrifuged for 10 min at 1500 x *g* at 4ºC. The supernatant was collected for ELISA assay.

2.4.1.2 ELISA assay

The volumes of supernatant added to the ELISA wells were adjusted so that the reported values are within the linear range of the ELISA kit. For the experimental cell lines, 200 µL of the cell lysate was added instead of 100 µL. For the positive control, 50 µL was added instead of 100 µL. The generated PSMA concentration was then adjusted by the dilution factor to get the actual concentration per 2 million cells. Duplicates of the standard solutions (100 µL) were added in two columns of the ELISA micro plate. The EA.hy926 (200 µL), MCF-7 (200 µL), MDA-MB-231 (200 µL) and LNCaP (50 µL) cell supernatants were added to individual micro-plate wells in duplicates. The plate was covered with a plate sealer and incubated at 37°C for 90 minutes in an oven. Following incubation, the standard solutions and cell supernatant were carefully removed from each well followed by 3 wash steps to remove unbound compounds. The biotinylated detection antibody working solution (100 µL) was added to each well. The plate was sealed and gently agitated on a plate shaker. The plate was incubated at 37°C for one hour. Following incubation, the antibody working solution was decanted and the plate was washed five times with 350 µL of the wash buffer for two minutes at each wash interval. The HRP-streptavidin conjugate solution (100 µL) was

then added to each well. The plate was sealed and incubated at 37°C for 30 minutes. The conjugate solution was decanted after incubation and the wells were washed seven times with 350 µL wash buffer for two minutes at each wash interval. The substrate reagent used was tetramethyl benzidine (TMB) and 90 µL was added and the plate was incubated at 37°C for 15 minutes after which 50 µL of the stop solution was added and the absorbance was read at 450 nm on a Biotek® Synergy II microplate reader with a reference wavelength of 630 nm. Quantitation of PSMA protein in cell supernatants was extrapolated from the ELISA calibration curve generated from the standards.

2.4.1.3 Statistics for ELISA

A minimum of three independent inter-day repeats of duplicates were conducted for each cell line. The passage number for each culture at every repeat was recorded. Absorbance was measured and concentration was interpolated from the absorbance measurements. Statistical analysis was conducted using GraphPad® Prism 6 (GraphPad Software, Inc. La Jolla, California, USA). The concentration is expressed as the mean (± standard error of the mean) of the repeat measurements. Significant differences across different cell lines are represented by (*). Multiple comparisons of a Repeated measures one-way Analysis of Variance (ANOVA).

2.4.1.4 ELISA reagents

Wash buffer

The was buffer was made by diluting 30 mL of wash buffer concentrate included in the kit into 720 mL of deionised water to make a 750 mL wash buffer working solution.

Standard working solution

The reference standard was diluted in the provided standard diluent and allowed to stand for 10 minutes. The mixture was mixed thoroughly with a pipette until fully dissolved. The standard stock solution provided 300 ng/mL PSMA. A serial dilution was made to provide standard solutions of 0, 4.69, 9.38, 18.75, 37.5, 75, 150 and 300 ng/mL.

Biotinylated primary antibody working solution

The stock solution (100X) was centrifuged at 200 x *g* for two minutes prior to use. It was diluted to a 1X working solution by adding 120 µL of the stock in 11 880 µL of the antibody diluent solution.

HRP conjugated secondary antibody working solution

The stock solution (100X) was centrifuged at 200 x *g* for two minutes prior to use. It was diluted to a 1X working solution by adding 120 µL of the stock in 11 880 µL of the secondary antibody diluent solution.

Protease inhibitor solution

Protease inhibitor solution (50 mL) was purchased from Sigma-Aldrich (St. Louis, USA) and was added to prevent protein degradation. The concentration of the protease inhibitor stock solution was 25X. For the working solution, 10µL of protease inhibitor was added to 240µL of PBS to make a 1in 25 working solution. The cells were resuspended in the protease inhibitor working solution.

3 Results and Discussion

3.1 Phase contrast microscopy and Crystal Violet assay – Optimisation

3.1.1 Cell detachment methods

Trypsin is a proteolytic enzyme which cleaves arginine and lysine at the C-terminal (Olsen *et al.,* 2004). A highly specific protease with proteolytic aggressiveness, trypsin is commonly used to detach adherent cells during cell culture (Huang *et al.,* 2010, Olsen *et al.,* 2004). Worryingly, the proteolytic activity of trypsin has been demonstrated to cleave a large population of cell membrane proteins (Huang *et al.,* 2010). As PSMA is a transmembrane protein, it may be cleaved by trypsin. As such, alternative methods of cell detachment should be comparatively assessed against trypsinisation. One alternative is mechanical scraping that involves physical removal of cells from the surfaces to which they are adherent without the potential of PSMA receptor enzymatic cleavage (Lin *et al.,* 2006, Mahabadi *et al.,* 2015). Mechanical scraping similar to trypsinisation has its own shortfalls. Mechanical dissociation has been shown to disrupt cellular membrane integrity (Mahabadi *et al.,* 2015). This could have an effect on cell viability and influence downstream assay outcomes negatively (Mahabadi *et al.,* 2015) and could also release intracellular proteases that could cleave numerous surface proteins.

3.1.2 Phase contrast microscopy

Scraped cells notably exhibited a substantial amount of clumping (red arrows) and clustering when compared to trypsinised cells (Figure 3.1). The mechanical force applied when scraping results in cell lysis, cells that are non-uniform in shape and cell clumps surrounded by substantial quantities of debris (Mahabadi *et al.,* 2015). When cells lyse, DNA, organelles and intracellular proteins leak out of the cells into the extracellular space (Newton *et al.,* 2017). Cellular DNA is naturally adhesive and upon leakage causes other cells and surrounding debris to aggregate into clusters and clump (Sakamoto *et al.,* 1999). Cell clumping creates and oxygen/nutrient gradient limiting access to critical nutrients when sub-culturing (Su and Lee, 2007). As a result the overall growth of the cells is affected over time (Su and Lee, 2007).

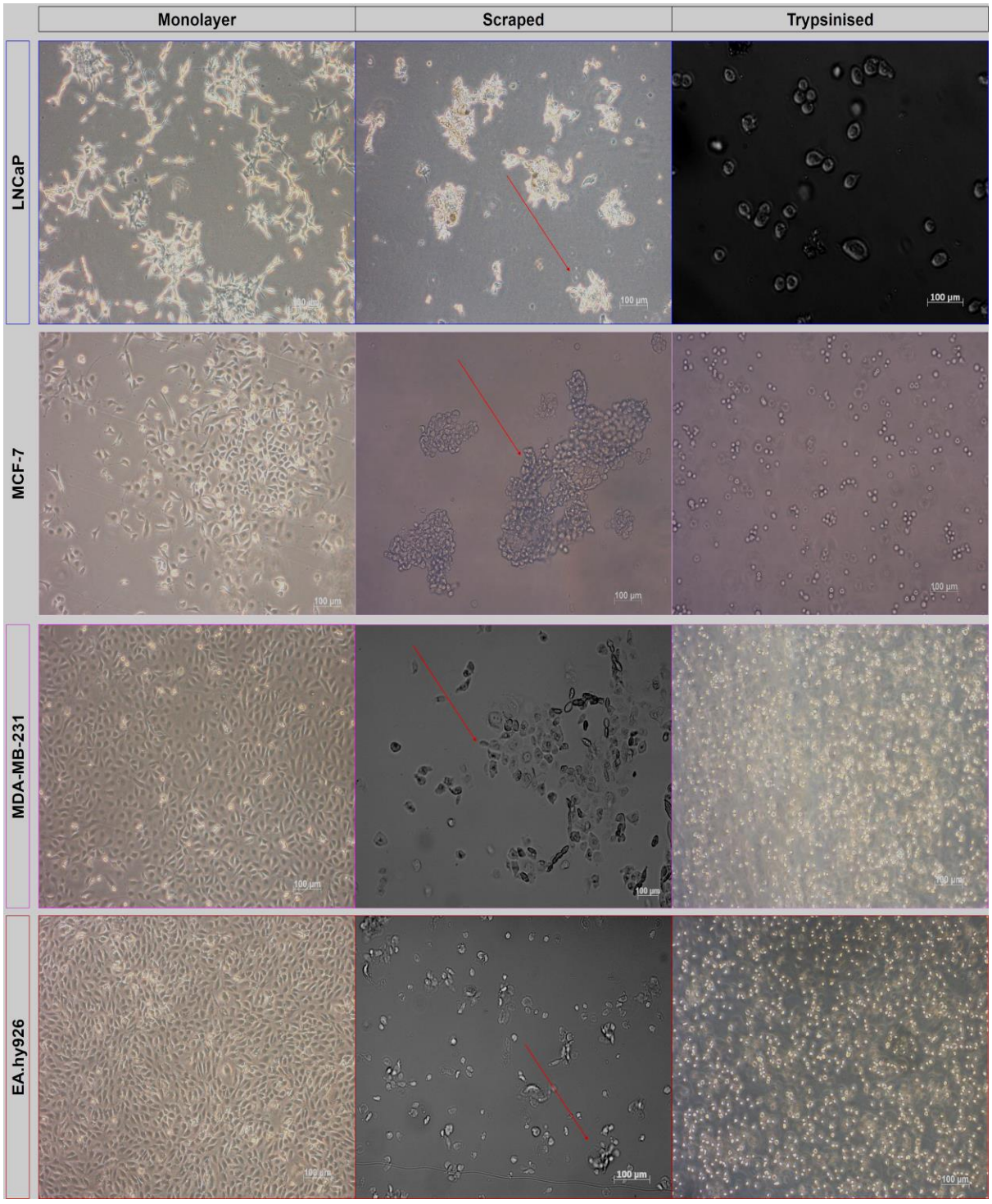

Figure 3-1 Monolayer, trypsinised and scraped images phase contrast images of trypsinised and scraped LNCaP MCF-7, MDA-MB-231 and EA.hy926 cells at 10X magnification. Red arrows indicate cell clustering. (Image brightness adjusted)

3.2 Crystal Violet assay

The limited access to nutrients in scraped cells added to the accumulation of debris compromises culture conditions and does not permit optimal cell growth after passaging. These negative effects on downline growth can be clearly observed when comparing the next generation Crystal Violet assay results of trypsinised versus scraped cell cultures. Cell number at 24 hours was used as starting point (100%). The increase in cell number at 48 and 72 hours was then calculated as a percentage increase from 24 hours. A consistent trend displaying lower cell numbers percentages for scraped cells was observed (Figure 3.2). Though statistically insignificant, trypsinised cells demonstrated higher cell number percentages at 48- and 72-hour culture times in all four cell cultures relative to the cell number at 24 hours. For trypsinised LNCaP cells (Figure 3.2A), cell number increased by ±56% after 48 hours and ±100% after 72 hours. Scraped LNCaP cell number contrastingly increased by 41% and 70% after 48 and 72 hours respectively. In EA.hy926 cells (Figure 3.1B), trypsinised cell number increased by ±32% and ±101% at 48 and 72 hours respectively. Scraped EA.hy926 cells reported lower cell number increases of ±29% at 48 hours and ±74% at 72 hours. The trypsinised MCF-7 cell number increased by ±48% after 48 hours and ±192% after 72 hours (Figure 3.2C) while scraped MCF-7 cells showed increases of ±46% at 48 hours and 164% at 72 hours. Triple negative MDA-MB-231 cells (Figure 3.2D) reported increases of ±162% after 48 hours and 545% after 72 hours in trypsinised cell number. Scraped cell number increased by 90% after 48 hours and 261% after 72 hours, in MDA-MB-231 cells

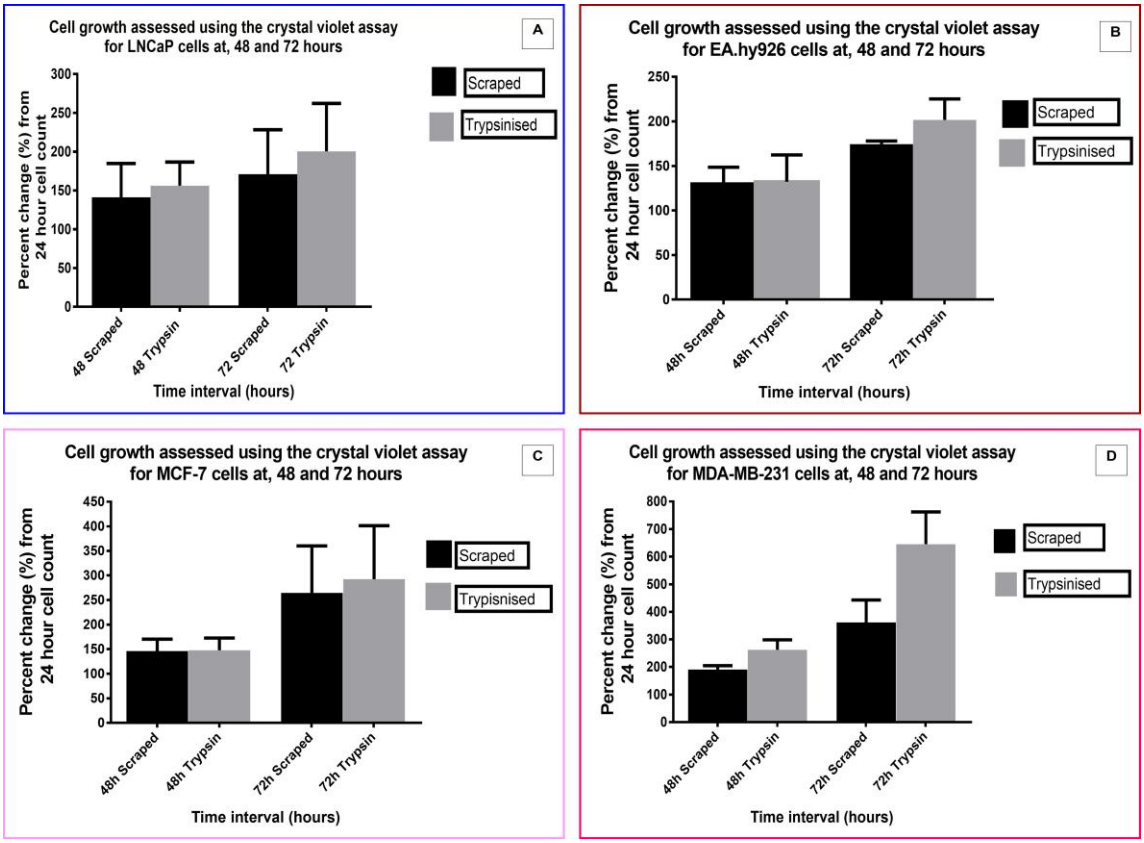

Figure 3-2 Graphs representing growth of LNCaP (A), Ea.hy926 (B), MCF-7 (C) and MDA-MB-231 (D) monolayer cells at 48 and 72 hour time intervals after scraping (black) or trypsinisation (grey) assessed by the Crystal Violet assay. N= 3 repeats, error bars are representative of standard error of the mean (SEM).

A characteristic mammalian cell growth curve presents a sigmoidal log phase proliferation (Figure 3.2). The curve typically shows a lag phase, log phase, stationary phase for growth and death phase (Nagabhushanam, 1997). Switches in growth phases depend on time and culture conditions that change (Nagabhushanam, 1997, Pan *et al.,* 2017). These changes include nutrient depletion and/or waste accumulation which drives the transition in growth phases (Pan *et al.,* 2017).

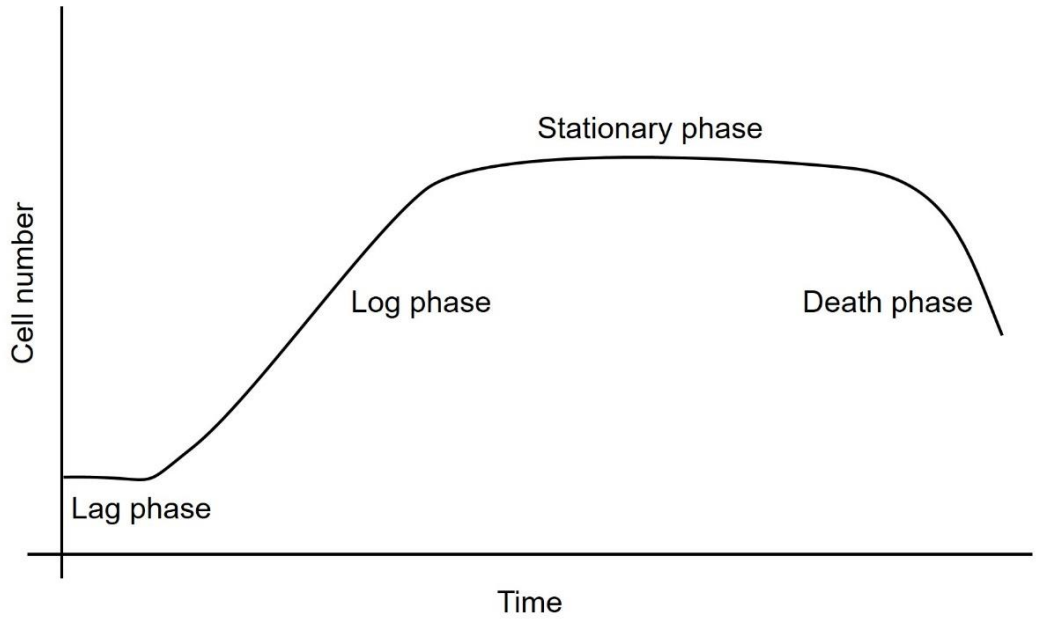

Figure 3-3 Graph of the typical growth phases of mammalian cells in culture (Used with permission)

Cells are typically in a lag phase in the first 24 hours of growth (Nagabhushanam, 1997). Cells in the lag phase do not divide, they are recovering from stress as a result of sub-culturing and simultaneously acclimatising to their new growth conditions (Nagabhushanam, 1997). At 24 hours sub-culturing, the cells were most likely in their lag phase of growth hence; a significant discrepancy in cell number compared to longer culture times would be expected. Cell numbers had increased by 48 hours and 72 hours in both trypsinised and scraped cells. It can be reasoned that cells moved from their initial lag phase to a logarithmic growth phase. In the exponential phase of growth, cells access the nutrients surrounding them and the rate of proliferation begins to increase resulting in the observed increase in cell numbers (Nagabhushanam, 1997, Pan *et al.,* 2017). Simultaneously, the growth disadvantages conferred by scraping were disclosed. Mechanically scraped cells over time, consistent with literature, reported lower percentage increases in cell number contrasted to trypsinised cells (Bundscherer *et al.,* 2013, Huang *et al.,* 2010). The longer the cells were cultured the higher the cell numbers in both detachment methods. However, trypsinisation appears to be a superior method of cell detachment in that cell proliferation capacity is preserved.

Over and above cell proliferation preservation, trypsinisation has the least damaging effect on cell morphology (Batista *et al.,* 2010). Favourably, trypsinisation provides unclustered single cell suspensions preserving a typical round cell morphology (Mahabadi *et al.,* 2015). Using scraping to release the cells appears not to achieve this. The clumping of the cells means that, they cannot be used for other experiments such as flow cytometry which

depends on single cell suspensions. Although trypsin digestion can potentially cleave the transmembrane PSMA, which is an undesirable outcome, cells were trypsinised to release them for further downline culturing and preparation of free cells for marker assays. Tykvart et al. (2014) probed for PSMA on LNCaP cells using the YPSMA-1 monoclonal antibody. The cells generated satisfactory, reproducible and useful data in that study. Based on their success, PSMA was probed downstream utilising trypsinised cells of all the cells used in this study and the same antibody and no obstacles were encountered.

3.3 Indirect flow cytometry - PSMA identification

Data generated utilising flow cytometry demonstrated PSMA positive but different intensity signals in all four of the probed cell lines. The depicted figures below the fluorescent intensity is represented on the x-axis in log scale while the number of events (or individual cells) is on the y-axis in the form of histograms. The histograms on the right represent an increasing shift in fluorescence from the histogram of control cells on the left that would represent the background and non-specific binding of fluorophore.

3.3.1 LNCaP cells – Flow cytometry

The generated univariate histograms disclosed LNCaP cells predictably express abundant PSMA levels (Figure 3.4). Using a logarithmic scale, the unstained sample (blue) peaked just above 4th decade with an intensity value ±14 800 (Figure 3.4A). The stained sample (red) peaked above the 5th decade with an intensity value of ±152 720 (Figure 3-4B). The difference in florescence between the unstained and stained sample was more than ten-fold.

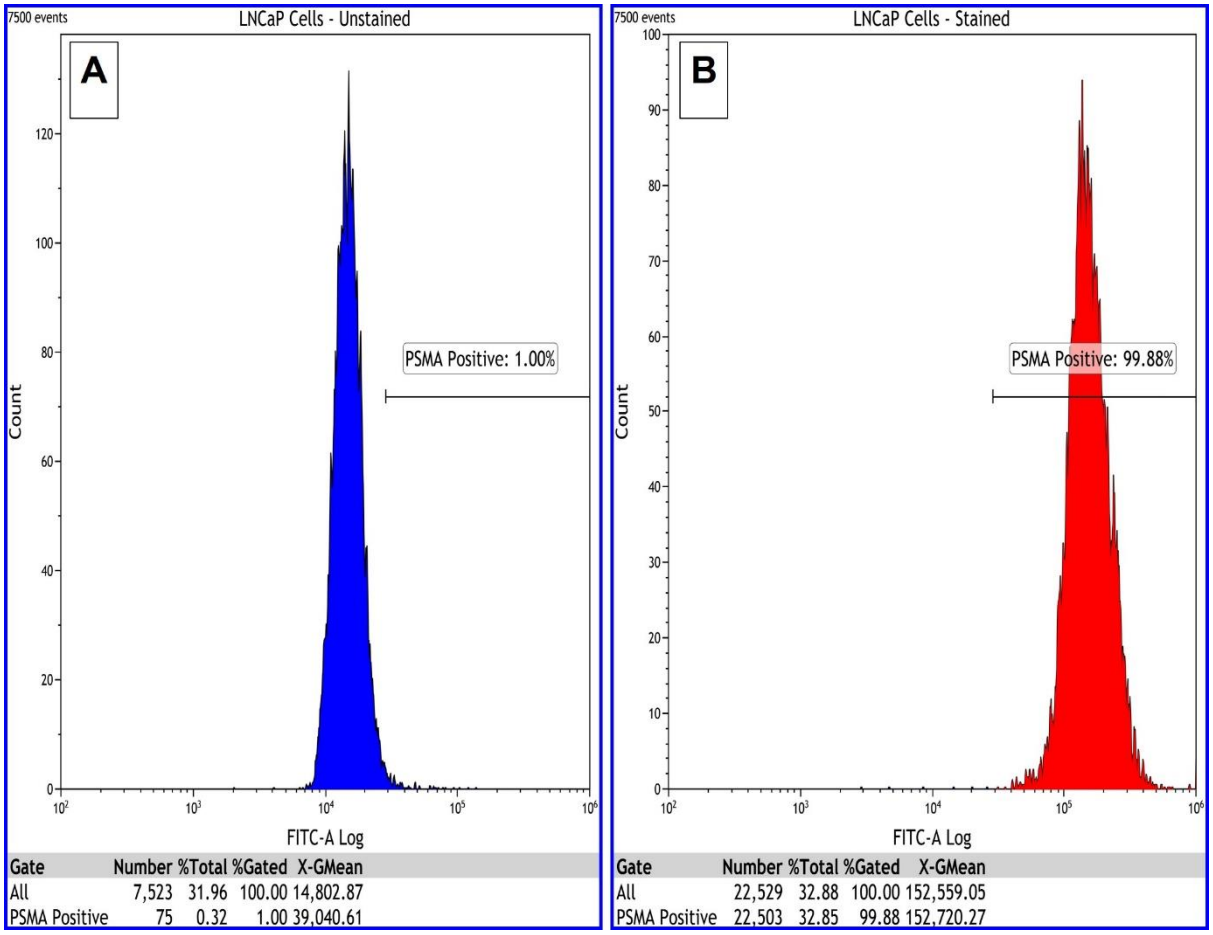

Figure 3-4 Flow cytometry histogram depicting PSMA binding in unstained (A) and stained (B) LNCaP cells (7500 events x 3 repeats). Note the gate position has remained constant.

Fluorescence intensity shares a linear relationship with concentration (Brown and Wittwer, 2000). The higher the fluorescence, the more abundant the antigen. The elevated fluorescence intensity identified for LNCaP cells is directly proportional to the expressed PSMA concentration. This increased concentration confirms the utility of PSMA in clinical prostate cancer diagnosis and therapy. Additionally, the results demonstrated above stand in continuity with published literature on PSMA expression in LNCaP cells (Abdolahi *et al.,* 2013, Tykvart *et al.,* 2014). Identifying PSMA expression in LNCaP cells did not speak to the aim of this study but confirmed that the logic and methodology was applicable for the study and confirmed that the LNCaP cells could be used as positive control cells for PSMA expression. A fundamental point of departure from which PSMA expression in the breast carcinoma cell lines could be investigated was established.

3.3.2 MCF-7 cells – Flow cytometry

The MCF-7 cells also proved to be PSMA positive (Figure 3.5). They presented with a percentage expression of 99.89%. The unstained MCF-7 histogram (pink) peaked about the 4th decade with a fluorescence intensity value of ±8 130 (Figure 3.5A). The histogram for the stained cells (red) shifted to peak above the 4th decade at ±$10^{4.586}$ with a corresponding fluorescence intensity value of ±38 630 (Figure 3.5B).

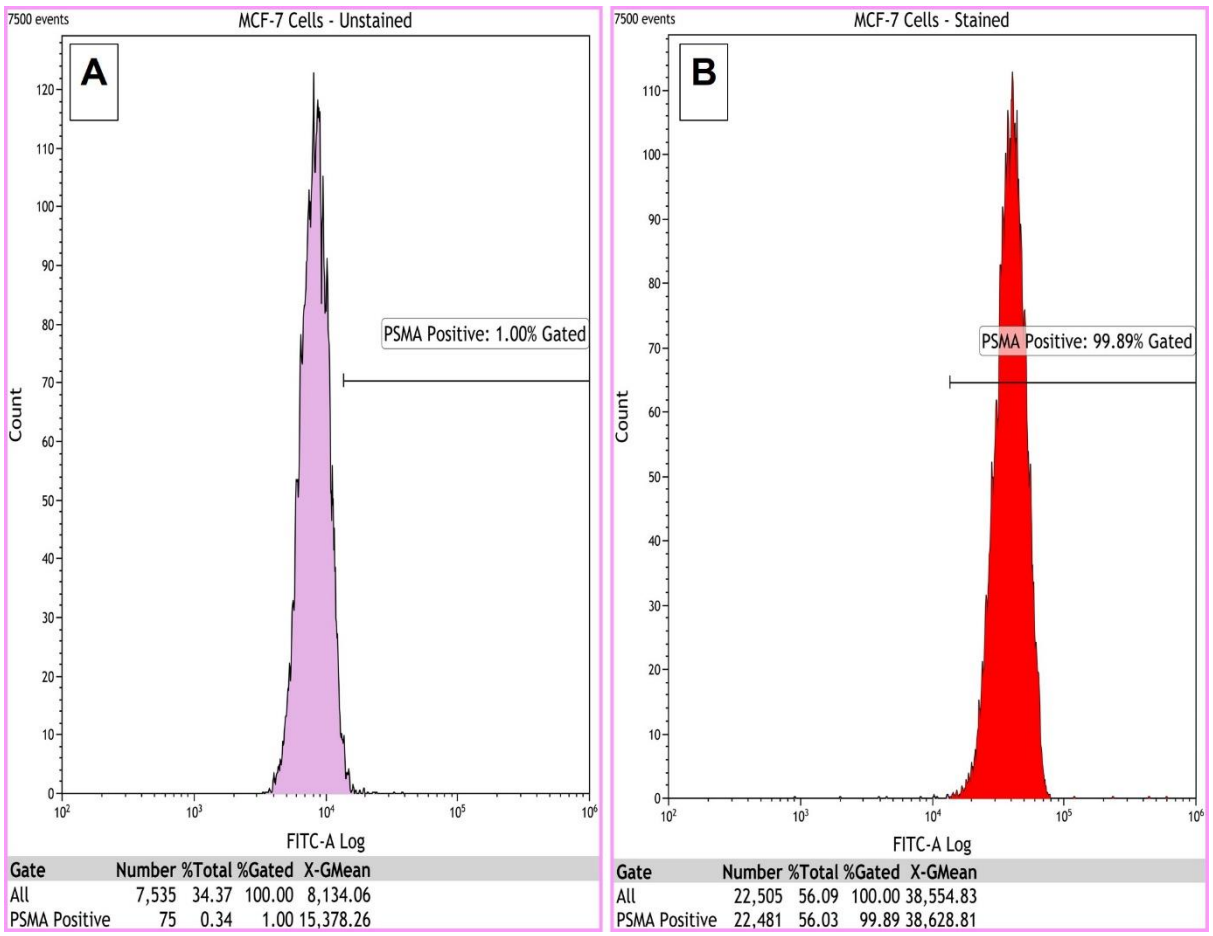

Figure 3-5 Flow cytometry histogram depicting PSMA binding in unstained (A) and stained (B) MCF-7 cells (7500 events x 3 repeats). Note the gate position has remained constant.

Expression of PSMA is associated with cancer aggression, metastatic progression and increased malignancy (Chen *et al.,* 2017). Characteristics which are not characteristics associated with MCF-7 cells. The MCF-7 cells are poorly-aggressive, non-invasive and considered to have low metastatic potential (Feng *et al.,* 2018, Shirazi *et al.,* 2011). More specifically, MCF-7 cells are generally considered to be PSMA negative (Xu *et al.,* 2018). The above result displayed contrasting information.

In support of this result, there is literature documented expression of PSMA genes in ER/PR positive breast carcinomas (Dharmasiri *et al.,* 2009, Gala *et al.,* 1998). Utilising reverse transcription polymerase chain reaction (RT-PCR), Gala *et al* (1998) reported PSMA positive detection signals above 50% in MCF-7 cells (Gala *et al.,* 1998). In addition, other luminal A cell lines have also been reported to express PSMA. Epithelial T-47D cells are ER/PR positive and were similarly originally isolated from the pleural effusions of metastatic breast adenocarcinoma (Aka and Lin, 2012). The expression data of PSMA on the human protein atlas (HPA) revealed positive identification in luminal A breast carcinoma T-47D cells (Thul *et al.,* 2017). While they are different cell lines and have different protein profiles, MCF-7 and T-47D cell cultures share several proteins that are involved in proliferation and cancer development (Aka and Lin, 2012).

To further confirm the result, formalin fixed MCF-7 cells were also tested for PSMA expression. Treatment of histological slices with methanol dehydrates the tissue and removes lipids, precipitating the proteins, while formalin is an aldehyde that crosslinks proteins (Hobro and Smith, 2017). Formalin fixed MCF-7 cultures were PSMA positive and fluorescence peaked at ±15 490. The fluorescent advantage that methanol has over formalin is its removal of lipids leading to a brighter signal hence the observed difference in fluorescence intensity (Hobro and Smith, 2017). Cytometric identification utilising different fixatives in MCF-7 cells along with literature reported PSMA identification in T-47D cells suggests PSMA expression as being reliably positive in luminal A carcinomic cultures. Its exact function and location is yet to be elucidated in MCF-7 cells. What is important is that flow cytometric identification of PSMA in these MCF-7 cell lines serves as an introductory premise to investigate any arising questions. Despite positive PSMA expression in MCF-7 cells, the fluorescence intensity was four times less that demonstrated by the LNCaP positive control cells, indicating an approximately of four times greater PSMA expression in the LNCaP cell line.

3.3.3 MDA-MB-231 cells – Flow cytometry

The MDA-MB-231 also displayed positive PSMA expression (Figure 3.6). The unstained MDA-MB-231 histogram (magenta) peaked at about the 4th decade. The unstained fluorescence intensity was recorded at ±8 800 (Figure 3.6A). This is contrasted to the stained cells where the histogram (red) peaked at ±$10^{4.598}$. Fluorescence intensity in the stained MDA-MB-231 cells was recorded at ±39 140 (Figure 3.6B).

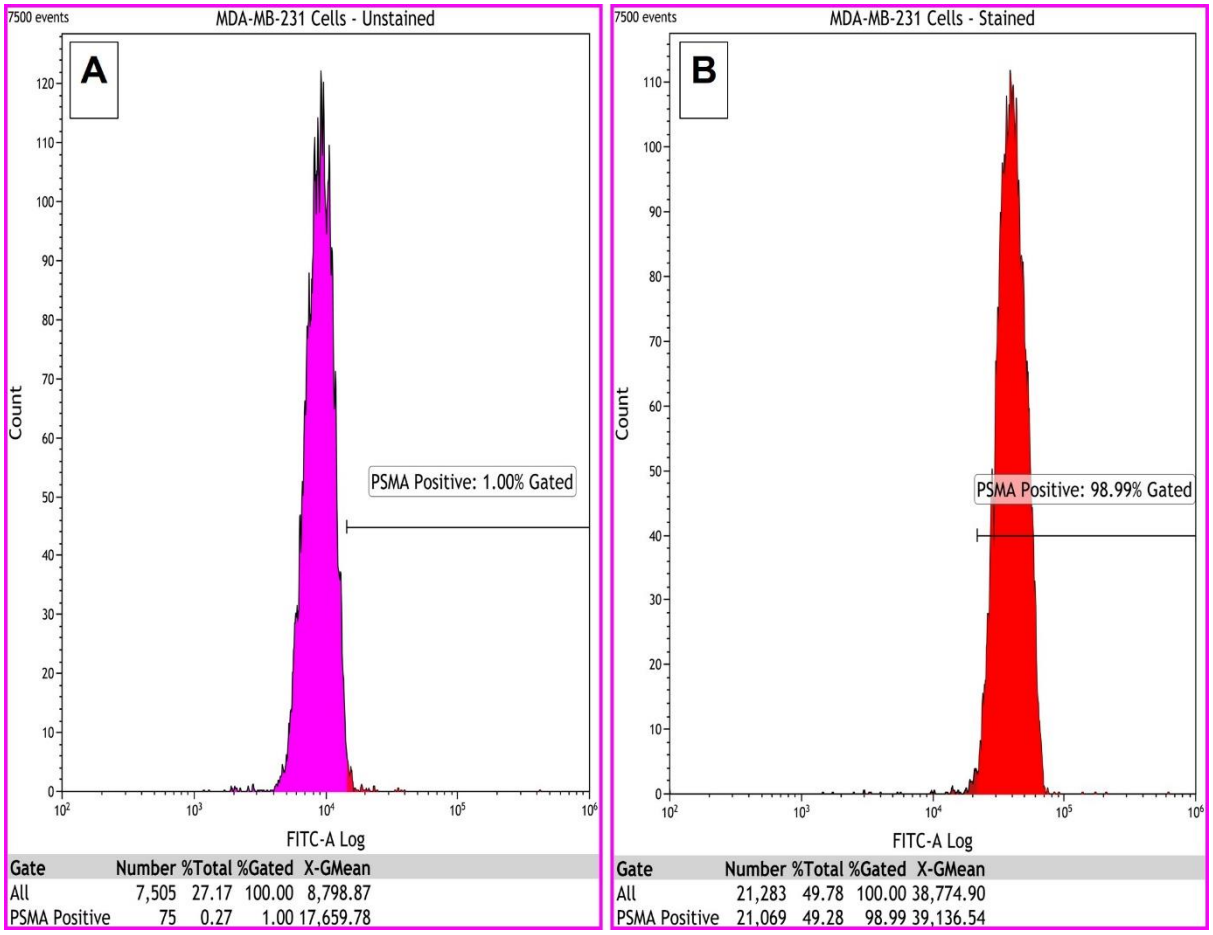

Figure 3-6 Flow cytometry histogram depicting PSMA binding in unstained (A) and stained (B) MDA-MB-231 cells (7500 events x 3 repeats). Note the gate position has remained constant.

Wernicke *et al* (2014) investigated the expression of PSMA in breast carcinoma and endothelial cell lines. In their study, invasive breast carcinomas exhibiting larger tumour size, higher nuclear grade, absence of ER/PR, and high Ki-67 abundance presented with higher PSMA expression (Wernicke *et al.,* 2014). Equally, Kasoha *et al* (2017) investigated PSMA expression in normal and cancerous breast tissue and their results confirmed those of Wernicke *et al*. Expression of PSMA was more abundant in carcinomas with the aforementioned pathophysiological parameters (Kasoha *et al.,* 2017, Wernicke *et al.,* 2014).

Basal MDA-MB-231 cells demonstrate high aggressiveness, ER/PR absence, invasiveness, higher tumour grade and poorer prognosis (Holliday and Speirs, 2011). The pathophysiological profile supports higher PSMA expression which is confirmed in this study. Although PSMA expression was present and abundant, it was four times less than the levels seen in the LNCaP cells, similar to the levels seen in MCF-7 cells. Be that as it may, this

cytometric identification of PSMA in MDA-MB-231 cells presents a valuable opportunity. This is because, triple negative carcinomas characteristically lack established targets for diagnostic and therapeutic application (Feng *et al.,* 2018). A number of approaches have been studied to address the diagnostic and therapeutic demands of TNBC yet, to date none have realised their anticipated success. There is a demand for new contemporary approaches in TNBC management (Aysola *et al.,* 2013, Board, 2020a). The identification of PSMA in MDA-MB-231 cells in this study may provide an as yet unexplored paradigm in clinical TNBC management. Additional research is necessary to validate the location, function and exact kinetics of PSMA in MDA-MB-231 cells.

3.3.4 MCF-7 cells and MDA-MB-231 cells – Flow cytometry

Luminal A MCF-7 cells and basal triple negative MDA-MB-231 individually exhibited PSMA expression. Assessment of the results revealed marginal differences in measured fluorescence intensity values between these two cell lines (Figure 3.7). The MDA-MB-231 cells intrinsically possess the pathophysiological landscape associated with elevated PSMA expression and expectedly exhibited higher PSMA concentration. Despite this fact, the cytometric identification of PSMA in breast carcinomas of differential molecular classification is indicative of its potential in broad breast cancer management.

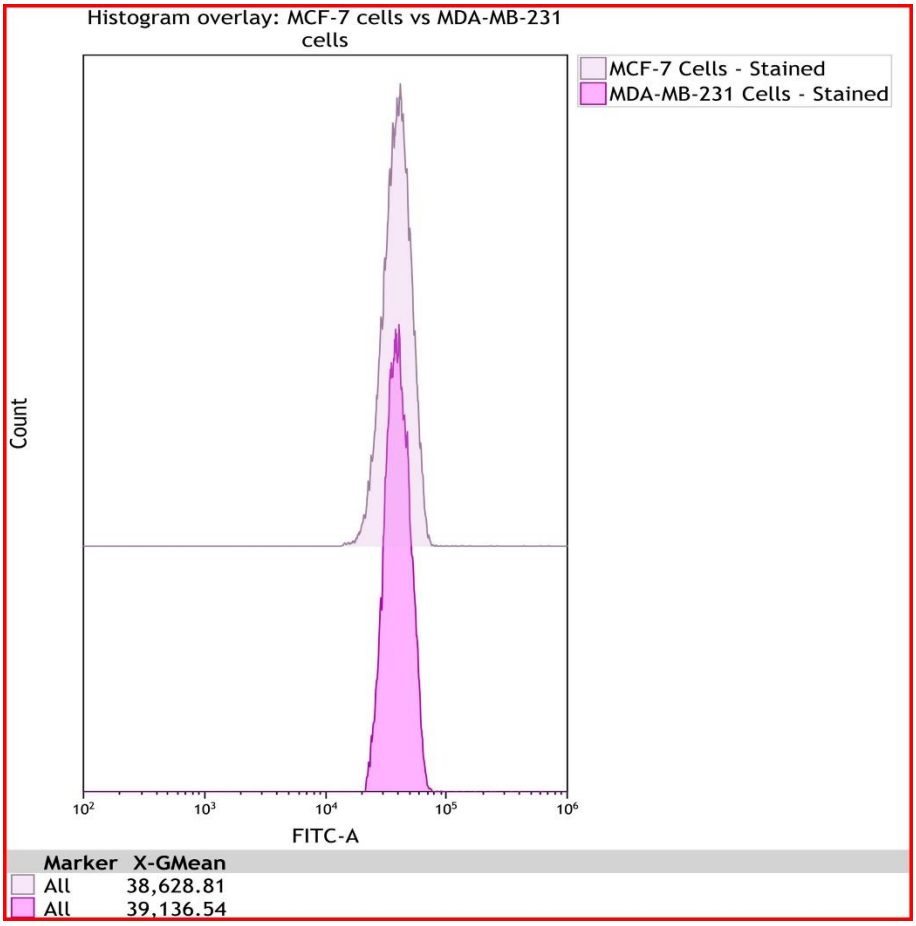

Figure 3-7 Half offset histogram overlay representing MCF-7 fluorescence intensity compared to MDA-MB-231 fluorescence intensity.

Ziegler *et al* (2014) studied the proteomic differences between MDA-MB-231 and MCF-7 cells (Ziegler *et al.,* 2014). The study focused on plasma membrane (PM) proteins in an attempt to identify new oncogenic targets for breast cancer therapy. The MDA-MB-231 cells totalled 6483 PM proteins while MCF-7 cells produced 5704 PM proteins (Ziegler *et al.,* 2014). Their study also revealed that the two cell lines shared 3500 PM proteins between them. This figure means that more than 50% of the PM proteins identified overlap between cell lines that are molecularly different (Ziegler *et al.,* 2014). That being the case, the identification of PSMA utilising flow cytometry in both MCF-7 and MDA-MB-231 cells is conceivable. The PSMA antigen may possibly be a shared PM protein expressed in MDA-MB-231 and MCF-7 cells. The more aggressive and metastatic MDA-MB-231 cells exhibited more PM proteins than MCF-7 cells (Ziegler *et al.,* 2014). Additional novel unidentified target proteins other than PSMA may be present in these cells which can be directed toward TNBC management. The presence of a particular protein does not automatically make them viable diagnostic and therapeutic targets. Similar to this study, these potential targets need to be

identified, localised studied and validated to confirm their possible application in managing a challenging cancer subtype.

3.3.5 EA.hy926 cells – Flow cytometry

The reported expression of PSMA in tumour-associated neovasculature presented an interesting dimension for investigation through endothelial EA.hy926 cells (Wernicke *et al.,* 2014). The endothelial EA.hy926 cells also presented with positive PSMA expression (Figure 3.8). The unstained histogram (brown) peaked around the 4th decade with a fluorescence intensity of ±11 830 (Figure 3.8A). The histogram shifted in the stained cells (red) peaking at ±$10^{4.530}$ with a fluorescence intensity of ±33 900 (Figure 3.8B).

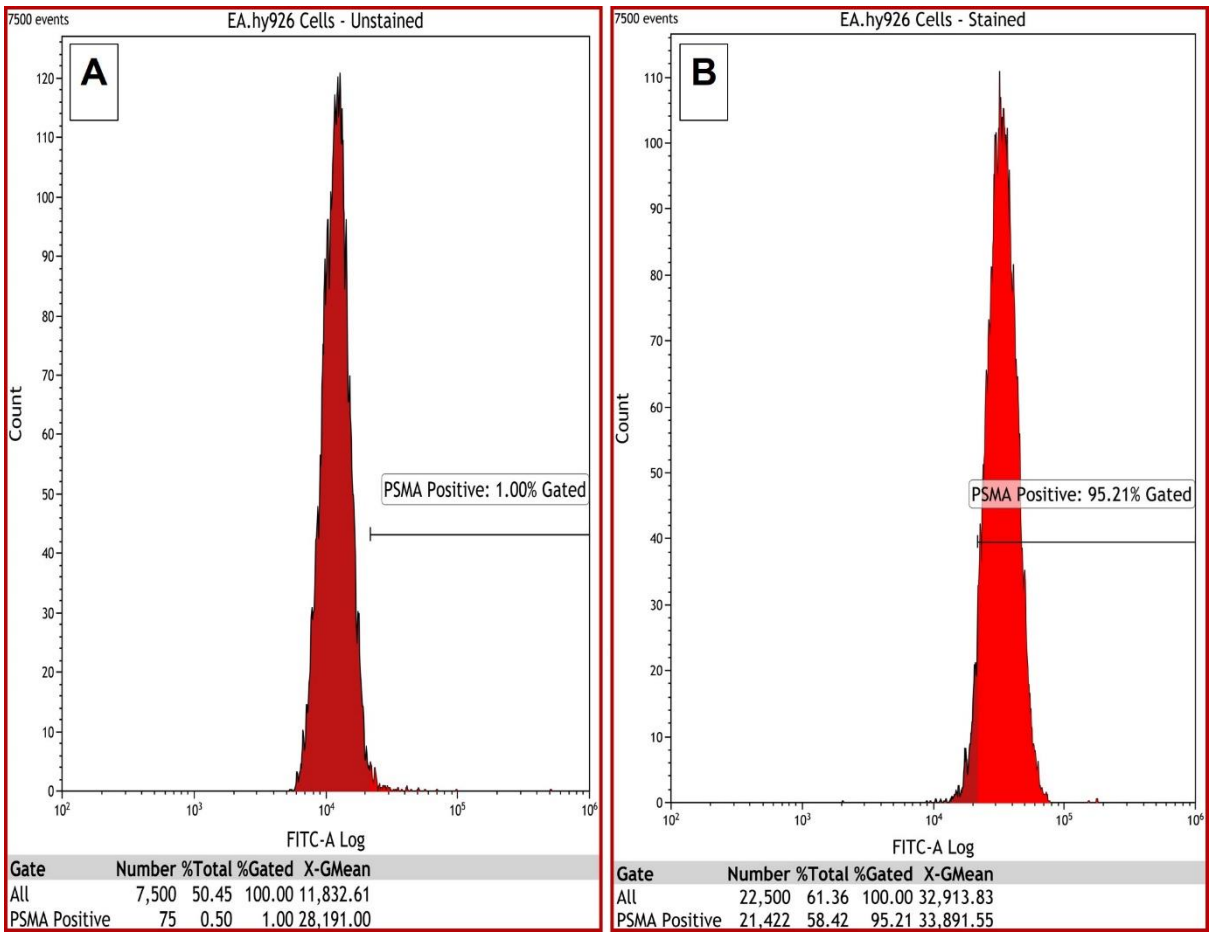

Figure 3-8 Flow cytometry histogram depicting PSMA binding in unstained (A) and stained (B) EA.hy926 cells (7500 events x 3 repeats). Note the gate position has remained constant.

Normal vasculature does not express PSMA however, consistently PSMA has been localised in tumorous neovasculature. So much so that it has been implicated in regulation of angiogenesis (Sathekge *et al.,* 2017). Angiogenesis is initiated by endothelial cells (Wang *et*

al., 2015). Furthermore, angiogenesis is rare in adults. It usually occurs as a result of pathology, contributing to cancerous tumour growth and metastasis (Conway *et al.,* 2006). In culture, EA.hy926 cells retain their endothelial characteristics and can be manipulated to exhibit a pro-angiogenic phenotype (Baranska *et al.,* 2005). The cells are used in research to understand the interactions of endothelial cells and tumorous cells in order to understand tumour angiogenesis (Lu *et al.,* 2009).

The EA.hy926 cells have been reported to express a differential proteomic profile compared to the HUVEC's, from which they were originally isolated (Baranska *et al.,* 2005). Comparative two-dimensional gel electrophoresis revealed great similarity exists in the expressed proteins between HUVEC's and EA.hy926 cells (Baranska *et al.,* 2005). In the same analysis, consistently, specific proteomic differences were observed. Proteins that were expressed in HUVEC's were unidentifiable in EA.hy926 cells conversely, several proteins that are not expressed in primary HUVEC's were identified in EA.hy926 cells (Baranska *et al.,* 2005). Similarly, A549 cells, from which the EA.hy926 hybrid cell line was derived also show significant proteomic differences when compared to EA.hy926 cells (Lu *et al.,* 2009). More particularly, 28 proteins that are linked to cell proliferation, differentiation, apoptosis, invasion and metastasis are differentially expressed between EA.hy926 cells and A549 cells (Lu *et al.,* 2009). Again, these features also support PSMA expression in the EA.hy926 cell line (Wernicke *et al.,* 2014).

Taken together, the expression of PSMA by HUVEC's can be deductively eliminated. This is because PSMA expression has been identified only in tumour neovasculature but not in normal vasculature endothelium (Wang *et al.,* 2015). The PSMA promoter and PSMA enhancer (PSME) are located within the FOLH1 gene and together regulate the expression of PSMA (Lee *et al.,* 2003). Noss *et al* (2002) reported that PSME transcribes PSMA in tumour neovasculature, however this region is generally absent in normal vascular endothelium (Noss *et al.,* 2002). On the other hand A549 cells are lung cancer cells which have been reported to express PSMA (Schmidt *et al.,* 2017).

The expression of PSMA in EA.hy926 may be linked to their lung carcinoma make up. Lung cancer is highly invasive, aggressive, rapidly metastasising and shows a high tumour grade (Lemjabbar-Alaoui *et al.,* 2015). These characteristics are conducive for PSMA expression. Utilising histology, both Wang *et al* (2015) and Schmidt *et al* (2017) investigated the expression of PSMA in lung cancer (Schmidt *et al.,* 2017, Wang *et al.,* 2015). The studies reported the highest levels of expression in the lung neovasculature endothelial cells. This is

supported by other published literature on endothelial cell expression in non-prostatic solid tumours (Haffner *et al.,* 2009, Schmidt *et al.,* 2017, Wang *et al.,* 2015). The lung carcinoma A549 cells possibly provide the endothelial HUVEC's with the ability to express PSMA.

The EA.hy926 cells present pathophysiological characteristics that typify the ability to express PSMA (Lu *et al.,* 2009). However, to-date, this study is the only one to report PSMA expression these cells. Proteomic differences between EA.hy926 cells and their two parent cells exist but identical proteins equally overlap between them (Baranska *et al.,* 2005, Lu *et al.,* 2009). There is no reason why PSMA cannot be expressed by these hybrid cells. Especially when considering the lung carcinoma origin of EA.hy926 cells and the reported expression of PSMA by these lung carcinoma cells. The flow cytometric identification of expression of PSMA in EA.hy926 cells extends the knowledge related to non-prostatic PSMA expression. However, EA.hy926 cells would still need to be subjected to further probing regarding PSMA so as to elucidate the location and exact mechanisms of this reported expression.

3.3.6 Flow cytometry – All cells

Univariate flow cytometry histograms revealed positive PSMA expression in all the probed cell lines. Qualitatively, fluorescence was displayed across all the probed cell lines. Quantitatively, fluorescence intensity differed across all four cell lines (Figure 3.9). Quantitatively, the measured fluorescence was significantly greater in LNCaP cells when compared to the other three cell lines. As the positive control, the LNCaP cells expectedly showed the highest fluorescence intensity. Fluorescence intensity in this case translates directly into PSMA concentration. Basal MDA-MB-231 cells show the second highest concentration of PSMA closely followed by the luminal A MCF-7 cells. The difference in fluorescence between the two breast carcinoma cell lines was however insignificant. The EA.hy926 showed the lowest fluorescence of PSMA, though only slightly less than the breast adenocarcinoma cells. The difference in fluorescence between the endothelial EA.hy926 cells and the breast carcinoma cells was not statistically significant. Of interest was the fact that in initial studies where permeabilisation of the cell membranes was not performed the breast adenocarcinoma cells did not show the fluorescent signal increase seen after permeabilisation which would imply that the PSMA in the breast adenocarcinoma cells is distributed intracellularly.

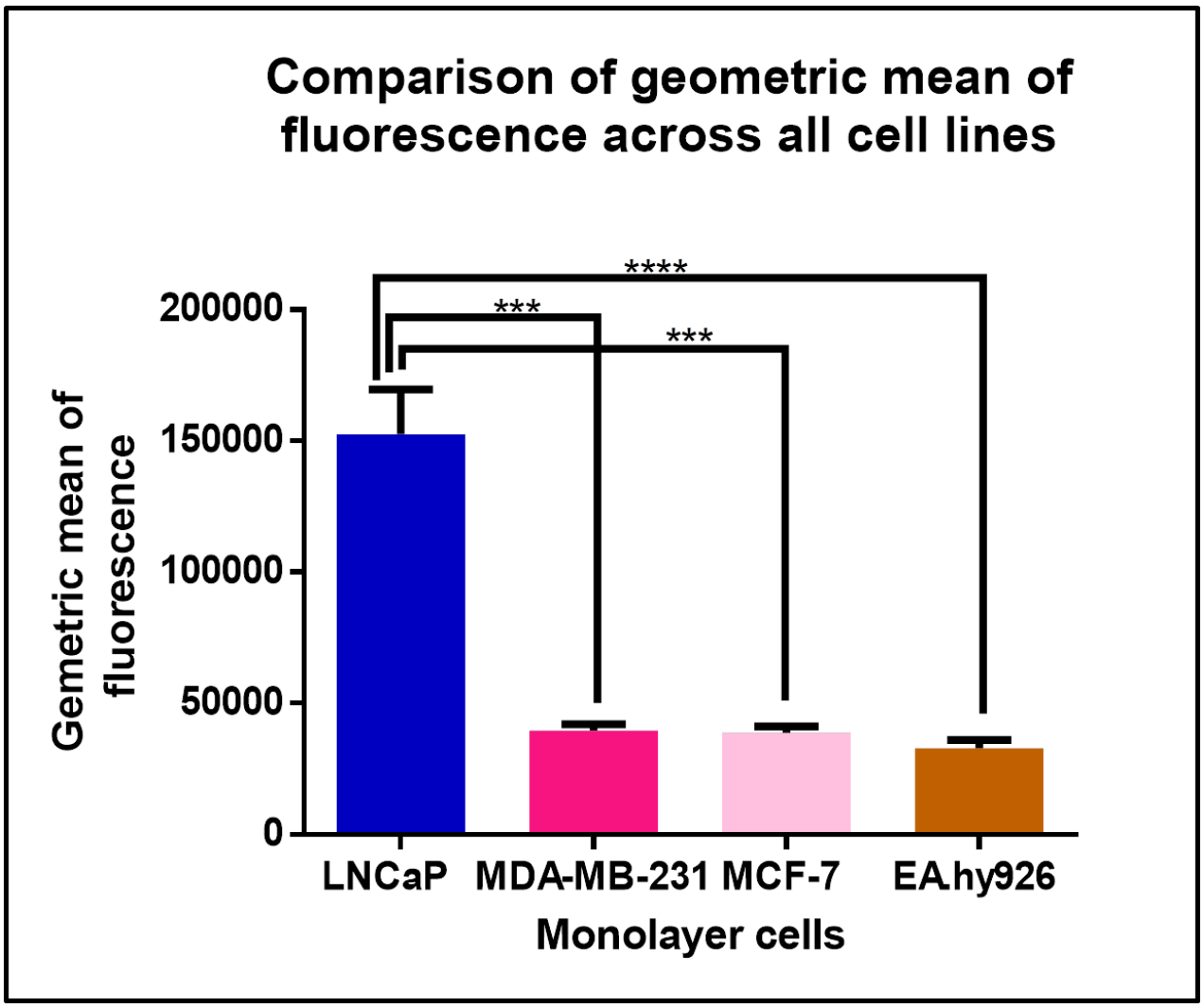

Figure 3-9 Fluorescence intensity comparison across all cell lines. N= 3 independent repeats, (P <0.0001), error bars are representative of standard error of the mean (SEM). Significant differences across different cell lines are represented by (*). Multiple comparisons of a Repeated measures one-way Analysis of Variance (ANOVA).

Flow cytometry coupled to the use of fluorescently tagged antibodies against PSMA proved more than adequate in identification of PSMA on the different cells used in this study. In an attempt to assess the robustness and evaluate the continuity of this positive result, PSMA expression was probed using immunofluorescence and assessed microscopically. Following identification, immunofluorescence was undertaken to elucidate on the location of PSMA in the positive control LNCaP cells and the investigational EA.hy926, MCF-7 and MDA-MB-231 cell lines.

3.4 Indirect immunofluorescence analysis – PSMA localisation

3.4.1 LNCaP cells – Confocal microscopy

Confocal microscopy where both the cell nucleus and the PSMA could be detected simultaneously in 3D stacked scan to provide high resolution spatial distribution information. Again the confocal microscopy using the same fluorescently tagged antibody as used for the flow cytometry revealed positive PSMA staining with spatial localisation in LNCaP prostate adenocarcinoma cells (Figure 3.10). The cells demonstrated intense green FITC fluorescence apparently located in the cell membrane (white arrow). Fluorescence was also diffusely distributed around the cell cytoplasm (blue arrow). The DAPI counterstain (turquoise) disclosed nuclear DNA and did not interfere with the FITC fluorescence. The control LNCaP cells without anti-PSMA antibody did not show any considerable fluorescence (Figure 3-10) indicating specificity of YPMSA-1 antibody in the localisation of PSMA in permeabilised LNCaP cells.

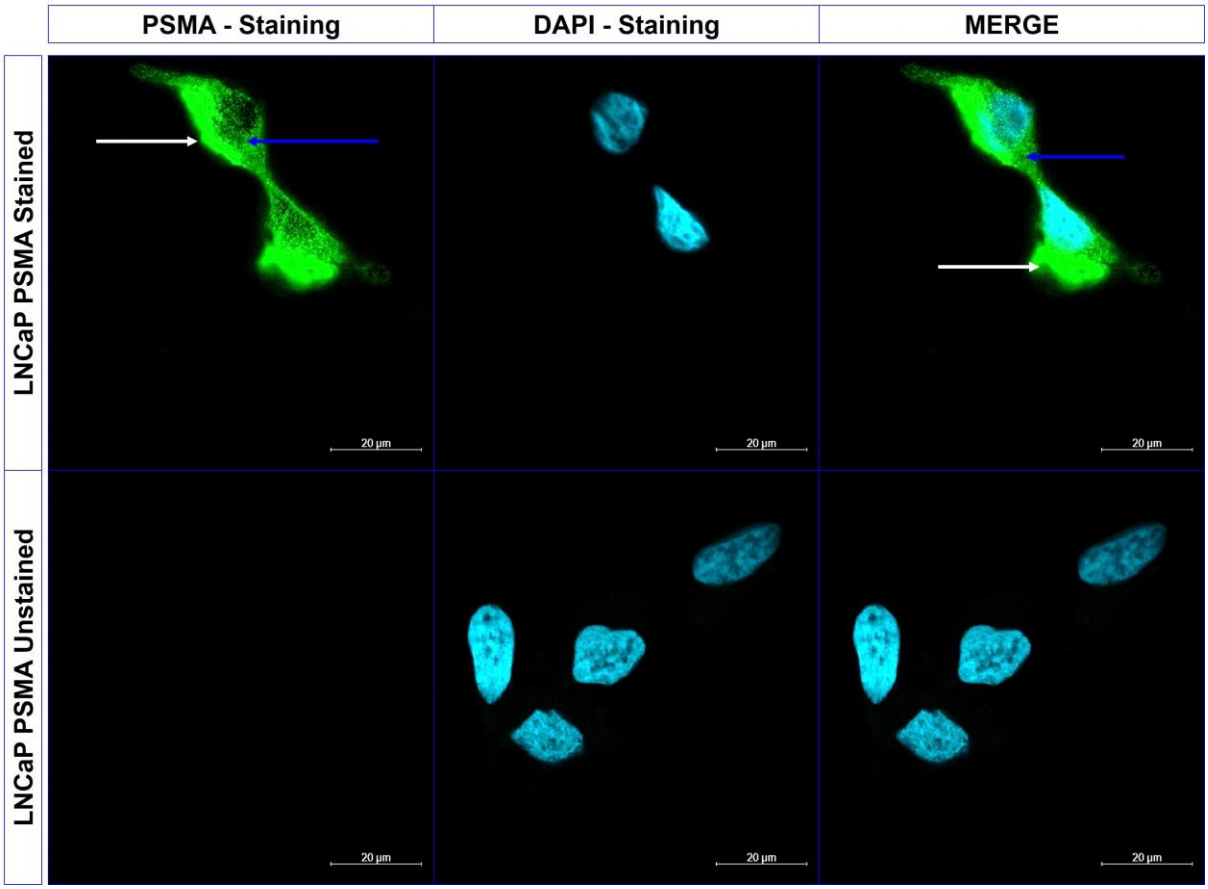

Figure 3-10 Confocal fluorescent microscopy images of LNCaP cells stained with anti-PSMA primary antibody counterstained with a FITC labelled secondary antibody. Turquoise DAPI stains reveal the cell nucleus while, the green indicates PSMA antigen localisation. Control LNCaP cells stained with DAPI but not exposed to anti-PSMA antibodies are shown in the bottom row of images confirming that there was no non-specific binding. Images were taken at 100X magnification. Blue arrow indicates strong cytosolic green fluorescence and white arrows show membrane associated green fluorescence. (Image brightness adjusted)

Localisation of PSMA in LNCaP cells produced results that support the antigen identification undertaken using flow cytometry with the added information of spatial distribution on and in the cells. This consistent finding extends beyond the two methods used in this study to published literature where expression of PMSA is well documented in plasma membrane and the cytoplasm of prostate LNCaP cells (Dowling *et al.,* 2019, Ristau *et al.,* 2014, Thul *et al.,* 2017, Tykvart *et al.,* 2014). The observed fluorescence showed differential intensity between the membrane and the cytoplasm. Green fluorescence around the plasma membrane appeared more intense compared to the dispersed green within the cytoplasm. As fluorescence is directly concentration dependant, it can be deduced that PSMA is more concentrated at the cell membrane than in the cytoplasm of LNCaP cells (Brown and Wittwer, 2000).

3.4.2 MCF-7 cells – Confocal microscopy

The PSMA antigen was positively localised within MCF-7 cells (Figure 3.11) and appeared not to locate to the cell plasma membrane. Intense green fluorescence was consistently detected in relatively small isolated circular regions within the cell (white arrow). Disseminated cytoplasmic green intensity was also seen in the MCF-7 cells (blue arrow). The control with no tagged antibody showed no green fluorescence, indicative of antibody specificity whilst concurrently confirming the observed green intensity as PSMA. Nuclear DAPI staining was observed and did not interfere with FITC fluorescence. The isolated spots of green intensity indicated by the white arrow in MCF-7 cells did not border the cell membrane. Closer inspection reveals that these regions are not just a circular mass of green fluorescence. The green intensity shows a vesicle-like staining pattern and appears to accumulate in the cytoplasmic portion near the cell membrane but not directly on the surface of the cell membrane. The intensity in these circular regions is visibly greater than the green fluorescence dispersed within the cytoplasm indicating PSMA concentration is greatest in these vesicle-like structures than in the cell cytosol.

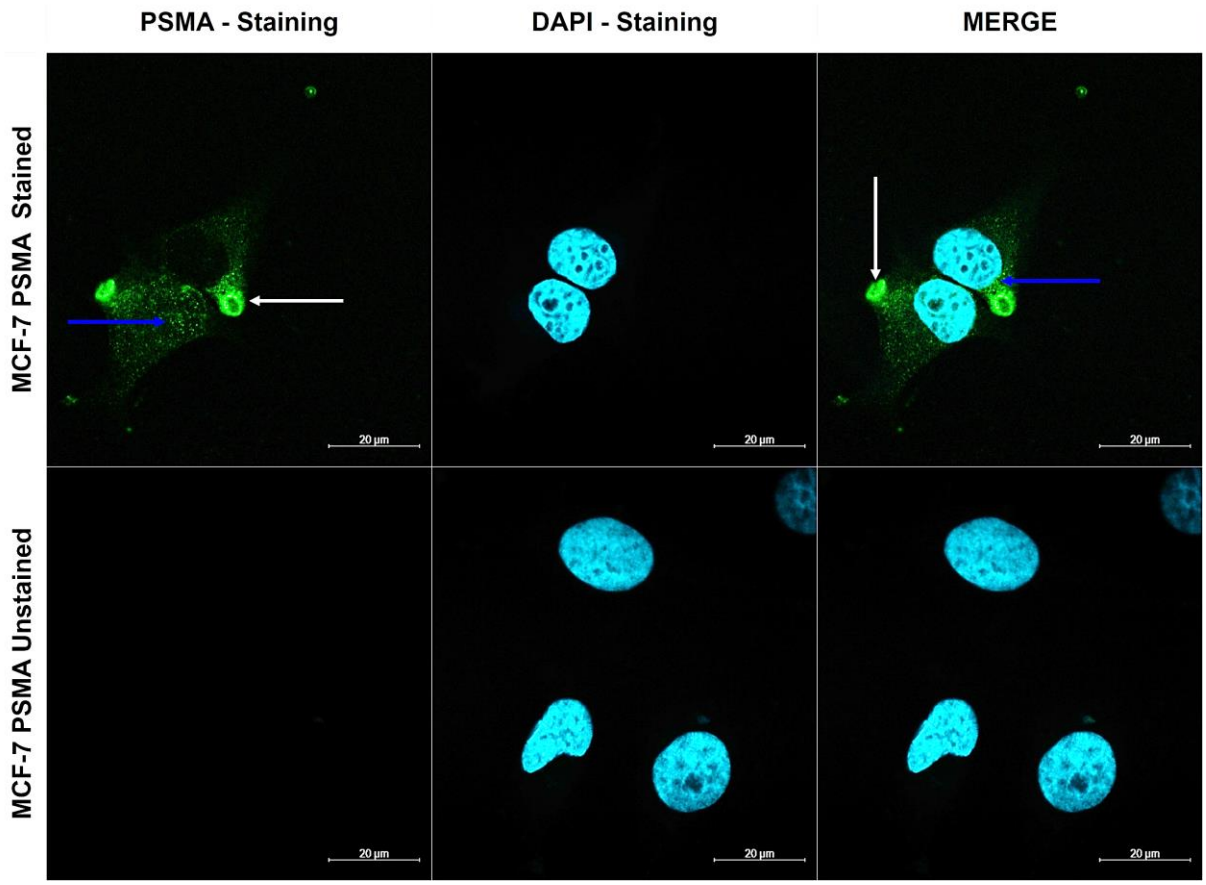

Figure 3-11 Confocal fluorescent microscopy images of MCF-7 cells stained with anti-PSMA primary antibody counterstained with a FITC labelled secondary antibody. Turquoise DAPI stains reveal the cell nucleus while, the green indicates PSMA antigen localisation. Control cells not treated with anti-PSMA antibody do not show green fluorescence, showing that there was no non-specific biding. Images were taken at 100X magnification. Blue arrows indicate diffuse cytosolic fluorescence and white arrows indicate circular intracellular fluorescence accumulation. (Image brightness adjusted)

The generated confocal microscopy images from MCF-7 cells were compared to LNCaP immunoelectron image results generated by Troyer *et al*, (1997) (Figure 3.12). Their study aimed to establish exactly where the diffuse PSMA staining in the cytoplasm was coming from. The PSMA-antibody complex (black arrow of left side image) in the LNCaP cells showed accumulation at the intracellular boundary of the cell membrane (Figure 3.12A). They also reported that localisation of PSMA at the cytoplasmic border of the cell membrane showed a ring-like staining pattern (Troyer *et al.,* 1997). A pattern which is strikingly similar to that seen in confocal MCF-7 images (Figure 3.12B).

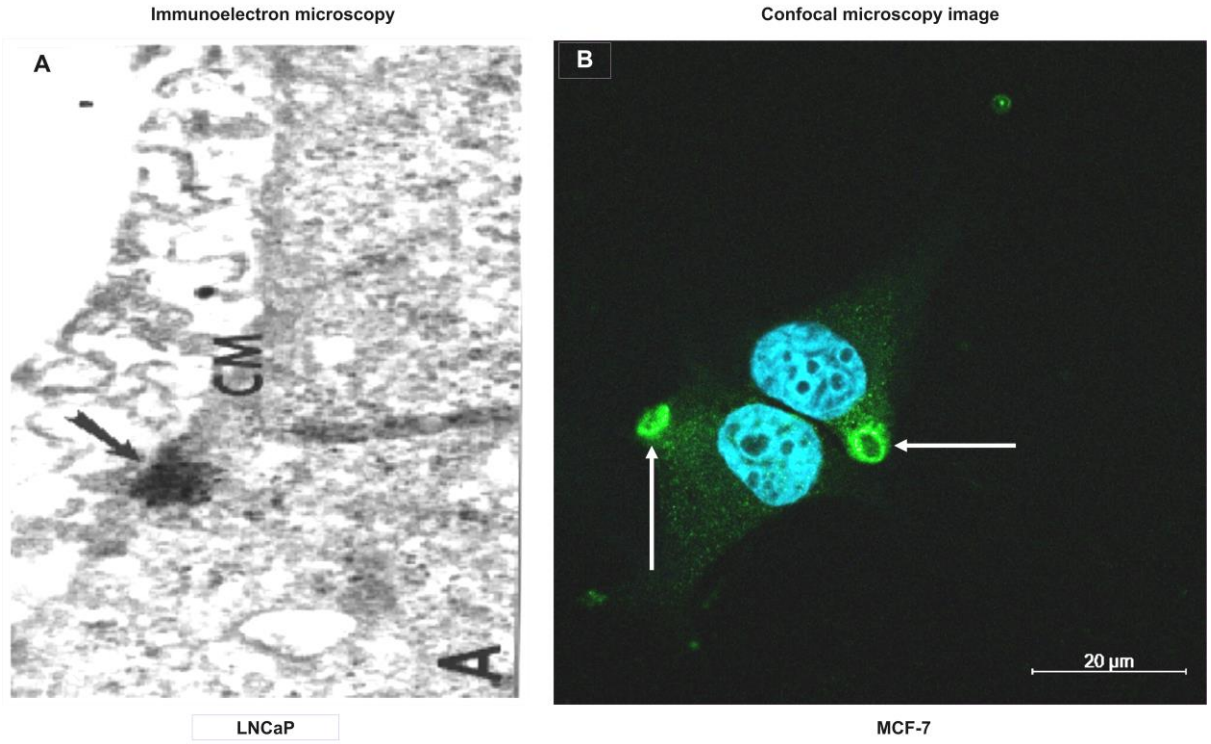

Figure 3-12 MCF-7 cells visualised using confocal microscopy (B) contrasted with LNCaP immunoelectron microscopy image (A). Cell membrane (CM) (Troyer et al., 1997). White arrow indicates circular intracellular accumulation of fluorescence. (Used with permission). (Image brightness adjusted). Magnification (A) x97000

From the confocal microscopy images the location of the PSMA in MCF-7 cells cannot be determined conclusively and may be found at the cytoplasmic border of the cell. Although the expression pattern is similar to that seen in LNCaP immunoelectron localisation the antibodies used bind different epitopes. The antibody used is this study, YPSMA-1 is reported to bind to the extracellular portion of PSMA (Tykvart *et al.,* 2014). The antibody used in the LNCaP immunoelectron microscopy by Troyer *et al*, (1997), 7E11-C5.3 binds on the intracellular portion of PSMA (Tykvart *et al.,* 2014). What is seen in the MCF-7 cells in this study is the binding of an antibody targeting the extracellular portion of PSMA, but clearly accumulating intracellularly in what appears to be a vesicle of some sort. The two antibodies used in these two studies provide different information and it appears that a different distribution of PSMA is evident in MCF-7 cells.

At the membrane, PSMA can undergo unprompted internalisation through endocytic trafficking (Figure 3.13) (Rajasekaran *et al.,* 2005). Ligand biding similarly induces internalisation of PSMA (Rajasekaran *et al.,* 2005). Endocytosis occurs through interaction of cytoplasmic domain of PSMA with clathrin-coated pits (Ghosh and Heston, 2004, Rajasekaran *et al.,* 2005). Receptors can be internalised for delivery of their ligands into the

cell (red circle), digestion in lysosomes (green circle) or recycling (brown circle) (Ghosh and Heston, 2004, Rajasekaran *et al.,* 2005).

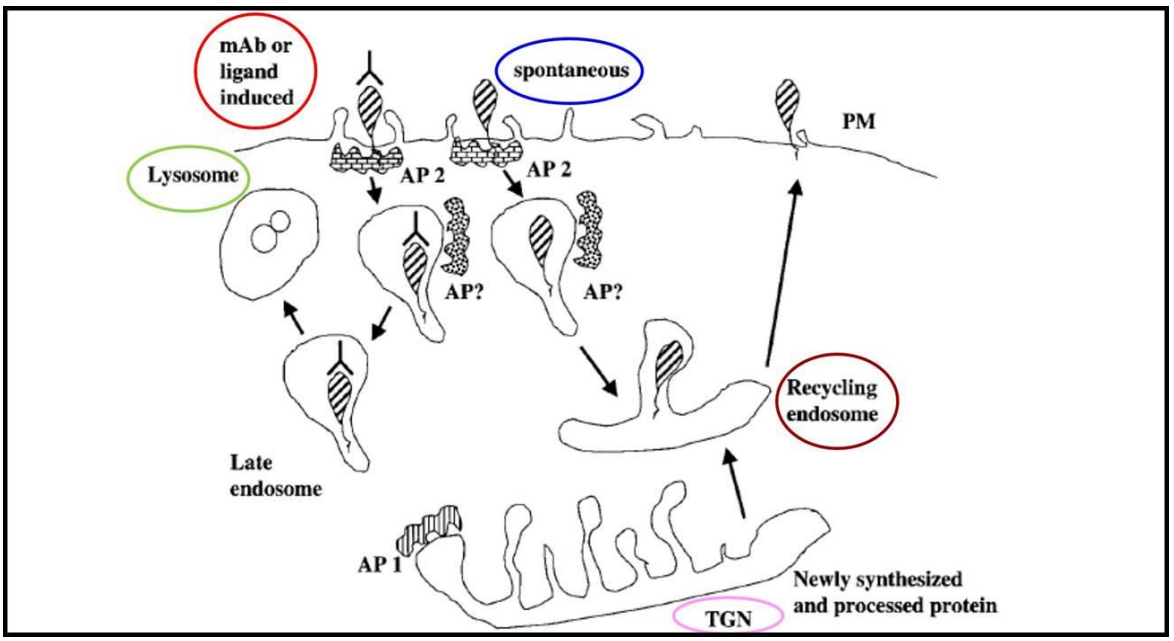

Figure 3-13 Graphical representation of the transportation, digestion and recycling of PSMA (Ghosh and Heston, 2004). Trans Golgi network (TGN), plasma membrane (PM), Adaptor complexes (AP). Brown circle indicates PSMA recycling, the pink circle shows the Trans Golgi network, the red circle indicates PSMA internalisation and the green circle indicate PSMA lysosome digestion. (Used with permission)

In the MCF-7 cells, these circles of green fluorescence close to the cell membrane may be PSMA that has been internalised spontaneously. In the presence of antibody, the rate of internalisation increases, however, the cells were fixed before antibody staining thus ligand induced internalisation was not possible (Nguyen *et al.,* 2016). At the same time, the vesicle-shaped green fluorescence could be PSMA that is being recycled back to the membrane for homeostasis but does not explain the apparent total lack of other PSMA on the external surface of the plasma membrane. The study scope did not encompass PSMA internalisation and recycling so this aspect has not been pursued further. The proximity of the observed green circular fluorescence suggests any of these two possibilities may be occurring. Quite clearly PSMA expression in MCF-7 cells needs to be studied further to elucidate the unique pattern of expression observed in this study.

3.4.3 MDA-MB-231 cells – Confocal Microscopy

Consistent with the observed flow cytometric data showing the presence of PSMA on MDA-MB-231 cells PSMA could be localised in MDA-MB-231 cells by immunofluorescence. These triple-negative cells exhibited isolated ring-like (white arrow) areas of high green fluorescent intensity within the cells (Figure 3.14). A unique larger circle of green fluorescence was also

observed (yellow arrow). Diffuse cytoplasmic green fluorescence (blue arrow) was also seen in MDA-MB-231 cells. Counterstaining with DAPI showed nuclear DNA in all stained cells but the cells not treated with tagged antibody showed no green fluorescence.

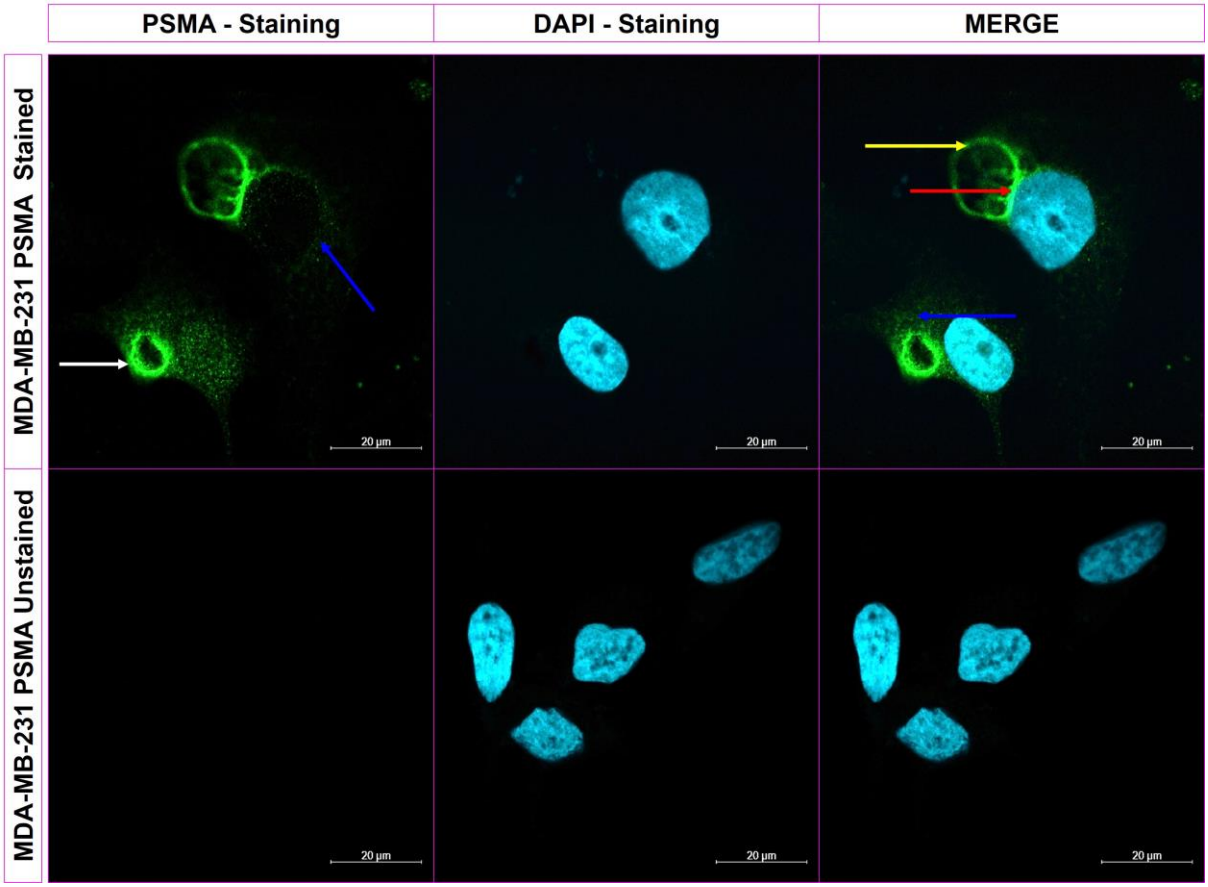

Figure 3-14 Confocal fluorescent microscopy images of MDA-MB-231 cells stained with anti-PSMA primary antibody counterstained with a FITC labelled secondary antibody. DAPI stain reveals the cell nucleus as turquoise while the green indicates PSMA antigen localisation. Control cells not treated with anti-PSMA antibodies indicating that there was no non-specific binding. Images were taken at 100X magnification. Blue arrow shows diffuse cytosolic fluorescence, red arrow shows fluorescence close to the nucleus. White arrow shows a smaller circle of green fluorescence and yellow arrow indicates bigger circle of green fluorescence (Image brightness adjusted)

The smaller circle of fluorescence (white arrow) shows closer proximity to the cell membrane than the nucleus. The fluorescence in the large circle was not evenly distributed. The circle exhibited an area that bordered around the nucleus which visibly showed brighter green fluorescent intensity (red arrow). Diffuse green fluorescence was seen inside the large ring showing it is located within the cell cytoplasm. The difference in fluorescent intensity observed between the areas of green fluorescence is directly related to PSMA concentration. In MDA-MB-231 cells, areas exhibiting brighter intensity would correspondingly show localised areas of high PSMA concentration.

The PSMA antigen has been reported to be expressed by the mitochondria of LNCaP cells (Ristau *et al.,* 2013, Troyer *et al.,* 1997). In LNCaP cells, mitochondrial PSMA expression was localised utilising immunoelectron microscopy and quantified using western blotting (Troyer *et al.,* 1997). This is important when considering where the mitochondria are located within these cells, typically in close proximity to the nucleus (Finichiu *et al.,* 2015). The confocal images generated in this study were compared to TEM images to elucidate how mitochondria localise in MDA-MB-231 (Figure 3.15). The TEM images showed several mitochondria (M) bordering the nucleus (N) (Figure 3.15A). This is the area where amplified green intensity (red arrow) in the large ring concentrated in MDA-MB-231 confocal microscopy images (Figure 3-15B).

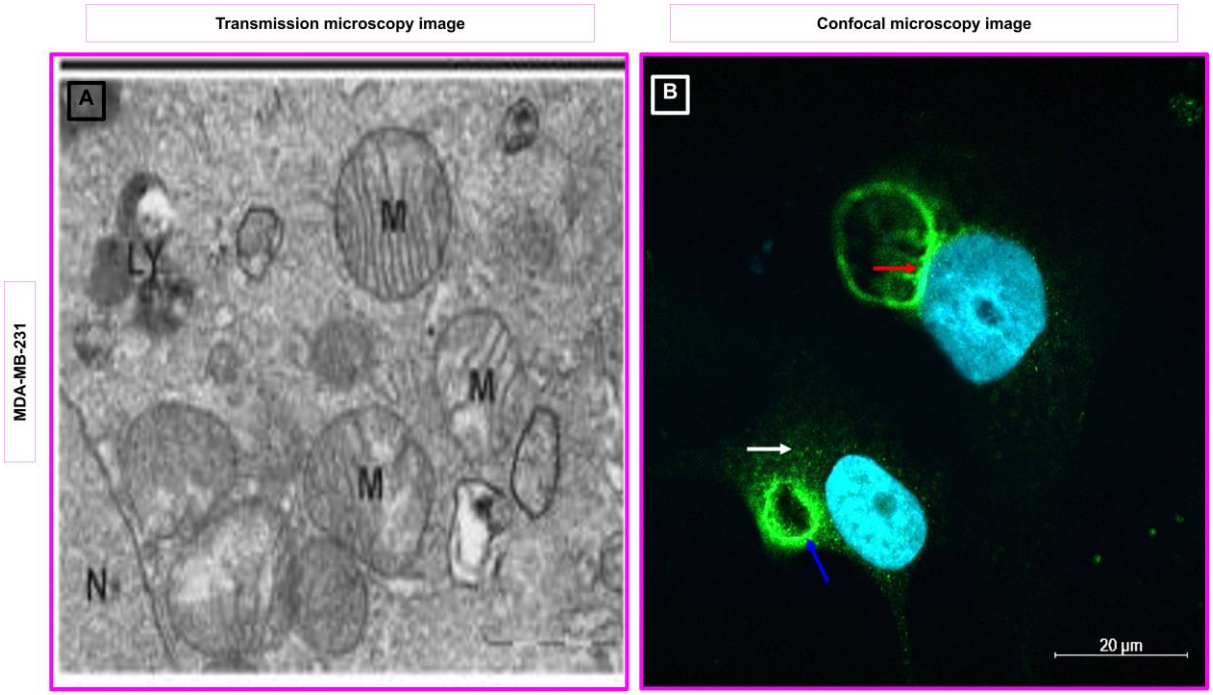

Figure 3-15 MDA-MB-231 cells visualised using transmission electron microscopy (TEM) (A) (Wojtkowiak et al., 2012) and confocal fluorescent microscopy (B). Mitochondria (M), nucleus (N) and lysosome (LY) (Wojtkowiak et al., 2012). Red arrow indicates fluorescence bordering the nucleus, blue arrow shows vesicular intracellular fluorescence and white arrows depict diffuse cytosolic accumulation. (TEM image used with permission). (Image brightness adjusted)

Another important peculiarity is the manner in which PSMA is reported to be expressed in the mitochondria. Troyer *et al* (1997) reported PSMA as being expressed on the outer membrane of the mitochondria. Based on the TEM image, the green fluorescence seen in the confocal microscopy image should display multiple small semicircles of green fluorescence about the nucleus. This was not the case as; the green fluorescence appears in a continuous line that borders the nucleus. Thus, attributing this pattern of expression to mitochondrial PSMA expression may be a possibility but it is unconvincing. Equally, within

the diffuse cytoplasmic green fluorescence is the appearance of granulated spots of green intensity. This granulated distribution may support mitochondrial association however it can only be confirmed through TEM aimed at PSMA localisation in the MDA-MB-231 cells.

The PSMA antigen could equally be internalised in MDA-MB-231 cells as was seen in MCF-7 cells. Especially considering the fluorescence intensity seen at the blue arrow. The fluorescence is close to the cell membrane and takes up a circular shape. It may be enclosed in an endosome ready for recycling or undergoing endocytic trafficking as a result of antibody binding.

The location where PSMA is recycled could possibly further explain the intensity seen around the nucleus. Recycling of PSMA occurs at the recycling endosomal compartment (REC) (Figure 3.16). The cytoplasmic domain of PSMA interacts with filamin A (light blue circle) and they form a complex that travels to the REC which is located at the near the nucleus of the cell (pink circle) (Ghosh and Heston, 2004, Grant and Donaldson, 2009).

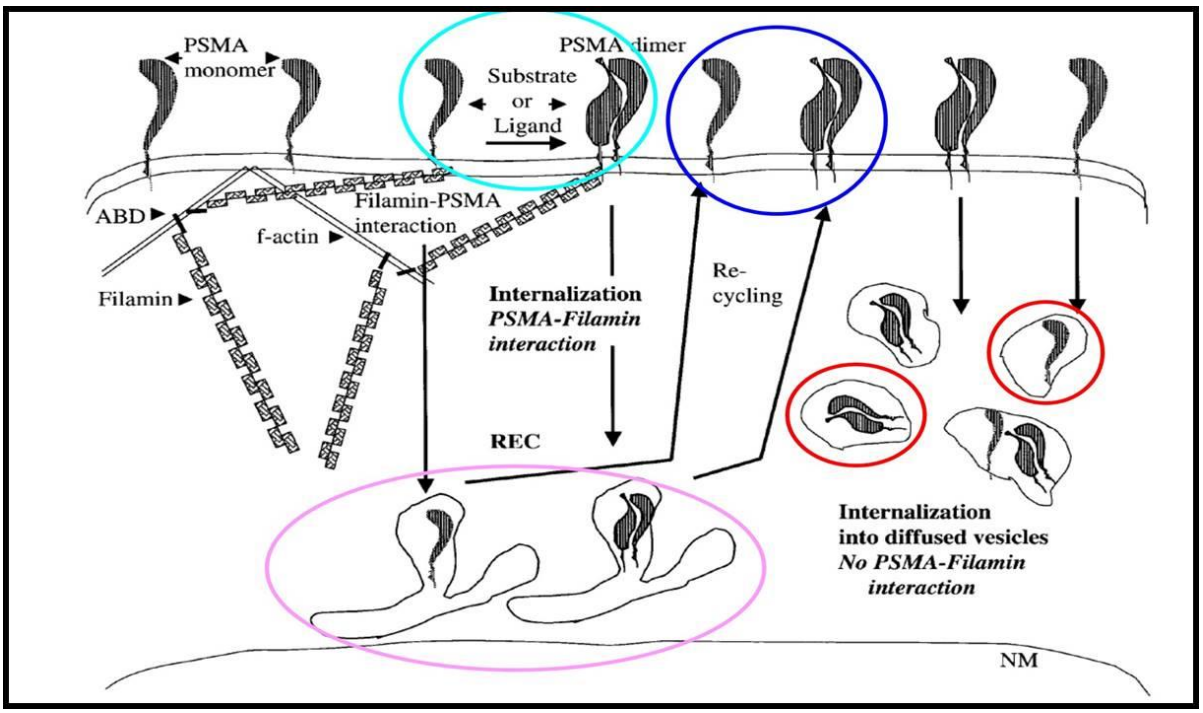

Figure 3-16 Graphical representation of PSMA recycling (Ghosh and Heston, 2004). Recycling endosomal compartment (REC) and nuclear membrane (NM). Pink circle indicates REC compartment, dark blue circle indicates REC trafficking, PSMA interacts with filamin A indicated by light blue circle and vesicle receptors are indicated by red circles. (Used with permission)

From the REC, the proteins are trafficked back to the membrane (dark blue circle). The green fluorescence seen at the red arrow may possibly be PSMA undergoing receptor recycling and accumulating in the REC. This was not experimentally confirmed.

Aside from the mitochondria, the Golgi apparatus and the endoplasmic reticulum (ER) are also found in close proximity of the nucleus (Cooper and Hausman, 2000). The ER extends from the nuclear membrane into the cytoplasm. It is the site of synthesis, folding as well as transport of secreted and integral membrane proteins (Schwarz and Blower, 2016). The PSMA antigen undergoes quality control in the ER before transport to the membrane is undertaken (Castelletti *et al.,* 2006). The Golgi apparatus receives proteins from the ER and organises them for transport in vesicles to the plasma membrane, lysosomes or for secretion (Cooper and Hausman, 2000). The transport of PSMA to the membrane has been suggested to be mediated by the Golgi apparatus through the *trans*-Golgi network (TGN) (Figure 3.13) (Christiansen *et al.,* 2003). Utilising the TGN (pink circle), PSMA is sorted and directed to the correct vesicle for transport to the cell membrane (Christiansen *et al.,* 2003, Christiansen *et al.,* 2005). Unusually, PSMA seems to be capable of leaving the ER without being correctly folded (Castelletti *et al.,* 2006). Usually, proteins are correctly folded In the ER and then move on to the Golgi apparatus where they can be transported to the membrane. The PSMA antigen appears to undergo correct folding in the Golgi apparatus. Once folded, PSMA is packaged and transported to the membrane in vesicles (Castelletti *et al.,* 2006, Christiansen *et al.,* 2005).

It is a possibility that the vesicle shaped green fluorescence at the white arrow is packaged PSMA on its way to the membrane. At the same time, PSMA could be in the Golgi awaiting vesicular transport to the cell membrane at the red arrow. These possibilities added to the possibility of PSMA being recycled and mitochondrial PSMA expression communicate a need to investigate the expression of PSMA in MDA-MB-231 cells further. The protein is present but appears to be expressed differentially. Further studies targeting internalisation, PSMA mitochondrial expression or folding in the Golgi will illuminate what is really happening in MDA-MB-231 cells.

3.4.4 MCF-7 and MDA-MB-231 cells – Confocal microscopy

There were similar and differing patterns of PSMA expression between MCF-7 and MDA-MB-231 cells (Figure 3.17). Similarly, they both showed low diffuse cytoplasmic green fluorescence (blue arrows). Both cells also showed isolated ringed regions on intense green fluorescence (white arrows) in the majority of the repeats, these circular regions of bright fluorescence were closer to the plasma membrane than they were to the nucleus. However, in some fields, the same type of circular areas of green fluorescence was seen close to the cell nucleus for both these breast cancer cell lines. This similarity in PSMA expression patterns shows that even though the two cell lines are genetically and molecularly different, there are similarities. The MDA-MB-231 cells in Figure 3.17 showed a unique larger circular pattern of expression with a specific area showing intense green fluorescence close to the

nucleus (red arrow). It can also be subjectively appreciated that the LNCaP cells visually showed a brighter and more disperse green fluorescence than both the MCF-7 and MDA-Mb-231 cells however this was not quantitatively evaluated.

Aside from the suggestion of PSMA being expressed in the mitochondria of MDA-MB-231 or being internalised in MCF-7 cells another simpler explanation may exist. In MDA-MB-231 and MCF-7 cells, PSMA may simply be an intracellular receptor. This is not exclusively different from the expression pattern of PSMA in the positive control. The LNCaP cells express PSMA in the mitochondria and in the cytoplasm, of which the latter was seen in this study when assaying by confocal microscopy (Ristau *et al.,* 2013, Troyer *et al.,* 1997). However, the LNCaP cells did not exhibit circular regions of green fluorescent intensity. The intracellular expression and distribution of PSMA in the breast adenocarcinoma cell lines appears to be different from that seen in the LNCaP cells.

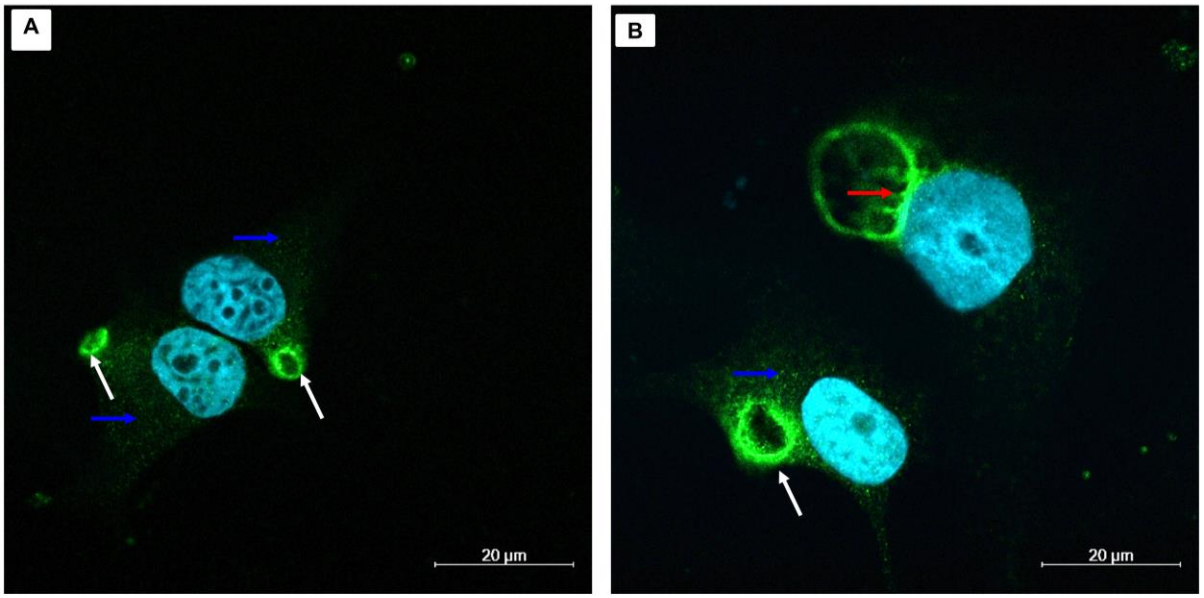

Figure 3-17 Confocal microscopy comparison of MDA-MB-231 images and MCF-7 images. Blue arrow indicates diffuse cytosolic accumulation, red arrow show fluorescence next to the nucleus and the white arrow indicates vesicular expression close to the membrane. (Image brightness adjusted)

Sathekge *et al* (2017) visualised breast tumours *in vivo* during PET imaging of a breast cancer patients while using ^{68}Ga-PSMA-11 as the radiotracer, which is a urea-based peptide inhibitor (Eder *et al.,* 2014, Sathekge *et al.,* 2017). Peptide inhibitors can generally cross the cell membrane and ^{68}Ga-PSMA-11 would be expected to cross cell plasma membranes (Barinka *et al.,* 2012, Eder *et al.,* 2014). Taking this into consideration along with the intense intracellular localisation of PSMA in MDA-MB-231 and MCF-7 breast cancer cells, the suggestion of PSMA being an intracellular receptor in breast cancer is strengthened.

The kinetics of the suggested possibilities regarding PSMA expression in breast cancer must still be investigated further. Several possibilities have been suggested but understandably these have to be confirmed experimentally. In both cell lines, immunoelectron microscopy seems a viable starting point in order to identify where PSMA accumulates in breast cancer cells. Using immunoelectron microscopy as a localising technique, internalisation and intracellular expression of PSMA in these cells can be investigated.

3.4.5 EA.hy926 – Confocal microscopy

The EA.hy926 cells also demonstrated positive PSMA expression using confocal microscopy images (Figure 3-16).

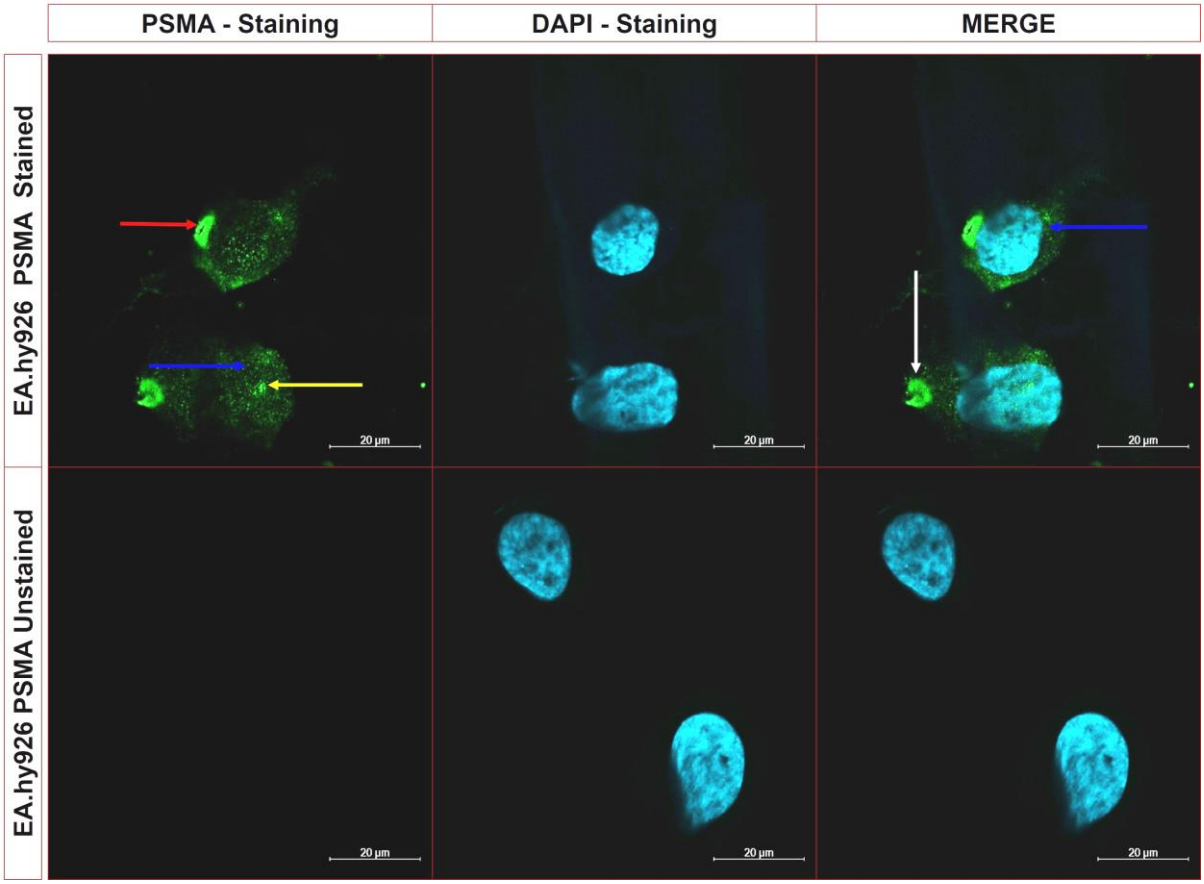

Figure 3-18 Confocal fluorescent microscopy images of EA.hy926 cells stained with anti-PSMA primary antibody counterstained with a FITC labelled secondary antibody. DAPI stain reveals the cell nucleus as turquoise while the green indicates PSMA antigen localisation. Controls not stained with anti-PSMA antibody showed no green fluorescence, indicating that there was no non-specific binding. Blue arrows indicate diffuse cytosolic fluorescence, white arrows show fluorescence close to the cell membrane, yellow arrows show fluorescence close to the nucleus and red arrows show fluorescence close to the plasma membrane. Images were taken at 100X magnification. (Image brightness adjusted)

Diffuse green fluorescence was seen in the cytoplasm (blue arrows) with distinct regions of intense green fluorescence seen close to or at the plasma membrane (white arrow), close to

the nucleus (yellow arrow) and on the plasma membrane (red arrow). The samples not treated with anti-PSMA antibody showed no green fluorescence. The areas of showing intense fluorescence correspond to high PSMA concentrations. The pattern of expression in the EA.hy926 shows similarity to that seen in MDA-MB-231 and MCF-7 but not the LNCaP cells. High green fluorescence intensity was seen around the nucleus, close to the plasma membrane and on the cell membrane of different cells from the same cultures. The suggested explanations of PSMA expression patterns discussed in MCF-7 and MDA-MB-231 cells extend to the EA.hy926 cells. Electron micrographs of EA.hy926 cells show mitochondria and Golgi located close to the nucleus (Figure 3.19). In the EA.hy926, PSMA expression is possibly juxtanuclear Golgi apparatus and mitochondria (red arrow). The green fluorescence seen at the membrane (yellow arrow) mimics the expression pattern but not intensity seen in LNCaP cells. The circular green fluorescence (blue arrow) could likewise be ligand induced receptor internalisation.

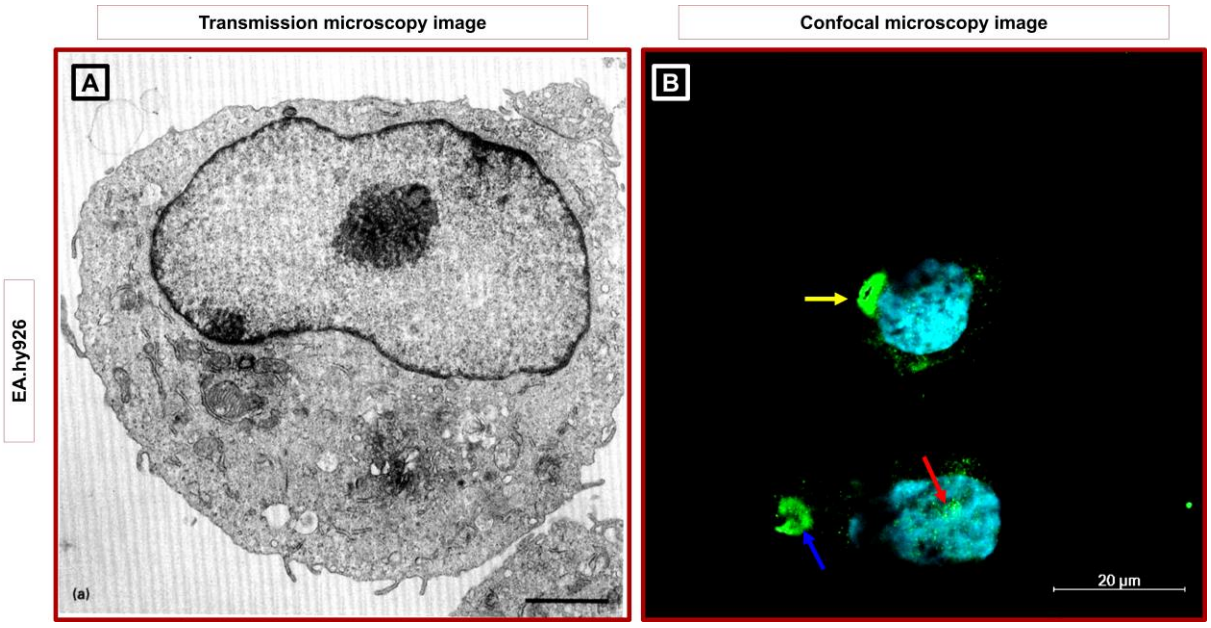

Figure 3-19 EA.hy926 cells visualised using TEM EA.hy926 cells (A) (Eremeeva and Silverman, 1998) and confocal fluorescent microscopy (B). Red arrow indicates intracellular nuclear associated fluorescence, blue arrow indicates intracellular circular fluorescence close to the membrane and yellow arrow shows fluorescence at the plasma membrane. (TEM image used with permission). (Image brightness adjusted)

Somatic cell hybrids like EA.hy926 cells are generated by fusion of nuclei from both their parent cells (Mak and Saunders, 2005). The same nuclei which provides the genetic information that directs protein expression (Newport and Forbes, 1987). Already discussed above is the inability of HUVEC's to express PSMA due to lack of the transcriptional machinery necessary for PSMA expression (Noss *et al.,* 2002). The positive localisation of PSMA in EA.hy926 cells could possibly be attributed to its lung cancer origin. Wang *et al*

(2015) in their study reported PSMA expression not only in the of endothelial cells of neovasculature but expression was also reported in lung adenocarcinoma tissue. The cellular location of the PSMA expression was however not reported (Wang *et al.,* 2015). Moreover, the antibody used in that study was the LS-C150527 FOLH1/PSMA antibody from Abcam (Wang *et al.,* 2015) which binds to the extracellular portion of PSMA similar to YPSMA-1 used in this study (Tykvart *et al.,* 2014).

The EA.hy926 cells should be probed to elucidate the exact location and kinetics of their PSMA expression. This becomes more pertinent when considering that flow cytometry and confocal microscopy both showed evidence of PSMA in these cells, a result which no other study has reported to date.

3.5 ELISA – PSMA quantification

Following proof of presence and localisation of PSMA in the different cell lines, the quantification utilising ELISA completed the picture of the investigation of non-prostatic expression of PSMA in MCF-7 and MDA-MB-231 cell lines. ELISA using different antibodies to those used for the previous two aspects of the study added empirical robustness to the generated data. The ELISA assay provided positive quantification of PSMA in all four of the probed cell lines (Figure 3.20).

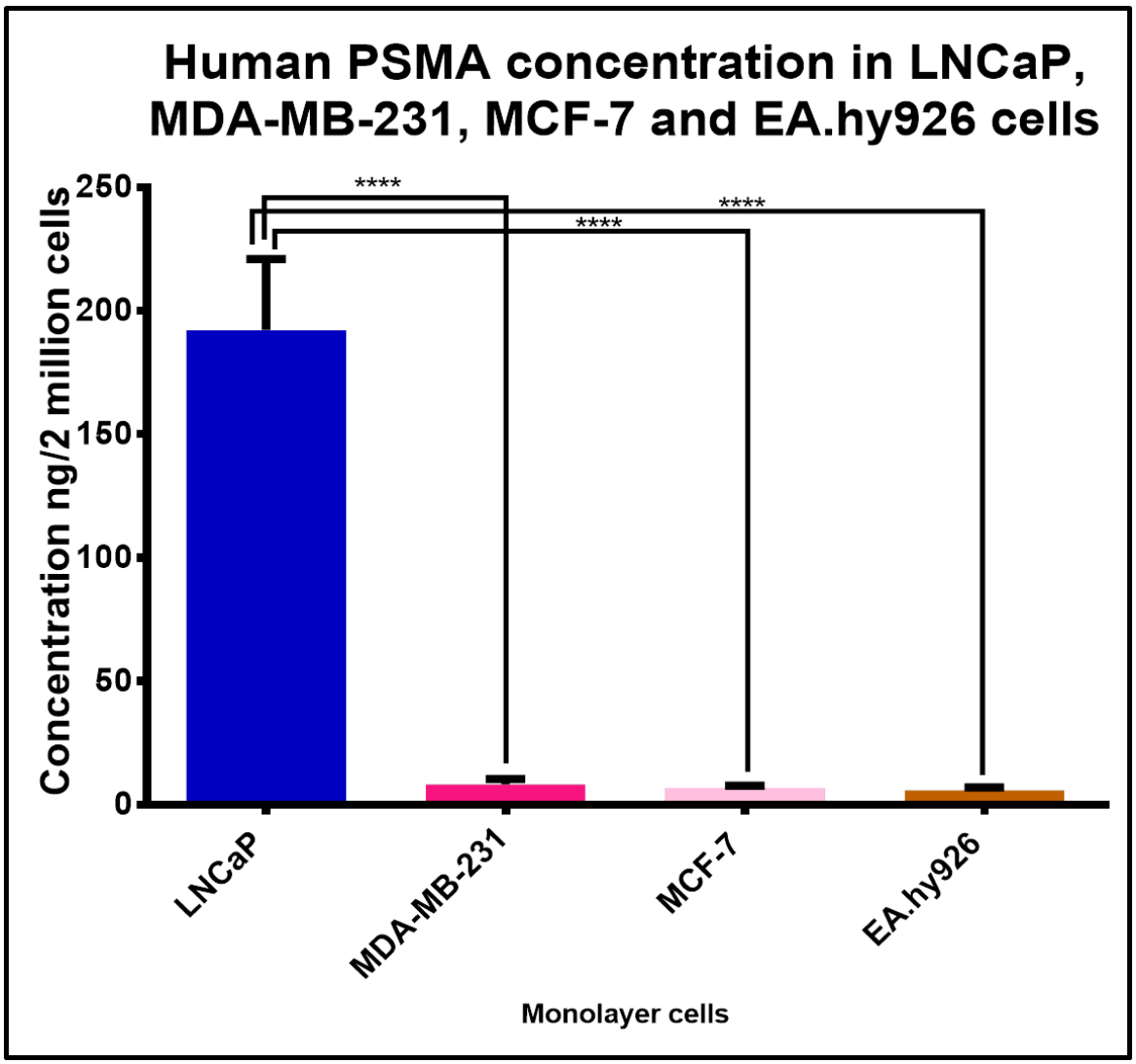

Figure 3-20 PSMA quantification utilising ELISA in LNCaP, MDA-MB-231, MCF-7 and EA.hy926 cell lysates. N= 3 repeats, (P <0.0001), error bars are representative of standard error of the mean (SEM). Significant differences across different cell lines are represented by (*). Multiple comparisons of a Repeated measures one-way ANOVA.

The absolute quantitation of PSMA utilising ELISA demonstrated support for the semi-quantitative flow cytometry results. As expected the LNCaP cell line exhibited the highest PSMA concentration, followed by MDA-MB-231, MCF-7 and EA.hy926 cells respectively (Table 3.1). The actual PSMA concentration in LNCaP was 384.3 ng/2 million cells. Experimental MDA-MB-231 and MCF-7 cells reported concentration figures of 4.1 ng/2 million cells and 3.5 ng/2 million cells respectively. The MDA-MB-231 cells had a slightly higher concentration of PSMA as was seen in the flow cytometry results although the difference in PSMA concentration was not statistically significant. Finally, EA.hy926 cells reporting figures of 2.9 ng/2 million cells. This was also similar to the flow cytometry results where they showed the lowest concentration. Significant differences in concentration were

observed between the positive control LNCaP and all the investigational cell lines. There were no significant differences observed in concentration between the MDA-MB-231 cells and the MCF-7 cells. Equally no significant difference was seen between EA.hy926 and both breast carcinoma cell lines.

Table 3.1 Table showing numeric values of PSMA quantified in LNCaP, MDA-MB-231, MCF-7 and EA.hy926 utilising ELISA. Multiple comparisons of a Repeated measures one-way ANOVA.

Comparisons	Mean 1 [C]	Mean 2 [C]	Mean difference	Significance
LNCaP vs MDA-MB-231	192,1	8,237	183,9	Yes
LNCaP vs MCF-7	192,1	6,932	185,2	Yes
LNCaP vs EA.hy926	192,1	5,805	186,3	Yes
MDA-MB-231 vs MCF-7	8,237	6,932	1,305	No
MDA-MB-231vs EA.hy926	8,237	5,805	2,432	No
MCF-7 vs EA.hy926	6,932	5,805	1,127	No

Considering that the positive identification of PSMA in breast adenocarcinoma cell lines is aimed at potential theranostic radiopharmaceutical applications, it must also be recalled that potential radiopharmaceutical targets should be selectively and abundantly expressed, accessible, stable and located on the surface or within the target cells (Lee *et al.,* 2019). In breast adenocarcinoma cell lines and endothelial EA.hy926 cells, PSMA is accessible as it was confidently identified, localised and quantified. Secondly, PSMA is located within the cells and appears to be intracellular although further studies will be required to reveal the exact location of the observed expression. Similarly, the stability of PSMA in these cells is yet to be investigated.

3.6 Breast tissue – Confocal microscopy

A concern may arise when considering that for effective targeting in the experimental cell lines, PSMA must be abundantly expressed in these cell lines. Looking at the ELISA results, PSMA concentration in experimental cell lines is approximately 100-times less than the concentration seen in LNCaP prostrate adenocarcinoma cells which are reported to overexpress PSMA by 100-1000 fold compared to equivalent non-carcinomic cells

(Udovicich *et al.,* 2017). From this, it can be deduced that PSMA concentration in EA.hy926, MCF-7 and MDA-MB-231 cells presents with concentrations comparable to or less than those seen in healthy prostatic tissue, although this is an assumption. There are well known inconsistencies that are sometimes seen between two-dimensional monolayer cultures and clinical heterogeneous tumour environments (Edmondson *et al.,* 2014). Monolayer cultures of cells do not fully represent the *in vivo* conditions but in this study incontestable evidence regarding PSMA expression in the non-prostrate cell lines was found. The clinical implications of these quantitative results demand further investigation. Heterogeneous tumour tissue samples that are representative of typical clinical tumour environments may provide more information of the distribution and extent of the non-prostatic PSMA expression seen in cultured cells used in this study.

Thus, although not an original aim of this study, unstained cryotome cut 60µm histology slices of a luminal A and a HER-2 positive breast tumour left over from a separate study were probed directly for PSMA expression. The aim was to evaluate the PSMA expression of two different samples of *ex vivo* breast tumour and assess whether PSMA was detectable in solid primary breast tumours. These two histological slices required tissue clearing using a standard operating procedure used by the confocal research group to allow clear 3D confocal images to be collected and to increase the laser penetration into the tissue slices.

Luminal A tissue is theoretically analogous to the MCF-7 cell line and PSMA expression was confirmed elevated (Figure 3.21), as indicated with the blue arrows. The pink arrow shows what appears to be membrane associated PSMA expression in luminal A tumour sample. The white circle depicts intense green fluorescence in multiple cells that appear to be clustered together, indicated by the DAPI nuclear staining.

The expression pattern appears to be slightly different in luminal A tumour samples compared to the *in vitro* 2D monolayers of MCF-7 cells (Figure 3.22). The red arrow on the tumour samples show PSMA being more membrane associated similar to the distribution of that seen in cultured LNCaP cells but not seen in MCF-7 cells (Figure 3.22B). They also show diffuse cytoplasmic fluorescence (blue arrow) similar to the cultured MCF-7 cells and appear to have an intracellular circular accumulation of green intense fluorescence shown by the white arrow.

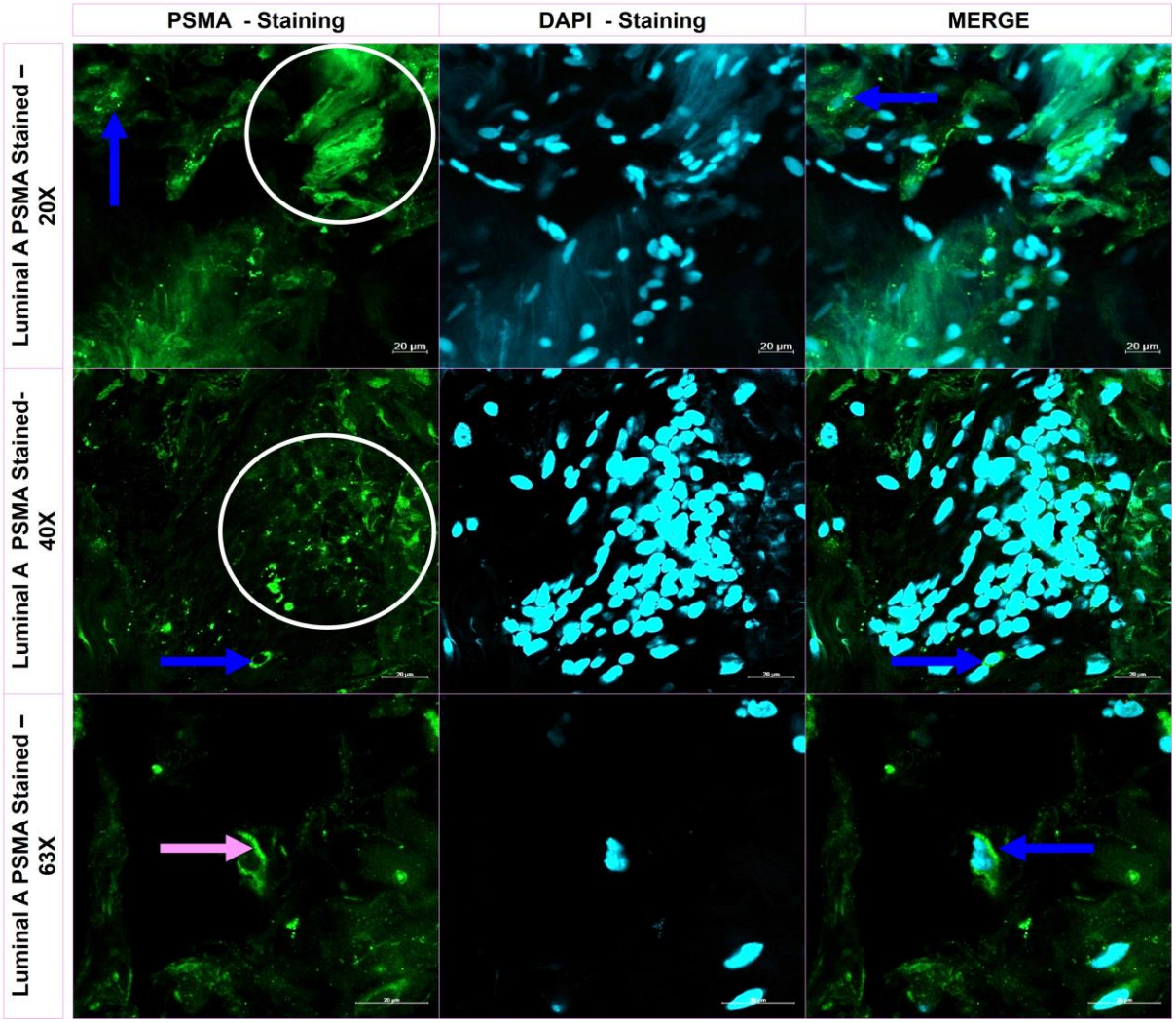

Figure 3-21 Confocal fluorescent microscopy images of luminal A tumour samples stained with anti-PSMA primary antibody counterstained with a FITC labelled secondary antibody. DAPI stain reveals the cell nuclei as turquoise while, the green indicates PSMA antigen localisation. Images were taken at 20X, 40X and 63X magnification. Blue arrows indicate intense green fluorescence, pink arrow indicate membrane associated fluorescence. The white circles indicate multiple cells showing intense green fluorescence (PSMA). (Image brightness adjusted)

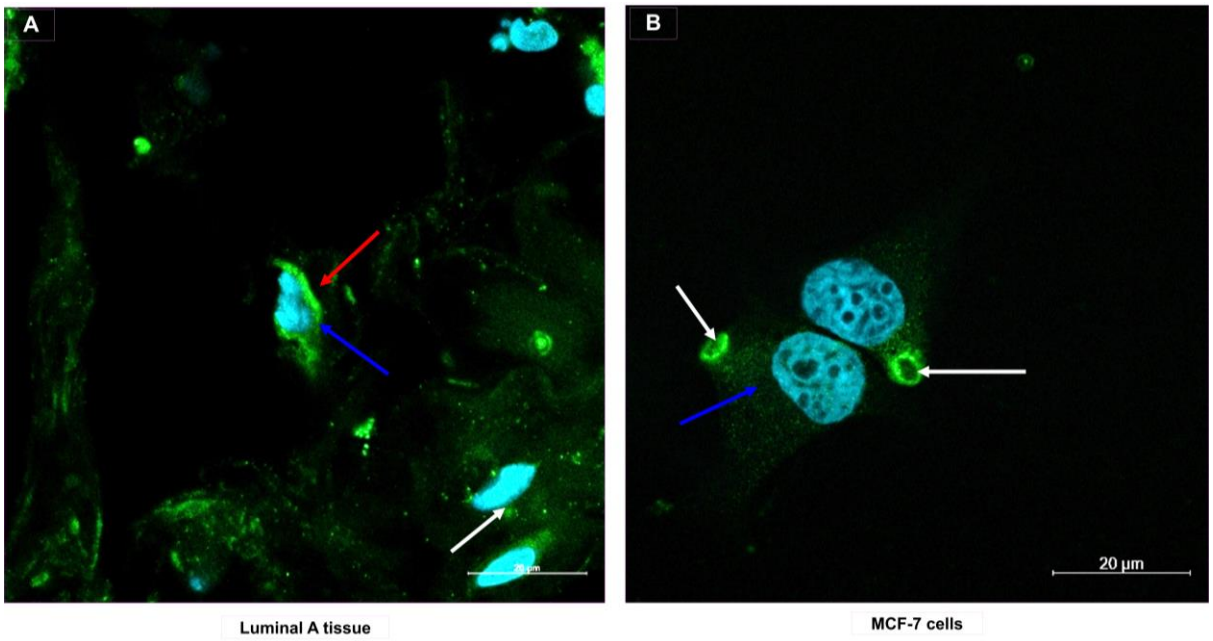

Figure 3-22 Luminal A tissue samples visualised using confocal fluorescent microscopy (63X magnification) (A) compared with MCF-7 cells (B). MCF-7 (100X magnification). Red arrow shows membrane associated fluorescence in tissue samples, blue arrows show diffuse cytosolic fluorescence and white arrow shows circular accumulation in MCF-7 cells. (Image brightness adjusted)

Taken together this shows that the PSMA expression visible in cultured adenocarcinoma monolayers extends to heterogeneous *ex vivo* breast tumour samples. The PSMA was positively identified in different samples of the same subtype. This is in spite of the limitations of the representative monolayer cultures (Yamada and Cukierman, 2007). Interestingly, 30% of genes have been reported to be differentially expressed between cultured cells and *in vivo* tissues (Birgersdotter *et al.,* 2005). Thus, the expression of PSMA by the MDA-MB-231 and MCF-7 cell lines probably indicates a functional requirement for the PSMA protein in breast cancer Consistency of PSMA expression in breast carcinoma is being observed that hierarchically matches the aggressiveness. Positive PSMA expression has been demonstrated *in vitro* in two-dimensional monolayer cultures, in *ex vivo* breast tumour samples and in a recent clinical case could indicate *in situ* primary breast and metastatic tumours of a cancer patient. Supporting results from this study, expression of PSMA has also been reported in carcinomic and healthy breast tissue by Kasoha *et al* (2017), utilising histology techniques. In breast cancer tumour cells, PSMA expression appears constitutively persistent and necessary for reasons not yet understood.

Ex vivo triple negative basal tumour samples could not be sourced for this study, but HER-2 positive tumour tissue samples were probed for PSMA presence utilising confocal microscopy. As a subtype this cancer shows increased aggressiveness, faster tumour

growth rates and poor prognosis (Feng *et al.,* 2018). These characteristics are associated with PSMA expression and in this study these tumours correspondingly displayed positive PSMA localisation (Figure 3.23). Diffuse cytoplasmic fluorescence is indicated by the white arrow, demonstrating comparability with all the probed cell lines and solid tumour samples. Membrane associated expression was seen comparable to the positive control LNCaP cell cultures (blue arrows). In totality, this study has reliably localised PSMA in different breast cancer subtypes. These are triple negative two-dimensional MDA-MB-231 cultures, luminal A type MCF-7 two-dimensional monolayer cultures, but also important is finding PSMA in histological samples from *ex vivo* breast tumour samples including a HER-2 positive type breast tumour samples.

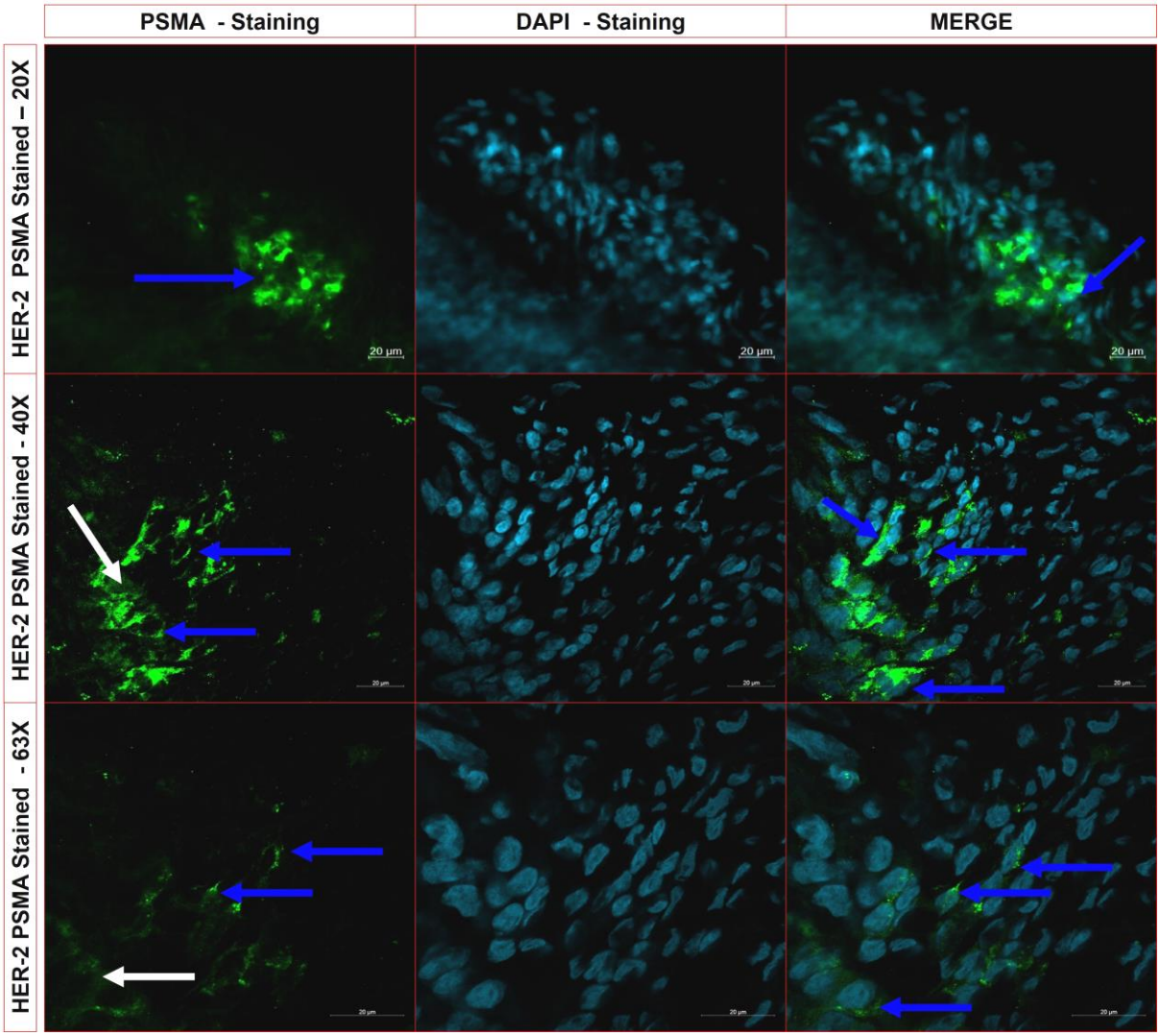

Figure 3-23 Confocal fluorescent microscopy images of HER-2 positive tumour samples stained with anti-PSMA primary antibody and counterstained with a FITC labelled secondary antibody. DAPI stain reveals the cell nucleus as turquoise while, the green indicates PSMA localisation. Images were taken at 20X, 40X and 63X magnification. White arrows indicate intracellular fluorescence and blue arrows indicate membrane associated fluorescence. (Image brightness adjusted)

These different cells show similar expression patterns related to a common mammary origin. At the same time, they also present their own unique peculiarities, showing divergence due to their pathophysiological differences. In this study, confirmed PSMA expression has been described at a cellular level in MCF-7 and MDA-MB-231 breast adenocarcinoma cell lines for the first time. A result which was confirmed when compared to *ex vivo* tumour samples which are representative of clinical breast cancer environments. Positive identification as a result of experimental phenomenon can be confidently ruled out.

The expression of PSMA in breast adenocarcinoma cell lines was probed utilising three different complementary methods where two different monoclonal antibodies with different haptens were targeted. Robust and reliable methods were used and each independently identified PSMA expression in all the probed adenocarcinoma and tumour samples.

Considering that several candidate oncogenic targets appear to be constitutively expressed in cancer cells arising from tissues different (Lili *et al.,* 2014, Ziegler *et al.,* 2014), it may not be an unanticipated result that PSMA is expressed in breast cancer as this study shows. Breast and prostate cancers share several pathogenic similarities even though they originate from different tissues including oncogenic proteins. (Risbridger *et al.,* 2010). The once considered prostate-unique PSA protein is now known to be produced in female periurethral glands (Yu and Berkel, 1999, Biswas *et al.,* 2011). Additionally, PSA has been detected in breast and ovarian tissues (Melegos *et al.,* 1997). The overlap in pathogenic characteristics of the prostate and breast cancers extends beyond molecular similarities to predisposing factors, mortality rates and applied chemotherapeutic inventions (Risbridger *et al.,* 2010, Hu *et al.,* 2011, Castro and Eeles, 2012). Results from this study show that PSMA appears to be one of the many cancer-associated proteins that is constitutively expressed between these two carcinomas although in significantly different amounts.

Consultation of the Human Protein Atlas (HPA) database for proteins adds to the discussion about the presence and abundance of PSMA across different tissues. A consensus data sheet for PSMA mRNA expression was compiled by the HPA. The data is made up of HPA internally generated mRNA sequence data, mRNA sequence data from the Genotype-Tissue Expression (GTEx) project and Cap Analysis of Gene Expression (CAGE) data from the FANTOM5 project. The normalised expression (NX) value represents the maximum expression value derived from the three data sources used (Thul *et al.,* 2017). The consensus datasheet resulting from that study identified PSMA gene expression in the prostate, breast, liver, cervix and lung tissues (identified with black rectangles in Figure 3-24). This adds further support for the results of this study by providing published results of a

completely different approach to whether PSMA can be found in different tissue types. It is also worth noting that the tissue assessed for the HPA were non-cancerous tissues.

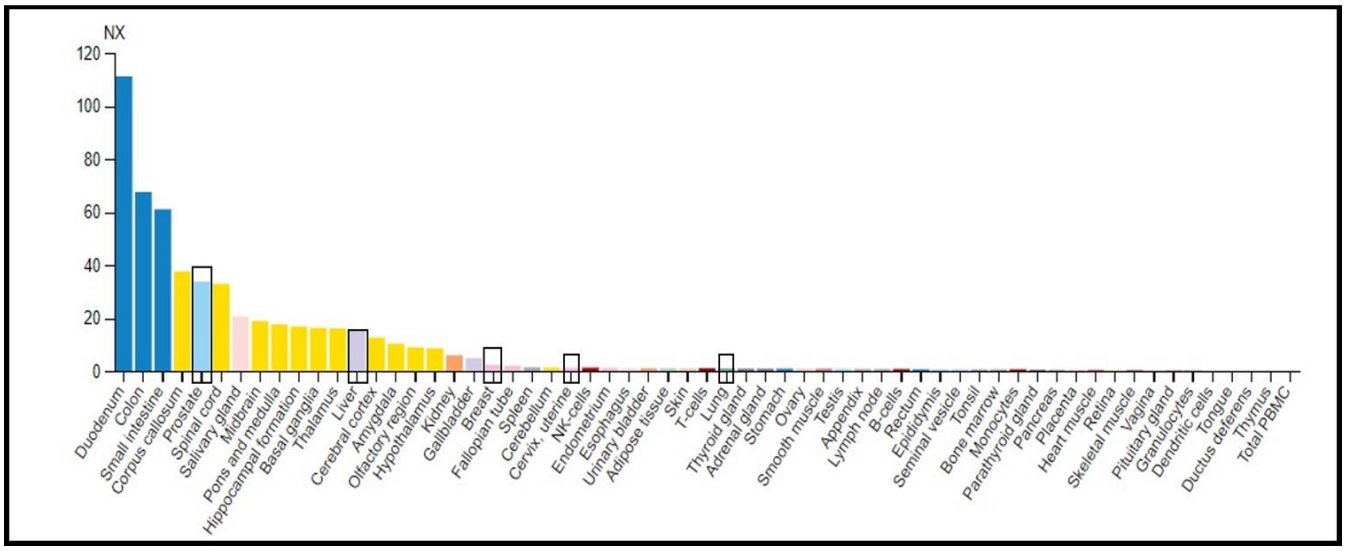

Figure 3-24 Consensus PSMA RNA sequence data form of HPA internally generated RNA sequence data, RNA sequence data from the Genotype-Tissue Expression (GTEx) project and Cap Analysis of Gene Expression (CAGE) data from FANTOM5 project (Thul et al., 2017). The black rectangles indicate PSMA expression in prostate, liver, breast, cervix and lung tissue from highest to lowest. (Used with permission)

Pathological tissue was also probed for PSMA expression by the HPA. The results showed PSMA expression in prostate, breast and lung carcinoma amongst others (Figure 3.25) (Thul *et al.*, 2017). The highest expression was reported in prostate cancer. Breast carcinoma similarly displayed expression and identification in lung carcinoma links to the EA.hy926 identification in this study.

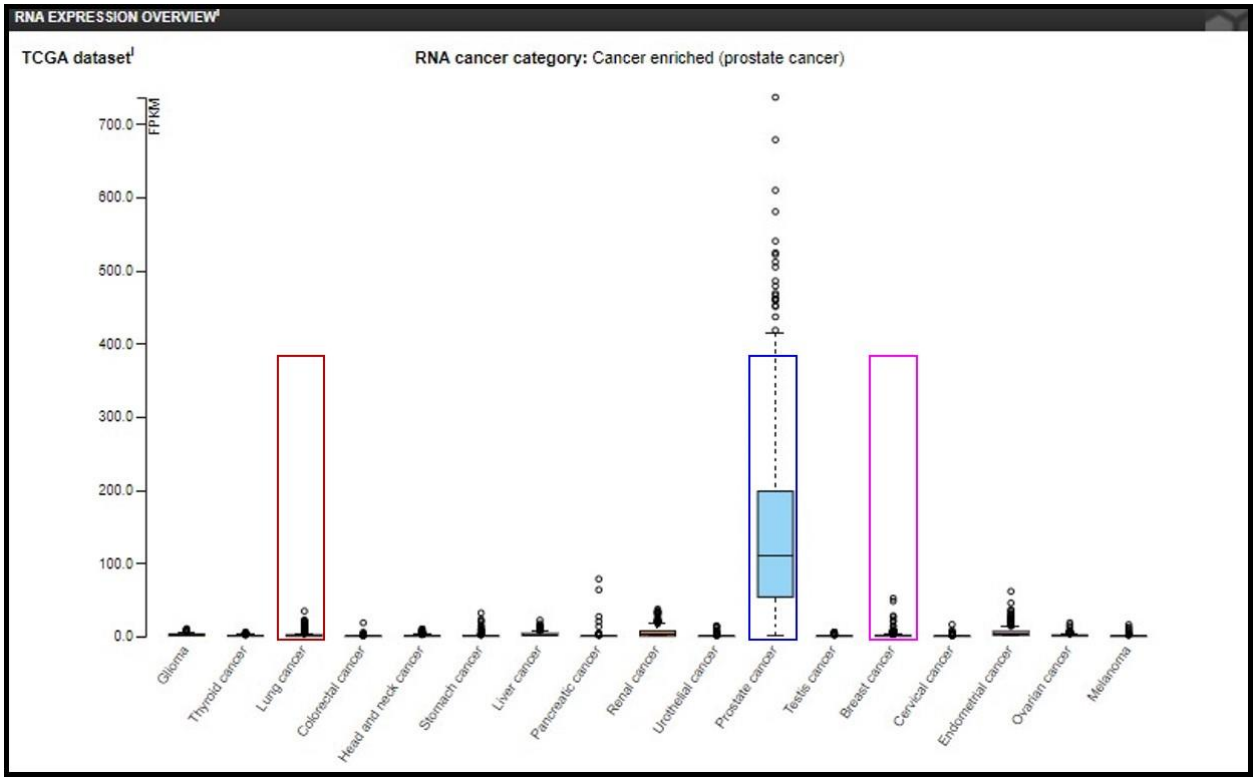

Figure 3-25 Consensus PSMA RNA expression in pathological tissue data form of HPA internally generated mRNA sequence data (Thul et al., 2017). The brown rectangle indicates PSMA expression in lung cancer, the blue rectangles indicate PSMA expression in prostate cancer and the pink rectangle indicates PSMA expression in breast cancer. (Used with permission)

The folate hydrolase activity of PSMA could be a starting point to elucidate its oncologic function in non-prostatic carcinomas. Folate hydrolase activity of PSMA and its influence on proliferation, suggests a possible analogous function in the PSMA positive cell lines of this study. Folate antagonists such as MTX and 5-FU are regularly used in breast cancer chemotherapy (Allegra *et al.,* 1986, Visentin *et al.,* 2012). In EA.hy926 cells, folate starvation and dihydrofolate reductase down-regulation results in inhibited cell proliferation (Fei *et al.,* 2016). The investigational cell lines in that study exhibited folate associated proliferation (Oppenheim *et al.,* 2000, Sambi *et al.,* 2019). The MCF-7 cells exhibit moderate expression of folate receptors while MDA-MB-231 cells overexpress folate receptors (Fernández *et al.,* 2018, Sambi *et al.,* 2019). This infers a greater folate dependency in MDA-MB-231 cells in comparison to MCF-7 cells. Although statistically insignificant, the higher PSMA concentration reported in this study and the pathophysiological characteristics associated with MDA-MB-231 cells is aligned with this inference.

4 Concluding discussion

Breast and prostate cancer present among the most prevalent carcinomic malignancies in women and men respectively. Both malignancies display an average increase in the number of new cases reported every year. Breast cancer occurs in the mammary glands of both females and males. Consequently, the global cancer disease burden continues to grow. The impact of this increasing burden is heaviest in low- and middle-income countries. More than half of the diagnosed breast cancer cases manifest in low- and middle-income countries. The cornerstone of breast cancer control is early diagnosis and subsequent therapeutic intervention. However, the majority of affected patients in low- and middle-income countries have poor access to early detection screening and cannot afford the high cost of treatment. Moreover, the conventional diagnostic and treatment options demonstrate intrinsic limitations that in some cases put the patient at risk. As a result, research aimed at developing superior diagnostic and therapeutic alternatives has become pertinent.

One of the evaluated methods of cancer diagnosis and therapy is non-invasive PET scanning. Where conventional diagnostic and treatment techniques experience challenges, PET scanning has realised oncological success. One particularly successful application has been through targeting of the PSMA protein. The protein is an 80-100 kDa type II membrane protein that has folate hydrolase activity. Presently, PET based PSMA radiotracers are realising increasing oncological success in prostate cancer theranostics. Expression of PSMA was initially understood as being restricted to the prostate gland however, non-prostatic expression of PSMA in the vasculature of other cancers is well studied and reported. Beyond the neovasculature of many cancers, researchers recently reported PSMA accumulation in solid breast tumour tissue. This non-prostatic expression of PSMA in breast tissue meant that the success experienced in prostate cancer theranostics could possibly extend into breast cancer.

Therefore, the aim of this study was to investigate the possible expression of PSMA in the well-established MCF-7 and MDA-MB-231 breast adenocarcinoma cell lines. To achieve this, flow cytometry and confocal microscopy were used in conjunction with antibodies raised against the human PSMA for identification and localisation respectively. An ELISA assay was also undertaken as a method of quantitatively assessing PSMA expression in these investigational cell lines. LNCaP prostate adenocarcinoma cells were used as a positive control due to their reported high expression of PSMA, while endothelial hybrid EA.hy926 cells were used to gain insight into the endothelial association of PSMA expression in other

carcinomas. An initial pilot study was undertaken to determine the effects of different cell detachment methods on cell counts. The Crystal Violet assay and phase contrast microscopy were used to assess cell count and morphology following scraping or trypsinisation as the method of releasing cells for downline passaging or experimental use.

Scraping was demonstrated as having a negative effect on the cell count when compared to trypsinisation. Cell numbers were measured after 24-, 48- and 72-hour culturing intervals. At each of these time points, trypsinisation showed higher cell numbers across all cell lines when compared to mechanical scraping. Considering the effect on cell morphology, phase contrast microscopy revealed mechanical scraping as having a negative effect in all cell lines. Scraped cells generally exhibited clustering and clumping which had negative effects on their viability and proliferative outcomes. The clumping of the cells also meant that they could not be used for other experiments such as flow cytometry which depends on single cell suspensions. Trypsinisation was therefore selected as the better cell dissociation method. Although there was a concern for proteolytic cleavage of PSMA, consultation of literature reported that sufficient robust data can be generated when probing for PSMA utilising trypsinisation as a cell releasing method if sufficient time was allowed for surface protein recovery.

Flow cytometry aimed at identification of PSMA expression revealed positive PSMA expression in EA.hy926, MCF-7, MDA-MB-231 and LNCaP cells. Significant differences were seen between the positive control and the three investigational cell lines. Statistically, there was no significant difference between MDA-MB-231 cells and MCF-7 cells. As expected, the positive control LNCaP showed the highest concentration of PSMA, presenting with a geometric fluorescence mean value of 152 720. Triple-negative MDA-MB-231 cell line which intrinsically presents with a pathophysiological environment promoting PSMA expression showed the second highest but much lower concentration of PSMA. The geometric mean fluorescence in MDA-MB-231 cells was measured at 39 140. Luminal A type MCF-7 cells were slightly less with a geometric mean fluorescence value of 38 630. The MCF-7 cells do not demonstrate the pathophysiological profile that enhances PSMA expression. Despite this characteristic, other Luminal A cell lines have been shown to express PSMA and PSMA genes have also been reported as being active in MCF-7 cells. The EA.hy926 cell lines reported the lowest concentration of PSMA with geometric mean fluorescence values measured at 32 400. Notably, this was the first study to positively identify PSMA in EA.hy926 cells. These cells are somatic cell hybrids of the lung carcinoma

A549 cell line and primary HUVEC's. The expression becomes more fathomable when considering that lung cancer has been identified as expressing PSMA both in tumour tissue and in the neovasculature associated with the tumour.

Following the positive identification of PSMA expression in the three experimental cell lines utilising flow cytometry, a second fluorescent technique using the same anti-PSMA antibodies was used. This was the confocal microscopy that due to the magnification, revealed the location of the PSMA expression in the cells. The LNCaP cells exhibited increased concentration around the cell membrane and also showed diffuse cytosolic PSMA expression. The MCF-7, MDA-MB-231 and EA.hy926 cells all exhibited different PSMA expression pattern compared to the positive control LNCaP cells. The cells showed circular, vesicle like PSMA expression bordering the cell membrane. This could possibly indicate spontaneous PSMA internalisation either for recycling or lysosome degradation or potentially exposed areas of PSMA in the membrane due to permeabilisation. The MDA-MB-231 and EA.hy926 cells exhibited intense circular regions of high PSMA concentrations in what could be close to the nucleus. This expression pattern could be linked to accumulation in the REC or packaging in the TGN for transport to the cell membrane. Studies to confirm these possibilities were not undertaken; however, an important feature observed was the similarity of the data derived from the two complementary methods when assessing PSMA expression in these cell lines.

The ELISA undertaken on cell lysates revealed the same trend seen in the flow cytometry and confocal microscopy results (assays in which intact cells were used). Significant differences were seen between the LNCaP cells and MCF-7, MDA-MB-231 and EA.hy926 investigational cell lines. Statistically, there was no significant difference between MDA-MB-231 cells and MCF-7 cells. The LNCaP cells showed the highest concentration of PSMA, measuring at 384.3 ng/2 million cells. The PSMA concentration was measured at 3.5 ng/2 million cells in MCF-7 cells, 4.1 ng/2 million cells in MDA-MB-231 cells and 2.9 ng/2 million cells in EA.hy926 cells. As seen in the flow cytometry results, MDA-MB-231 cells showed slightly higher PSMA concentration compared to MCF-7 cells. Once again EA.hy926 cells exhibited the lowest values of PSMA concentration. Of particular concern was the 100-fold difference in PSMA concentration between the positive control (LNCaP cells) and the investigational cell lines. This has implications on the potential clinical applications of PSMA targeting in breast cancer. However, when considering that PSMA has been located during

PET scans in clinical breast cancer cases, the measured concentration reported in these breast cancer cell lines appears to be sufficient for clinical translation.

The representative limitations of two-dimensional monolayer cell culture were addressed through probing of PSMA in heterogeneous ex vivo breast tumour samples. Luminal A and HER-2 subtype tumour samples were tissue cleared then PSMA was localised utilising 3-D confocal microscopy. The results showed positive PSMA binding in both samples. This showed continuity between monolayer cultures and heterogeneous tumour samples when considering PSMA expression. The expression pattern seen in Luminal A tissue samples and representative model MCF-7 cell line differed. These differences are yet to be investigated.

In conclusion, this study, has demonstrated PSMA expression in EA.hy926, MCF-7 and MDA-MB-231 cell line cultures for the first time. Secondly, through this study, PSMA was positively identified and localised in three different breast cancer subtypes over and above the endothelial expression in EA.hy926 cells. Literature consultation created a precedent for the positive expression of PSMA in the non-prostatic samples used in this study. In some instances, continuity was demonstrated between literature and data collected from this study. The data generated and the data available consistently detected PSMA in non-prostatic tissue.

Theranostics is an emerging field that at present is addressing the shortfalls of conventional cancer management by utilising contemporary scientific approaches. The hypothetical application of theranostics targeting PSMA could be tested based on this study's result. The successful prostate cancer theranostics through targeting PSMA may conceivably be realised is other carcinomas, particularly breast carcinomas. There are however persisting questions. One being; how does the pattern of PSMA expression exhibited by the experimental in vitro cell lines differ from the one seen in the positive control. At this point, various reasons can be tabled as to why this is the case. However, extension of this study into further research is the only way to elucidate and definitively conclude on the nature of PSMA expression in the cells probed during this study.

4.1 Limitations and recommendations

The assessment of cell proliferation utilising the Crystal Violet assay was sufficient but addition of a method that assesses metabolic activity following dissociation would have added more support to the results. Addition of a method such as the 3-[4, 5-dimethylthiazole-

2-yl]-2, 5-diphenyltetrazolium bromide (MTT) assay or the resazurin assay would have elucidated more on the metabolic status of the cells following dissociation.

The MCF-7 cells were compared to a tumour sample equivalent to Luminal A type cancer but the LNCaP, MDA-MB-231 and EA.hy926 cells were not compared to equivalent tumorous tissue. Comparison of the PSMA expression pattern seen in the tested cells to their equivalent tumour type sample would have expounded on the differences and similarities between the monolayers and tissue samples with regard to the expression of PSMA. Moreover, comparison between hormone responsive and triple-negative carcinomas could have been evaluated to provide more heterogeneous samples that better representation of the *in vivo* tumour environment.

The expression pattern in the investigational cell lines was different from the anticipated membrane associated expression of PSMA. Immunoelectron microscopy would have elucidated where exactly in the cell the PSMA was accumulating and with which organelles it is associated. Moreover, PSMA internalisation, recycling and trafficking studies were not undertaken. These studies would have given definite answers regarding the intracellular accumulation of PSMA in the investigational cell lines. Another paradigm that was not explored is the formation of filopodia and their association to the cell membrane. The formation of filopodia is associated with Filamin A which interacts with PSMA to facilitate receptor recycling. These studies could have been undertaken to elucidate further on the intracellular nature of PSMA expression in the investigational cell lines.

Folate hydrolysis studies could have been undertaken to expound on the potential role of PSMA in the investigational cell lines. Folate starvation or increasing folate in growth media could have given more information regarding PSMA kinetics in the investigational cell lines. Cell cycle analysis with simultaneous PSMA probing would have also further elucidated PSMA expression kinetics. Information such as which stage of the cell cycle shows the most abundant expression of PSMA would have along with the generated results provided more information on the kinetics of PSMA expression.

A definite negative control would have also extended the comparison landscape. Incorporation of cells that don't express PSMA such as PC-3 prostate carcinoma cells would have been supportive in this study as a negative control. Notwithstanding the aforementioned limitations, the data generated from this study showed reliability, reproducibility and comparability. The results from this study generated many questions that stimulate future research.

4.2 Future work

The expression of PSMA in monolayer breast carcinoma cell lines has been confidently confirmed. Future work has to look at more representative samples to elucidate the kinetics of PSMA in non-prostatic carcinomas. Three dimensional spheroids and organoids can be assessed to confirm the tissue sample probing of PSMA. Animal studies that include the use of mammary tumours that are generated in athymic mice of other animal models can provide more information of the clinical theranostic potential of PSMA targeting in breast cancer. Furthermore, considering the extent of non-prostatic tissue expression of PSMA as reported in different protein databases, investigation should be extended to other carcinomas beyond breast cancer. The folate hydrolase association of PSMA and the role of folate in cancer may mean that PSMA is a ubiquitous antigen that can be applied as a theranostic target in more carcinomas than previously thought. Folate hydrolysis studies should be undertaken to elucidate and pin point the exact function of PSMA in the non-prostatic cells. Their expression pattern appears to be different from prostate tissue and as such, the function may equally be different.

5 References

ABDOLAHI, M., SHAHBAZI-GAHROUEI, D., LAURENT, S., SERMEUS, C., FIROZIAN, F., ALLEN, B. J., BOUTRY, S. & MULLER, R. N. 2013. Synthesis and in *Vitro* Evaluation of Mr Molecular Imaging Probes Using J591 Mab-Conjugated Spions for Specific Detection of Prostate Cancer. *Contrast Media & Molecular Imaging,* 8**,** 175-184.

AHMED, A., ZAHID, I., LADIWALA, Z. F. R., SHEIKH, R. & MEMON, A. S. 2018. Breast Self-Examination Awareness and Practices in Young Women in Developing Countries: A Survey of Female Students in Karachi, Pakistan. *Journal of Education and Health Promotion,* 7.

AKA, J. A. & LIN, S.-X. 2012. Comparison of Functional Proteomic Analyses of Human Breast Cancer Cell Lines T47d and Mcf7. *PloS One,* 7**,** e31532.

ALBAGOUSH, S. A. & LIMAIEM, F. 2018. Her2. *Statpearls [Internet].* StatPearls Publishing.

ALKABBAN, F. M. & FERGUSON, T. 2019. Cancer, Breast. *Statpearls [Internet].* StatPearls Publishing.

ALLEGRA, C., FINE, R., DRAKE, J. & CHABNER, B. 1986. The Effect of Methotrexate on Intracellular Folate Pools in Human Mcf-7 Breast Cancer Cells. Evidence for Direct Inhibition of Purine Synthesis. *Journal of Biological Chemistry,* 261**,** 6478-6485.

ALZAHRANI, A. S., ALSHAIKH, O., TULI, M., AL-SUGAIR, A., ALAMAWI, R. & AL-RASHEED, M. M. 2012. Diagnostic Value of Recombinant Human Thyrotropin–Stimulated 123i Whole-Body Scintigraphy in the Follow-up of Patients with Differentiated Thyroid Cancer. *Clinical Nuclear Medicine,* 37**,** 229-234.

ANAMPA, J., MAKOWER, D. & SPARANO, J. A. 2015. Progress in Adjuvant Chemotherapy for Breast Cancer: An Overview. *BMC Medicine,* 13**,** 195.

ARNETH, B. 2020. Tumor Microenvironment. *Medicina,* 56**,** 15.

AYSOLA, K., DESAI, A., WELCH, C., XU, J., QIN, Y., REDDY, V., MATTHEWS, R., OWENS, C., OKOLI, J. & BEECH, D. J. 2013. Triple Negative Breast Cancer–an Overview. *Hereditary Genetics: Current Research,* 2013.

BAILEY, D. L., TOWNSEND, D. W., VALK, P. E. & MAISEY, M. N. 2005. *Positron Emission Tomography*, Springer.

BAJOU, K., LEWALLE, J. M., MARTINEZ, C. R., SORIA, C., LU, H., NOËL, A. & FOIDART, J. M. 2002. Human Breast Adenocarcinoma Cell Lines Promote Angiogenesis by Providing Cells with Upa-Pai-1 and by Enhancing Their Expression. *International Journal of Cancer,* 100**,** 501-506.

BANERJEE, S. R., PULLAMBHATLA, M., BYUN, Y., NIMMAGADDA, S., GREEN, G., FOX, J. J., HORTI, A., MEASE, R. C. & POMPER, M. G. 2010. 68ga-Labeled Inhibitors of Prostate-Specific Membrane Antigen (Psma) for Imaging Prostate Cancer. *Journal of Medicinal Chemistry,* 53**,** 5333-5341.

BARANSKA, P., JERCZYNSKA, H., PAWLOWSKA, Z., KOZIOLKIEWICZ, W. & CIERNIEWSKI, C. S. 2005. Expression of Integrins and Adhesive Properties of Human Endothelial Cell Line Ea. Hy 926. *Cancer Genomics-Proteomics,* 2**,** 265-269.

BARBER, L., GERKE, T., MARKT, S. C., PEISCH, S. F., WILSON, K. M., AHEARN, T., GIOVANNUCCI, E., PARMIGIANI, G. & MUCCI, L. A. 2018. Family History of Breast or Prostate Cancer and Prostate Cancer Risk. *Clinical Cancer Research,* 24**,** 5910-5917.

BARINKA, C., ROJAS, C., SLUSHER, B. & POMPER, M. 2012. Glutamate Carboxypeptidase Ii in Diagnosis and Treatment of Neurologic Disorders and Prostate Cancer. *Current Medicinal Chemistry,* 19**,** 856-870.

BARNARD, M. E., BOEKE, C. E. & TAMIMI, R. M. 2015. Established Breast Cancer Risk Factors and Risk of Intrinsic Tumor Subtypes. *Biochimica et Biophysica Acta (BBA)-Reviews on Cancer,* 1856**,** 73-85.

BATISTA, U., GARVAS, M., NEMEC, M., SCHARA, M., VERANIČ, P. & KOKLIC, T. 2010. Effects of Different Detachment Procedures on Viability, Nitroxide Reduction Kinetics

and Plasma Membrane Heterogeneity of V-79 Cells. *Cell Biology International,* 34**,** 663-668.
BIRGERSDOTTER, A., SANDBERG, R. & ERNBERG, I. Gene Expression Perturbation in *Vitro*—a Growing Case for Three-Dimensional (3d) Culture Systems. *Seminars in Cancer Biology*, 2005. Elsevier, 405-412.
BISWAS, T., DATTA, A. & SEN, P. 2011. Prostate-Specific Antigen in Females: A New Tool?
BOARD, P. A. T. E. 2014. Breast Cancer Treatment During Pregnancy (Pdq®): Patient Version. *PDQ Cancer Information Summaries [Internet]*.
BOARD, P. A. T. E. 2019. Male Breast Cancer Treatment (Pdq®). *Pdq Cancer Information Summaries [Internet].* National Cancer Institute (US).
BOARD, P. A. T. E. 2020a. Breast Cancer Treatment (Adult)(Pdq®). *Pdq Cancer Information Summaries [Internet].* National Cancer Institute (US).
BOARD, P. A. T. E. 2020b. Prostate Cáncer Treatment (Pdq®). *Pdq Cancer Information Summaries [Internet].* National Cancer Institute (US).
BOUCHELOUCHE, K. & CHOYKE, P. L. 2016. Psma Pet in Prostate Cancer–a Step Towards Personalized Medicine. *Current Opinion in Oncology,* 28**,** 216.
BRAY, F., FERLAY, J., SOERJOMATARAM, I., SIEGEL, R. L., TORRE, L. A. & JEMAL, A. 2018. Global Cancer Statistics 2018: Globocan Estimates of Incidence and Mortality Worldwide for 36 Cancers in 185 Countries. *CA: A Cancer Journal for Clinicians,* 68**,** 394-424.
BREWER, N. T., SALZ, T. & LILLIE, S. E. 2007. Systematic Review: The Long-Term Effects of False-Positive Mammograms. *Annals of Internal Medicine,* 146**,** 502-510.
BREWSTER, A. M., CHAVEZ-MACGREGOR, M. & BROWN, P. 2014. Epidemiology, Biology, and Treatment of Triple-Negative Breast Cancer in Women of African Ancestry. *The Lancet Oncology,* 15**,** e625-e634.
BROWN, M. & WITTWER, C. 2000. Flow Cytometry: Principles and Clinical Applications in Hematology. *Clinical Chemistry,* 46**,** 1221-1229.
BUNDSCHERER, A., MALSY, M., LANGE, R., HOFMANN, P., METTERLEIN, T., GRAF, B. M. & GRUBER, M. 2013. Cell Harvesting Method Influences Results of Apoptosis Analysis by Annexin V Staining. *Anticancer Research,* 33**,** 3201-3204.
CAPITANIO, S., NORDIN, A. J., NORAINI, A. R. & ROSSETTI, C. 2016. Pet/Ct in Nononcological Lung Diseases: Current Applications and Future Perspectives. *European Respiratory Review,* 25**,** 247-258.
CASALE, J. & CRANE, J. S. 2019. Fluorouracil. *Statpearls [Internet].* StatPearls Publishing.
CASTELLETTI, D., FRACASSO, G., ALFALAH, M., CINGARLINI, S., COLOMBATTI, M. & NAIM, H. Y. 2006. Apical Transport and Folding of Prostate-Specific Membrane Antigen Occurs Independent of Glycan Processing. *Journal of Biological Chemistry,* 281**,** 3505-3512.
CASTRO, E. & EELES, R. 2012. The Role of Brca1 and Brca2 in Prostate Cancer. *Asian Journal of Andrology,* 14**,** 409.
CHAVEZ, K. J., GARIMELLA, S. V. & LIPKOWITZ, S. 2010. Triple Negative Breast Cancer Cell Lines: One Tool in the Search for Better Treatment of Triple Negative Breast Cancer. *Breast Disease,* 32**,** 35.
CHEN, Y., CHATTERJEE, S., LISOK, A., MINN, I., PULLAMBHATLA, M., WHARRAM, B., WANG, Y., JIN, J., BHUJWALLA, Z. M. & NIMMAGADDA, S. 2017. A Psma-Targeted Theranostic Agent for Photodynamic Therapy. *Journal of Photochemistry and Photobiology B: Biology,* 167**,** 111-116.
CHRISTIANSEN, J. J., RAJASEKARAN, S. A., INGE, L., CHENG, L., ANILKUMAR, G., BANDER, N. H. & RAJASEKARAN, A. K. 2005. N-Glycosylation and Microtubule Integrity Are Involved in Apical Targeting of Prostate-Specific Membrane Antigen: Implications for Immunotherapy. *Molecular Cancer Therapeutics,* 4**,** 704-714.
CHRISTIANSEN, J. J., RAJASEKARAN, S. A., MOY, P., BUTCH, A., GOODGLICK, L., GU, Z., REITER, R. E., BANDER, N. H. & RAJASEKARAN, A. K. 2003. Polarity of Prostate Specific Membrane Antigen, Prostate Stem Cell Antigen, and Prostate

Specific Antigen in Prostate Tissue and in a Cultured Epithelial Cell Line. *The Prostate,* 55**,** 9-19.
COMŞA, Ş., CIMPEAN, A. M. & RAICA, M. 2015. The Story of Mcf-7 Breast Cancer Cell Line: 40 Years of Experience in Research. *Anticancer Research,* 35**,** 3147-3154.
CONWAY, R. E., PETROVIC, N., LI, Z., HESTON, W., WU, D. & SHAPIRO, L. H. 2006. Prostate-Specific Membrane Antigen Regulates Angiogenesis by Modulating Integrin Signal Transduction. *Molecular and Cellular Biology,* 26**,** 5310-5324.
COOPER, G. M. & HAUSMAN, R. 2000. A Molecular Approach. *The Cell. 2nd ed. Sunderland, MA: Sinauer Associates*.
COOPERBERG, M. R. & CHAN, J. M. 2017. Epidemiology of Prostate Cancer. Springer.
DAHLBOM, M. 2017. *Physics of Pet and Spect Imaging*, CRC Press.
DESCOTES, J.-L. 2019. Diagnosis of Prostate Cancer. *Asian Journal of Urology,* 6**,** 129-136.
DHARMASIRI, U., BALAMURUGAN, S., ADAMS, A. A., OKAGBARE, P. I., OBUBUAFO, A. & SOPER, S. A. 2009. Highly Efficient Capture and Enumeration of Low Abundance Prostate Cancer Cells Using Prostate-Specific Membrane Antigen Aptamers Immobilized to a Polymeric Microfluidic Device. *Electrophoresis,* 30**,** 3289-3300.
DI ZAZZO, E., GALASSO, G., GIOVANNELLI, P., DI DONATO, M. & CASTORIA, G. 2018. Estrogens and Their Receptors in Prostate Cancer: Therapeutic Implications. *Frontiers in Oncology,* 8**,** 2.
DIECI, M. V., VERNACI, G. & GUARNERI, V. 2019. Escalation and De-Escalation in Her2 Positive Early Breast Cancer. *Current Opinion in Oncology,* 31**,** 35-42.
DING, H. & WU, F. 2012. Image Guided Biodistribution and Pharmacokinetic Studies of Theranostics. *Theranostics,* 2**,** 1040.
DONYA, M., RADFORD, M., ELGUINDY, A., FIRMIN, D. & YACOUB, M. H. 2015. Radiation in Medicine: Origins, Risks and Aspirations. *Global Cardiology Science and Practice,* 2014**,** 57.
DOWLING, M., SAMUELSON, J., FADL-ALLA, B., PONDENIS, H. C., BYRUM, M., BARGER, A. M. & FAN, T. M. 2019. Overexpression of Prostate Specific Membrane Antigen by Canine Hemangiosarcoma Cells Provides Opportunity for the Molecular Detection of Disease Burdens within Hemorrhagic Body Cavity Effusions. *PloS One,* 14**,** e0210297.
DU, Y. & DIZDAREVIC, S. 2017. Molecular Radiotheragnostics in Prostate Cancer. *Clinical Medicine,* 17**,** 458.
DUCKER, G. S. & RABINOWITZ, J. D. 2017. One-Carbon Metabolism in Health and Disease. *Cell Metabolism,* 25**,** 27-42.
EASTHAM, J. 2017. Prostate Cancer Screening. *Investigative and Clinical Urology,* 58**,** 217-219.
EDER, M., NEELS, O., MÜLLER, M., BAUDER-WÜST, U., REMDE, Y., SCHÄFER, M., HENNRICH, U., EISENHUT, M., AFSHAR-OROMIEH, A. & HABERKORN, U. 2014. Novel Preclinical and Radiopharmaceutical Aspects of [68ga] Ga-Psma-Hbed-Cc: A New Pet Tracer for Imaging of Prostate Cancer. *Pharmaceuticals,* 7**,** 779-796.
EDER, M., SCHÄFER, M., BAUDER-WÜST, U., HULL, W.-E., WÄNGLER, C., MIER, W., HABERKORN, U. & EISENHUT, M. 2012. 68ga-Complex Lipophilicity and the Targeting Property of a Urea-Based Psma Inhibitor for Pet Imaging. *Bioconjugate Chemistry,* 23**,** 688-697.
EDGELL, C.-J., MCDONALD, C. C. & GRAHAM, J. B. 1983. Permanent Cell Line Expressing Human Factor Viii-Related Antigen Established by Hybridization. *Proceedings of the National Academy of Sciences,* 80**,** 3734-3737.
EDMONDSON, R., BROGLIE, J. J., ADCOCK, A. F. & YANG, L. 2014. Three-Dimensional Cell Culture Systems and Their Applications in Drug Discovery and Cell-Based Biosensors. *Assay and Drug Development Technologies,* 12**,** 207-218.
EFESOY, O., BOZLU, M., ÇAYAN, S. & AKBAY, E. 2013. Complications of Transrectal Ultrasound-Guided 12-Core Prostate Biopsy: A Single Center Experience with 2049 Patients. *Turkish Journal of Urology,* 39**,** 6.

EMMETT, L., WILLOWSON, K., VIOLET, J., SHIN, J., BLANKSBY, A. & LEE, J. 2017. Lutetium 177 Psma Radionuclide Therapy for Men with Prostate Cancer: A Review of the Current Literature and Discussion of Practical Aspects of Therapy. *Journal of Medical Radiation Sciences,* 64**,** 52-60.

EREMEEVA, M. E. & SILVERMAN, D. J. 1998. *Rickettsia Rickettsii* Infection of the Ea. Hy 926 Endothelial Cell Line: Morphological Response to Infection and Evidence for Oxidative Injury. *Microbiology,* 144**,** 2037-2048.

EVANS, J. C., MALHOTRA, M., CRYAN, J. F. & O'DRISCOLL, C. M. 2016. The Therapeutic and Diagnostic Potential of the Prostate Specific Membrane Antigen/Glutamate Carboxypeptidase Ii (Psma/Gcpii) in Cancer and Neurological Disease. *British Jjournal of Pharmacology,* 173**,** 3041-3079.

FEI, Z., GAO, Y., QIU, M., QI, X., DAI, Y., WANG, S., QUAN, Z., LIU, Y. & OU, J. 2016. Down-Regulation of Dihydrofolate Reductase Inhibits the Growth of Endothelial Ea. Hy926 Cell through Induction of G1 Cell Cycle Arrest Via up-Regulating P53 and P21waf1/Cip1 Expression. *Journal of Clinical Biochemistry and Nutrition***,** 15-64.

FENG, Y., SPEZIA, M., HUANG, S., YUAN, C., ZENG, Z., ZHANG, L., JI, X., LIU, W., HUANG, B. & LUO, W. 2018. Breast Cancer Development and Progression: Risk Factors, Cancer Stem Cells, Signaling Pathways, Genomics, and Molecular Pathogenesis. *Genes & Diseases,* 5**,** 77-106.

FERNÁNDEZ, M., JAVAID, F. & CHUDASAMA, V. 2018. Advances in Targeting the Folate Receptor in the Treatment/Imaging of Cancers. *Chemical Science,* 9**,** 790-810.

FINICHIU, P. G., LARSEN, D. S., EVANS, C., LARSEN, L., BRIGHT, T. P., ROBB, E. L., TRNKA, J., PRIME, T. A., JAMES, A. M. & SMITH, R. A. 2015. A Mitochondria-Targeted Derivative of Ascorbate: Mitoc. *Free Radical Biology and Medicine,* 89**,** 668-678.

FLORES, O., SANTRA, S., KAITTANIS, C., BASSIOUNI, R., KHALED, A. S., KHALED, A. R., GRIMM, J. & PEREZ, J. M. 2017. Psma-Targeted Theranostic Nanocarrier for Prostate Cancer. *Theranostics,* 7**,** 2477.

FOSS, C., MEASE, R., CHO, S., KIM, H. & POMPER, M. 2012. Gcpii Imaging and Cancer. *Current Medicinal Chemistry,* 19**,** 1346-1359.

GALA, J.-L., HEUSTERSPREUTE, M., LORIC, S., HANON, F., TOMBAL, B., VAN CANGH, P., DE NAYER, P. & PHILIPPE, M. 1998. Expression of Prostate-Specific Antigen and Prostate-Specific Membrane Antigen Transcripts in Blood Cells: Implications for the Detection of Hematogenous Prostate Cells and Standardization. *Clinical Chemistry,* 44**,** 472-481.

GHOSH, A. & HESTON, W. D. 2004. Tumor Target Prostate Specific Membrane Antigen (Psma) and Its Regulation in Prostate Cancer. *Journal of Cellular Biochemistry,* 91**,** 528-539.

GINSBURG, O., YIP, C. H., BROOKS, A., CABANES, A., CALEFFI, M., DUNSTAN YATACO, J. A., GYAWALI, B., MCCORMACK, V., MCLAUGHLIN DE ANDERSON, M. & MEHROTRA, R. 2020. Breast Cancer Early Detection: A Phased Approach to Implementation. *Cancer,* 126**,** 2379-2393.

GODET, I. & GILKES, D. M. 2017. Brca1 and Brca2 Mutations and Treatment Strategies for Breast Cancer. *Integrative Cancer Science and Therapeutics,* 4.

GØTZSCHE, P. C. & JØRGENSEN, K. J. 2013. Screening for Breast Cancer with Mammography. *Cochrane Database of Systematic Reviews*.

GRANT, B. D. & DONALDSON, J. G. 2009. Pathways and Mechanisms of Endocytic Recycling. *Nature reviews Molecular Cell Biology,* 10**,** 597-608.

HAFFNER, M. C., KRONBERGER, I. E., ROSS, J. S., SHEEHAN, C. E., ZITT, M., MÜHLMANN, G., ÖFNER, D., ZELGER, B., ENSINGER, C. & YANG, X. J. 2009. Prostate-Specific Membrane Antigen Expression in the Neovasculature of Gastric and Colorectal Cancers. *Human Pathology,* 40**,** 1754-1761.

HANAHAN, D. & WEINBERG, R. A. 2000. The Hallmarks of Cancer. *Cell,* 100**,** 57-70.

HANNOODEE, M. & MITTAL, M. 2020. Methotrexate.

HARRIS, T. J. & MCCORMICK, F. 2010. The Molecular Pathology of Cancer. *Nature Reviews Clinical Oncology,* 7**,** 251.
HENDERSON, J. A. & FERGUSON, T. 2019. Breast Examination Techniques.
HOBRO, A. J. & SMITH, N. I. 2017. An Evaluation of Fixation Methods: Spatial and Compositional Cellular Changes Observed by Raman Imaging. *Vibrational Spectroscopy,* 91**,** 31-45.
HOLLIDAY, D. L. & SPEIRS, V. 2011. Choosing the Right Cell Line for Breast Cancer Research. *Breast Cancer Research,* 13**,** 215.
HOUSSAMI, N. 2017. Overdiagnosis of Breast Cancer in Population Screening: Does It Make Breast Screening Worthless? *Cancer Biology & Medicine,* 14**,** 1.
HU, R., DAWOOD, S., HOLMES, M. D., COLLINS, L. C., SCHNITT, S. J., COLE, K., MAROTTI, J. D., HANKINSON, S. E., COLDITZ, G. A. & TAMIMI, R. M. 2011. Androgen Receptor Expression and Breast Cancer Survival in Postmenopausal Women. *Clinical Cancer Research,* 17**,** 1867-1874.
HUANG, G.-L., KANG, C.-H., LEE, W.-C. & CHIANG, P.-H. 2019. Comparisons of Cancer Detection Rate and Complications between Transrectal and Transperineal Prostate Biopsy Approaches-a Single Center Preliminary Study. *BMC Urology,* 19**,** 1-8.
HUANG, H.-L., HSING, H.-W., LAI, T.-C., CHEN, Y.-W., LEE, T.-R., CHAN, H.-T., LYU, P.-C., WU, C.-L., LU, Y.-C. & LIN, S.-T. 2010. Trypsin-Induced Proteome Alteration During Cell Subculture in Mammalian Cells. *Journal of Biomedical Science,* 17**,** 36.
HUPE, M. C., PHILIPPI, C., ROTH, D., KÜMPERS, C., RIBBAT-IDEL, J., BECKER, F., JOERG, V., DUENSING, S., LUBCZYK, V. H. & KIRFEL, J. 2018. Expression of Prostate-Specific Membrane Antigen (Psma) on Biopsies Is an Independent Risk Stratifier of Prostate Cancer Patients at Time of Initial Diagnosis. *Frontiers in Oncology,* 8**,** 623.
HYATT, A. 2009. Advancing Nuclear Medicine through Innovation-National Research Council and Institute of Medicine of the National Academies* the National Academies Press, Joseph Henry Press; Isbn-13 978-0-309-11067-9; 2008;£ 28.99. *Journal of Radiotherapy in Practice,* 8**,** 165-166.
JADVAR, H. & BALLAS, L. K. 2018. Psma Pet: Transformational Change in Prostate Cancer Management? *Journal of Nuclear Medicine,* 59**,** 228-229.
JIN, X. & MU, P. 2015. Targeting Breast Cancer Metastasis. *Breast Cancer: Basic and Clinical Research,* 9**,** BCBCR. S25460.
KALASH, R. S., LAKSHMANAN, V. K., CHO, C.-S. & PARK, I.-K. 2016. Theranostics. *Biomaterials Nanoarchitectonics.* Elsevier.
KAMIŃSKA, M., CISZEWSKI, T., ŁOPACKA-SZATAN, K., MIOTŁA, P. & STAROSŁAWSKA, E. 2015. Breast Cancer Risk Factors. *Przeglad Menopauzalny Menopause Review,* 14**,** 196.
KAPOOR, M. & KASI, A. 2020. Pet Scanning.
KARSSEMEIJER, N., THIJSSEN, M., HENDRIKS, J. & VAN ERNING, L. 2012. *Digital Mammography: Nijmegen, 1998*, Springer Science & Business Media.
KASOHA, M., UNGER, C., SOLOMAYER, E.-F., BOHLE, R. M., ZAHARIA, C., KHREICH, F., WAGENPFEIL, S. & JUHASZ-BÖSS, I. 2017. Prostate-Specific Membrane Antigen (Psma) Expression in Breast Cancer and Its Metastases. *Clinical & Experimental Metastasis,* 34**,** 479-490.
KEEN, J. D. & KEEN, J. E. 2009. What Is the Point: Will Screening Mammography Save My Life? *BMC Medical Informatics and Decision Making,* 9**,** 18.
KELKAR, S. S. & REINEKE, T. M. 2011. Theranostics: Combining Imaging and Therapy. *Bioconjugate Chemistry,* 22**,** 1879-1903.
KHARKWAL, S. & SAMEER, A. M. 2014. Triple Test in Carcinoma Breast. *Journal of Clinical and Diagnostic Research: JCDR,* 8**,** NC09.
KIESS, A. P., BANERJEE, S., MEASE, R., ROWE, S., RAO, A., FOSS, C., CHEN, Y., YANG, X., CHO, S. & NIMMAGADDA, S. 2015. Prostate-Specific Membrane Antigen as a Target for Cancer Imaging and Therapy. *The quarterly journal of nuclear medicine and molecular imaging: official publication of the Italian Association of*

Nuclear Medicine (AIMN)[and] the International Association of Radiopharmacology (IAR),[and] Section of the Society of, 59**,** 241.
KINOSHITA, Y., KURATSUKURI, K., LANDAS, S., IMAIDA, K., ROVITO, P. M., WANG, C. Y. & HAAS, G. P. 2006. Expression of Prostate-Specific Membrane Antigen in Normal and Malignant Human Tissues. *World Journal of Surgery,* 30**,** 628-636.
KNISELY, A. T., STEWART, M. E., GARCIA, C., THOMAS, M. H., MODESITT, S. C. & RING, K. L. 2020. Evaluation of Breast Screening Strategies in a High Risk Breast and Ovarian Cancer Clinic. *Gynecologic Oncology Reports***,** 100587.
KONG, F.-L., FORD, R. J. & YANG, D. J. 2013. Managing Lymphoma with Non-Fdg Radiotracers: Current Clinical and Preclinical Applications. *BioMed Research International,* 2013.
KRAMER-MAREK, G. & CAPALA, J. 2012. The Role of Nuclear Medicine in Modern Therapy of Cancer. *Tumor Biology,* 33**,** 629-640.
KU, A., FACCA, V. J., CAI, Z. & REILLY, R. M. 2019. Auger Electrons for Cancer Therapy–a Review. *EJNMMI Radiopharmacy and Chemistry,* 4**,** 1-36.
KUENG, W., SILBER, E. & EPPENBERGER, U. 1989. Quantification of Cells Cultured on 96-Well Plates. *Analytical Biochemistry,* 182**,** 16-19.
LAIDLER, P., DULIŃSKA, J., LEKKA, M. & LEKKI, J. 2005. Expression of Prostate Specific Membrane Antigen in Androgen-Independent Prostate Cancer Cell Line Pc-3. *Archives of Biochemistry and Biophysics,* 435**,** 1-14.
LAKIS, S., KOTOULA, V., ELEFTHERAKI, A. G., BATISTATOU, A., BOBOS, M., KOLETSA, T., TIMOTHEADOU, E., CHRISAFI, S., PENTHEROUDAKIS, G. & KOUTRAS, A. 2014. The Androgen Receptor as a Surrogate Marker for Molecular Apocrine Breast Cancer Subtyping. *The Breast,* 23**,** 234-243.
LANGE, C. A. & YEE, D. 2008. Progesterone and Breast Cancer. *Women's Health,* 4**,** 151-162.
LEE, S.-J., LEE, K., YANG, X., JUNG, C., GARDNER, T., KIM, H.-S., JENG, M.-H. & KAO, C. 2003. Nfatc1 with Ap-3 Site Binding Specificity Mediates Gene Expression of Prostate-Specific-Membrane-Antigen. *Journal of molecular biology,* 330**,** 749-760.
LEE, S. T., BURVENICH, I. & SCOTT, A. Novel Target Selection for Nuclear Medicine Studies. Seminars in Nuclear Medicine, 2019. Elsevier.
LEMJABBAR-ALAOUI, H., HASSAN, O. U., YANG, Y.-W. & BUCHANAN, P. 2015. Lung Cancer: Biology and Treatment Options. *Biochimica et Biophysica Acta (BBA)-Reviews on Cancer,* 1856**,** 189-210.
LENZO, N. P., MEYRICK, D. & TURNER, J. H. 2018. Review of Gallium-68 Psma Pet/Ct Imaging in the Management of Prostate Cancer. *Diagnostics,* 8**,** 16.
LILI, L. N., MATYUNINA, L. V., WALKER, L. D., DANEKER, G. W. & MCDONALD, J. F. 2014. Evidence for the Importance of Personalized Molecular Profiling in Pancreatic Cancer. *Pancreas,* 43**,** 198.
LIN, R.-Z., CHOU, L.-F., CHIEN, C.-C. M. & CHANG, H.-Y. 2006. Dynamic Analysis of Hepatoma Spheroid Formation: Roles of E-Cadherin and B1-Integrin. *Cell and Tissue Research,* 324**,** 411-422.
LIU, B., GAO, S. & LI, S. 2017. A Comprehensive Comparison of Ct, Mri, Positron Emission Tomography or Positron Emission Tomography/Ct, and Diffusion Weighted Imaging-Mri for Detecting the Lymph Nodes Metastases in Patients with Cervical Cancer: A Meta-Analysis Based on 67 Studies. *Gynecologic and Obstetric Investigation,* 82**,** 209-222.
LIU, H., ZANG, C., FENNER, M., POSSINGER, K. & ELSTNER, E. 2003. Pparγ Ligands and Atra Inhibit the Invasion of Human Breast Cancer Cells in *Vitro*. *Breast Cancer Research and Treatment,* 79**,** 63-74.
LIU, T., JABBES, M., NEDROW-BYERS, J. R., WU, L. Y., BRYAN, J. N. & BERKMAN, C. E. 2011. Detection of Prostate-Specific Membrane Antigen on Huvecs in Response to Breast Tumor-Conditioned Medium. *International Journal of Oncology,* 38**,** 1349-1355.

LØBERG, M., LOUSDAL, M. L., BRETTHAUER, M. & KALAGER, M. 2015. Benefits and Harms of Mammography Screening. *Breast Cancer Research,* 17**,** 63.
LÓPEZ-ABENTE, G., MISPIRETA, S. & POLLÁN, M. 2014. Breast and Prostate Cancer: An Analysis of Common Epidemiological Features in Mortality Trends in Spain. *BMC Cancer,* 14**,** 874.
LU, Z. J., REN, Y. Q., WANG, G. P., SONG, Q., LI, M., JIANG, S. S., NING, T., GUAN, Y. S., YANG, J. L. & LUO, F. 2009. Biological Behaviors and Proteomics Analysis of Hybrid Cell Line Eahy926 and Its Parent Cell Line A549. *Journal of Experimental & Clinical Cancer Research,* 28**,** 16.
LUMACHI, F., BRUNELLO, A., MARUZZO, M., BASSO, U. & MM BASSO, S. 2013. Treatment of Estrogen Receptor-Positive Breast Cancer. *Current Medicinal Chemistry,* 20**,** 596-604.
MACEDO, G. S., ALEMAR, B. & ASHTON-PROLLA, P. 2019. Reviewing the Characteristics of Brca and Palb2-Related Cancers in the Precision Medicine Era. *Genetics and Molecular Biology,* 42**,** 215-231.
MADJAR, H. 2010. Role of Breast Ultrasound for the Detection and Differentiation of Breast Lesions. *Breast Care,* 5**,** 109-114.
MAHABADI, S., LABEED, F. H. & HUGHES, M. P. 2015. Effects of Cell Detachment Methods on the Dielectric Properties of Adherent and Suspension Cells. *Electrophoresis,* 36**,** 1493-1498.
MAK, T. W. & SAUNDERS, M. E. 2005. *The Immune Response: Basic and Clinical Principles*, Academic Press.
MANDRELL, R., GRIFFISS, J. & MACHER, B. 1988. Lipooligosaccharides (Los) of Neisseria Gonorrhoeae and Neisseria Meningitidis Have Components That Are Immunochemically Similar to Precursors of Human Blood Group Antigens. Carbohydrate Sequence Specificity of the Mouse Monoclonal Antibodies That Recognize Crossreacting Antigens on Los and Human Erythrocytes. *Journal of Experimental Medicine,* 168**,** 107-126.
MCKEITHEN, D., GRAHAM, T., CHUNG, L. W. & ODERO-MARAH, V. 2010. Snail Transcription Factor Regulates Neuroendocrine Differentiation in Lncap Prostate Cancer Cells. *The Prostate,* 70**,** 982-992.
MEISER, J., TUMANOV, S., MADDOCKS, O., LABUSCHAGNE, C. F., ATHINEOS, D., VAN DEN BROEK, N., MACKAY, G. M., GOTTLIEB, E., BLYTH, K. & VOUSDEN, K. 2016. Serine One-Carbon Catabolism with Formate Overflow. *Science Advances,* 2**,** e1601273.
MELEGOS, D. N., YU, H., ASHOK, M., WANG, C., STANCZYK, F. & DIAMANDIS, E. P. 1997. Prostate-Specific Antigen in Female Serum, a Potential New Marker of Androgen Excess. *The Journal of Clinical Endocrinology & Metabolism,* 82**,** 777-780.
MENEZES, G. L., KNUTTEL, F. M., STEHOUWER, B. L., PIJNAPPEL, R. M. & VAN DEN BOSCH, M. A. 2014. Magnetic Resonance Imaging in Breast Cancer: A Literature Review and Future Perspectives. *World Journal of Clinical Oncology,* 5**,** 61.
MOMENIMOVAHED, Z. & SALEHINIYA, H. 2019. Epidemiological Characteristics of and Risk Factors for Breast Cancer in the World. *Breast Cancer: Targets and Therapy,* 11**,** 151.
MORIMOTO, L., COALSON, J., MOWAT, F. & O'MALLEY, C. 2010. Factors Affecting Receipt of Chemotherapy in Women with Breast Cancer. *International Journal of Women's Health,* 2**,** 107.
MUNJAL, A. & GUPTA, N. 2020. Radiopharmaceuticals. *Statpearls [Internet].* StatPearls Publishing.
MURRAY, N. P., REYES, E., ORELLANA, N., FUENTEALBA, C. & DUEÑAS, R. 2014. A Comparative Performance Analysis of Total Psa, Percentage Free Psa, Psa Velocity, and Psa Density Versus the Detection of Primary Circulating Prostate Cells in Predicting Initial Prostate Biopsy Findings in Chilean Men. *BioMed Research International,* 2014.
NAGABHUSHANAM, R. 1997. *Fouling Organisms of the Indian Ocean*, CRC Press.

NAIRNE, J., IVESON, P. B. & MEIJER, A. 2015. Imaging in Drug Development. *Progress in Medicinal Chemistry.* Elsevier.

NASEEM, M., MURRAY, J., HILTON, J. F., KARAMCHANDANI, J., MURADALI, D., FARAGALLA, H., POLENZ, C., HAN, D., BELL, D. C. & BREZDEN-MASLEY, C. 2015. Mammographic Microcalcifications and Breast Cancer Tumorigenesis: A Radiologic-Pathologic Analysis. *BMC Cancer,* 15**,** 307.

NEWPORT, J. W. & FORBES, D. J. 1987. The Nucleus: Structure, Function, and Dynamics. *Annual Review of Biochemistry,* 56**,** 535-565.

NEWTON, J. M., VLAHOPOULOU, J. & ZHOU, Y. 2017. Investigating and Modelling the Effects of Cell Lysis on the Rheological Properties of Fermentation Broths. *Biochemical Engineering Journal,* 121**,** 38-48.

NGUYEN, D. P., XIONG, P. L., LIU, H., PAN, S., LECONET, W., NAVARRO, V., GUO, M., MOY, J., KIM, S. & RAMIREZ-FORT, M. K. 2016. Induction of Psma and Internalization of an Anti-Psma Mab in the Vascular Compartment. *Molecular Cancer Research,* 14**,** 1045-1053.

NOMURA, N., PASTORINO, S., JIANG, P., LAMBERT, G., CRAWFORD, J. R., GYMNOPOULOS, M., PICCIONI, D., JUAREZ, T., PINGLE, S. C. & MAKALE, M. 2014. Prostate Specific Membrane Antigen (Psma) Expression in Primary Gliomas and Breast Cancer Brain Metastases. *Cancer Cell International,* 14**,** 26.

NOSS, K. R., WOLFE, S. A. & GRIMES, S. R. 2002. Upregulation of Prostate Specific Membrane Antigen/Folate Hydrolase Transcription by an Enhancer. *Gene,* 285**,** 247-256.

NOUNOU, M. I., ELAMRAWY, F., AHMED, N., ABDELRAOUF, K., GODA, S. & SYED-SHA-QHATTAL, H. 2015. Breast Cancer: Conventional Diagnosis and Treatment Modalities and Recent Patents and Technologies. *Breast Cancer: Basic and Clinical Research,* 9**,** BCBCR. S29420.

O'KEEFE, D. S., BACICH, D. J., HUANG, S. S. & HESTON, W. D. 2018. A Perspective on the Evolving Story of Psma Biology, Psma-Based Imaging, and Endoradiotherapeutic Strategies. *Journal of Nuclear Medicine,* 59**,** 1007-1013.

OLSEN, J. V., ONG, S.-E. & MANN, M. 2004. Trypsin Cleaves Exclusively C-Terminal to Arginine and Lysine Residues. *Molecular & Cellular Proteomics,* 3**,** 608-614.

OPPENHEIM, E. W., NASRALLAH, I. M., MASTRI, M. G. & STOVER, P. J. 2000. Mimosine Is a Cell-Specific Antagonist of Folate Metabolism. *Journal of Biological Chemistry,* 275**,** 19268-19274.

PAN, X., DALM, C., WIJFFELS, R. H. & MARTENS, D. E. 2017. Metabolic Characterization of a Cho Cell Size Increase Phase in Fed-Batch Cultures. *Applied Microbiology and Biotechnology,* 101**,** 8101-8113.

PARISE, C. A. & CAGGIANO, V. 2014. Breast Cancer Survival Defined by the Er/Pr/Her2 Subtypes and a Surrogate Classification According to Tumor Grade and Immunohistochemical Biomarkers. *Journal of Cancer Epidemiology,* 2014.

PEARCE, A., HAAS, M., VINEY, R., PEARSON, S.-A., HAYWOOD, P., BROWN, C. & WARD, R. 2017. Incidence and Severity of Self-Reported Chemotherapy Side Effects in Routine Care: A Prospective Cohort Study. *Plos One,* 12**,** e0184360.

PRCIC, A., BEGIC, E. & HIROS, M. 2016. Usefulness of Total Psa Value in Prostate Diseases Diagnosis. *Acta Informatica Medica,* 24**,** 156.

PUGSLEY, M. & VEGA, E. 2011. An Overview of Colorimetric Assay Methods Used to Assess Survival or Proliferation of Mammalian Cells. *Proceedings of the Western Pharmacology Socety,* 54**,** 10-14.

RADHAKRISHNA, S., AGARWAL, S., PARIKH, P. M., KAUR, K., PANWAR, S., SHARMA, S., DEY, A., SAXENA, K., CHANDRA, M. & SUD, S. 2018. Role of Magnetic Resonance Imaging in Breast Cancer Management. *South Asian Journal of Cancer,* 7**,** 69.

RAJASEKARAN, A. K., ANILKUMAR, G. & CHRISTIANSEN, J. J. 2005. Is Prostate-Specific Membrane Antigen a Multifunctional Protein? *American Journal of Physiology-Cell Physiology,* 288**,** C975-C981.

RAVAL, A., DAN, T. D., WILLIAMS, N. L., PRIDJIAN, A. & DEN, R. B. 2016. Radioisotopes in Management of Metastatic Prostate Cancer. *Indian journal of urology: IJU: journal of the Urological Society of India,* 32**,** 277.

RISBRIDGER, G. P., DAVIS, I. D., BIRRELL, S. N. & TILLEY, W. D. 2010. Breast and Prostate Cancer: More Similar Than Different. *Nature Reviews Cancer,* 10**,** 205.

RISTAU, B., CUMMINGS, J., O'KEEFE, D. & BACICH, D. 2013. Psma Expression on the Mitochondrial Membrane of Prostate Cancer Cells Leads to a Folate-Dependent Increase in Cellular Proliferation. *The Journal of Urology,* 189**,** e403-e404.

RISTAU, B. T., O'KEEFE, D. S. & BACICH, D. J. The Prostate-Specific Membrane Antigen: Lessons and Current Clinical Implications from 20 Years of Research. *Urologic Oncology: Seminars and Original Investigations*, 2014. Elsevier, 272-279.

ROACH, P. J., FRANCIS, R., EMMETT, L., HSIAO, E., KNEEBONE, A., HRUBY, G., EADE, T., NGUYEN, Q. A., THOMPSON, B. D. & CUSICK, T. 2018. The Impact of 68ga-Psma Pet/Ct on Management Intent in Prostate Cancer: Results of an Australian Prospective Multicenter Study. *Journal of Nuclear Medicine,* 59**,** 82-88.

ROBINSON, D., VAN ALLEN, E. M., WU, Y.-M., SCHULTZ, N., LONIGRO, R. J., MOSQUERA, J.-M., MONTGOMERY, B., TAPLIN, M.-E., PRITCHARD, C. C. & ATTARD, G. 2015. Integrative Clinical Genomics of Advanced Prostate Cancer. *Cell,* 161**,** 1215-1228.

RYCYNA, K. J., BACICH, D. J. & O'KEEFE, D. S. 2013. Opposing Roles of Folate in Prostate Cancer. *Urology,* 82**,** 1197-1203.

SAHA, G. B. 2015. *Basics of Pet Imaging: Physics, Chemistry, and Regulations*, Springer.

SAITA, T., YAMAMOTO, Y., HOSOYA, K., YAMAMOTO, Y., KIMURA, S., NARISAWA, Y. & SHIN, M. 2017. An Ultra-Specific and Sensitive Sandwich Elisa for Imatinib Using Two Anti-Imatinib Antibodies. *Analytica Chimica Acta,* 969**,** 72-78.

SAKAMOTO, N., CHASTAIN, P. D., PARNIEWSKI, P., OHSHIMA, K., PANDOLFO, M., GRIFFITH, J. D. & WELLS, R. D. 1999. Sticky DNA: Self-Association Properties of Long Gaa· Ttc Repeats in R· R· Y Triplex Structures from Friedreich's Ataxia. *Molecular Cell,* 3**,** 465-475.

SAMBI, M., DECARLO, A., MALARDIER-JUGROOT, C. & SZEWCZUK, M. R. 2019. Next-Generation Multimodality of Nanomedicine Therapy: Size and Structure Dependence of Folic Acid Conjugated Copolymers Actively Target Cancer Cells in Disabling Cell Division and Inducing Apoptosis. *Cancers,* 11**,** 1698.

SARKAR, S., HORN, G., MOULTON, K., OZA, A., BYLER, S., KOKOLUS, S. & LONGACRE, M. 2013. Cancer Development, Progression, and Therapy: An Epigenetic Overview. *International Journal of Molecular Sciences,* 14**,** 21087-21113.

SATHEKGE, M., LENGANA, T., MODISELLE, M., VORSTER, M., ZEEVAART, J., MAES, A., EBENHAN, T. & VAN DE WIELE, C. 2017. 68 Ga-Psma-Hbed-Cc Pet Imaging in Breast Carcinoma Patients. *European Journal of Nuclear Medicine and Molecular Imaging,* 44**,** 689-694.

SCHMIDT, L. H., HEITKÖTTER, B., SCHULZE, A. B., SCHLIEMANN, C., STEINESTEL, K., TRAUTMANN, M., MARRA, A., HILLEJAN, L., MOHR, M. & EVERS, G. 2017. Prostate Specific Membrane Antigen (Psma) Expression in Non-Small Cell Lung Cancer. *PloS One,* 12.

SCHWARZ, D. S. & BLOWER, M. D. 2016. The Endoplasmic Reticulum: Structure, Function and Response to Cellular Signaling. *Cellular and Molecular Life Sciences,* 73**,** 79-94.

SEELY, J. & ALHASSAN, T. 2018. Screening for Breast Cancer in 2018—What Should We Be Doing Today? *Current Oncology,* 25**,** S115.

SGOUROS, G. 2019. Radiopharmaceutical Therapy. *Health Physics,* 116**,** 175.

SGOUROS, G., BODEI, L., MCDEVITT, M. R. & NEDROW, J. R. 2020. Radiopharmaceutical Therapy in Cancer: Clinical Advances and Challenges. *Nature Reviews Drug Discovery***,** 1-20.

SHAH, R., ROSSO, K. & NATHANSON, S. D. 2014. Pathogenesis, Prevention, Diagnosis and Treatment of Breast Cancer. *World Journal of Clinical Oncology,* 5**,** 283.

SHINOHARA, A., HANAOKA, H., SAKASHITA, T., SATO, T., YAMAGUCHI, A., ISHIOKA, N. S. & TSUSHIMA, Y. 2018. Rational Evaluation of the Therapeutic Effect and Dosimetry of Auger Electrons for Radionuclide Therapy in a Cell Culture Model. *Annals of Nuclear Medicine,* 32**,** 114-122.

SHIRAZI, F. H., ZARGHI, A., KOBARFARD, F., ZENDEHDEL, R., NAKHJAVANI, M., ARFAIEE, S., ZEBARDAST, T., MOHEBI, S., ANJIDANI, N. & ASHTARINEZHAD, A. 2011. Remarks in Successful Cellular Investigations for Fighting Breast Cancer Using Novel Synthetic Compounds. *Breast Cancer—Focusing Tumor Microenvironment, Stem Cells and Metastasis; Gunduz, M., Gunduz, E., Eds***,** 85-102.

SIEGEL, R. L., MILLER, K. D. & JEMAL, A. 2016. Cancer Statistics, 2016. *CA: A Cancer Journal for Clinicians,* 66**,** 7-30.

SILVER, D. A., PELLICER, I., FAIR, W. R., HESTON, W. & CORDON-CARDO, C. 1997. Prostate-Specific Membrane Antigen Expression in Normal and Malignant Human Tissues. *Clinical Cancer Research,* 3**,** 81-85.

SINGH, A. N. 2016. Positron Annihilation Spectroscopy in Tomorrow's Material Defect Studies. *Applied Spectroscopy Reviews,* 51**,** 359-378.

SMITH, H. R. 2015. Depression in Cancer Patients: Pathogenesis, Implications and Treatment. *Oncology Letters,* 9**,** 1509-1514.

STEPHEN, L., TAYLOR, S.-S., HUSSAIN, S. & LARRY, S. 2020. *Prostate Cancer,* Treasure Island (FL), StatPearls Publishing.

STRATTON, M. R. 1997. Pathology of Familial Breast Cancer: Differences between Breast Cancers in Carriers of Brca1 or Brca2 Mutations and Sporadic Cases. *The Lancet,* 349**,** 1505-1510.

SU, W. W. & LEE, K.-T. 2007. Plant Cell and Hairy Root Cultures–Process Characteristics, Products, and Applications. *Bioprocessing for Value-Added Products from Renewable Resources.* Elsevier.

TAN, M. E., LI, J., XU, H. E., MELCHER, K. & YONG, E.-L. 2015. Androgen Receptor: Structure, Role in Prostate Cancer and Drug Discovery. *Acta Pharmacologica Sinica,* 36**,** 3.

THIGPEN, D., KAPPLER, A. & BREM, R. 2018. The Role of Ultrasound in Screening Dense Breasts—a Review of the Literature and Practical Solutions for Implementation. *Diagnostics,* 8**,** 20.

THUL, P. J., ÅKESSON, L., WIKING, M., MAHDESSIAN, D., GELADAKI, A., BLAL, H. A., ALM, T., ASPLUND, A., BJÖRK, L. & BRECKELS, L. M. 2017. A Subcellular Map of the Human Proteome. *Science,* 356.

TIAN, J., RAN, B., ZHANG, C., YAN, D. & LI, X. 2018. Estrogen and Progesterone Promote Breast Cancer Cell Proliferation by Inducing Cyclin G1 Expression. *Brazilian Journal of Medical and Biological Research,* 51.

TOLKACH, Y., GEVENSLEBEN, H., BUNDSCHUH, R., KOYUN, A., HUBER, D., KEHRER, C., HECKING, T., KEYVER-PAIK, M.-D., KAISER, C. & AHMADZADEHFAR, H. 2018. Prostate-Specific Membrane Antigen in Breast Cancer: A Comprehensive Evaluation of Expression and a Case Report of Radionuclide Therapy. *Breast Cancer Research and Treatment,* 169**,** 447-455.

TROYER, J. K., BECKETT, M. L. & WRIGHT JR, G. L. 1997. Location of Prostate-Specific Membrane Antigen in the Lncap Prostate Carcinoma Cell Line. *The Prostate,* 30**,** 232-242.

TURNER, J. H. 2018. Recent Advances in Theranostics and Challenges for the Future. *The British Journal of Radiology,* 91**,** 20170893.

TYKVART, J., NAVRATIL, V., SEDLAK, F., COREY, E., COLOMBATTI, M., FRACASSO, G., KOUKOLIK, F., BAŘINKA, C., ŠÁCHA, P. & KONVALINKA, J. 2014. Comparative Analysis of Monoclonal Antibodies against Prostate-Specific Membrane Antigen (Psma). *The Prostate,* 74**,** 1674-1690.

UDOVICICH, C., PERERA, M., HOFMAN, M. S., SIVA, S., DEL RIO, A., MURPHY, D. G. & LAWRENTSCHUK, N. 2017. 68ga-Prostate-Specific Membrane Antigen-Positron

Emission Tomography/Computed Tomography in Advanced Prostate Cancer: Current State and Future Trends. *Prostate International,* 5**,** 125-129.
VERCHER-CONEJERO, J. L., PELEGRÍ-MARTINEZ, L., LOPEZ-AZNAR, D. & CÓZAR-SANTIAGO, M. D. P. 2015. Positron Emission Tomography in Breast Cancer. *Diagnostics,* 5**,** 61-83.
VIOLET, J. A. & HOFMAN, M. S. 2017. Prostate-Specific Membrane Antigen from Diagnostic to Therapeutic Target: Radionuclide Therapy Comes of Age in Prostate Cancer. *BJU International,* 120**,** 310-312.
VISENTIN, M., ZHAO, R. & GOLDMAN, I. D. 2012. The Antifolates. *Hematology/Oncology Clinics,* 26**,** 629-648.
WANG, H.-L., WANG, S.-S., SONG, W.-H., PAN, Y., YU, H.-P., SI, T.-G., LIU, Y., CUI, X.-N. & GUO, Z. 2015. Expression of Prostate-Specific Membrane Antigen in Lung Cancer Cells and Tumor Neovasculature Endothelial Cells and Its Clinical Significance. *PloS One,* 10.
WANG, L. 2017. Early Diagnosis of Breast Cancer. *Sensors,* 17**,** 1572.
WANG, Q.-E. 2015. DNA Damage Responses in Cancer Stem Cells: Implications for Cancer Therapeutic Strategies. *World Journal of Biological Chemistry,* 6**,** 57.
WERNICKE, A. G., VARMA, S., GREENWOOD, E. A., CHRISTOS, P. J., CHAO, K., LIU, H., BANDER, N. H. & SHIN, S. J. 2014. Prostate-Specific Membrane Antigen Expression in Tumor-Associated Vasculature of Breast Cancers. *Apmis,* 122**,** 482-489.
WILD, C., WEIDERPASS, E. & STEWART, B. 2020. World Cancer Report: Cancer Research for Cancer Prevention. *Lyon: International Agency for Research on Cancer*.
WOJTKOWIAK, J. W., ROTHBERG, J. M., KUMAR, V., SCHRAMM, K. J., HALLER, E., PROEMSEY, J. B., LLOYD, M. C., SLOANE, B. F. & GILLIES, R. J. 2012. Chronic Autophagy Is a Cellular Adaptation to Tumor Acidic Ph Microenvironments. *Cancer Research,* 72**,** 3938-3947.
XU, B., ZHOU, F., YAN, M.-M., CAI, D.-S., GUO, W.-B., YANG, Y.-Q., JIA, X.-H., ZHANG, W.-X., LI, T. & MA, T. 2018. Psma-Oriented Target Delivery of Novel Anticancer Prodrugs: Design, Synthesis, and Biological Evaluations of Oligopeptide-Camptothecin Conjugates. *International Journal of Molecular Sciences,* 19**,** 3251.
YAMADA, K. M. & CUKIERMAN, E. 2007. Modeling Tissue Morphogenesis and Cancer in 3d. *Cell,* 130**,** 601-610.
YAO, V. & BACICH, D. J. 2006. Prostate Specific Membrane Antigen (Psma) Expression Gives Prostate Cancer Cells a Growth Advantage in a Physiologically Relevant Folate Environment in *Vitro*. *The Prostate,* 66**,** 867-875.
YU, H. & BERKEL, H. 1999. Prostate-Specific Antigen (Psa) in Women. *The Journal of the Louisiana State Medical Society: official organ of the Louisiana State Medical Society,* 151**,** 209-213.
ZHENG, Y. & CANTLEY, L. C. 2019. Toward a Better Understanding of Folate Metabolism in Health and Disease. *Journal of Experimental Medicine,* 216**,** 253-266.
ZHENG, Y., LIN, T.-Y., LEE, G., PADDOCK, M. N., MOMB, J., CHENG, Z., LI, Q., FEI, D. L., STEIN, B. D. & RAMSAMOOJ, S. 2018. Mitochondrial One-Carbon Pathway Supports Cytosolic Folate Integrity in Cancer Cells. *Cell,* 175**,** 1546-1560. e17.
ZIEGLER, Y. S., MORESCO, J. J., TU, P. G., YATES III, J. R. & NARDULLI, A. M. 2014. Plasma Membrane Proteomics of Human Breast Cancer Cell Lines Identifies Potential Targets for Breast Cancer Diagnosis and Treatment. *PloS One,* 9.